THE
PHYSICAL REVIEW
A Journal of Experimental and Theoretical Physics Established by E. L. Nichols in 1893
VOL. 59, NO. 5 MARCH 1, 1941 SECOND SERIES

The Interaction of γ-Rays with Mesotrons

R. F. CHRISTY AND S. KUSAKA
Department of Physics, University of California, Berkeley, California
(Received December 31, 1940)

Differential cross sections for the production of a mesotron pair by a γ-ray and for the bremsstrahlung of a mesotron in the electromagnetic field of a nucleus have been calculated. Both the Proca wave field and the Kemmer matrix formulations of the theory for mesotrons of unit spin and unit magnetic moment were used. These differential cross sections have been integrated in the limit where the energies of the mesotrons and photon are large compared to the rest energy of the mesotron. For a pure Coulomb field, the integrated cross sections are $A\alpha Z^2e^4E^2/(\mu c^2)^4$ where for pair production $A=19/72$ and E is the γ-ray energy, and for bremsstrahlung $A=11/72$ and E is the initial mesotron energy. Since in these processes the important impacts are much closer than the nuclear radius, these cross sections do not describe correctly the electromagnetic effects in the neighborhood of an actual nucleus. The cross sections in a field of the form $(Ze/r)(1-e^{-r/d})$ where d is the nuclear radius and is taken to be $5\hbar Z^{1/3}/6\mu c$, are $B'\alpha Z^{2/3}e^4E/(\mu c^2)^3$ where E is defined as before and $B'=\pi/6$ and $\pi/18$ for pair production and bremsstrahlung, respectively. Since considerations of the validity of the Born approximation method used show that the leading terms in the cross sections lose their validity before they become dominant, terms of lower order which give cross sections increasing only logarithmically with the energy have been calculated by the method of virtual quanta. Further, to estimate the minimum values of the cross sections beyond the range of validity, the frequency integral in the virtual quantum calculation was cut off at $k/\mu c^2=\hbar c/e^2$.

I

THE absorption and production of the penetrating component of cosmic rays depend, among other processes, on the bremsstrahlung and pair production of mesotrons in matter. These processes are also involved in any account of the secondary soft radiation associated with the penetrating component under great thicknesses of matter. Oppenheimer, Snyder and Serber[1] have estimated that in a Coulomb field these cross sections are $\sim\alpha Z^2e^4E^2/(\mu c^2)^4$; whereas in an actual nuclear electric field, which they take to be a Coulomb field cut off at the nuclear radius $d\sim\hbar Z^{\frac{1}{3}}/\mu c$, the cross sections are $\sim\alpha Z^{5/3}e^4E/(\mu c^2)^3$. The large difference between these two forms is due to the high frequency Fourier components of the Coulomb field which are missing in the cut-off field. Kobayasi and Utiyama[2] have obtained similar expressions for the cross sections in a cut-off Coulomb field by the approximate method of virtual quanta. Because the approximations involved in this method lose their validity for just those small impact parameters and high frequencies which are most important, these results are still uncertain by a multiplicative factor of order unity.

[1] J. R. Oppenheimer, H. Snyder and R. Serber, Phys. Rev. **57**, 75 (1940).

[2] M. Kobayasi and R. Utiyama, Sci. Pap. Inst. Phys. Chem. Research, Tokyo **37**, 221 (1940). *Note added in proof.*—Since our manuscript was sent to press, a paper by M. Kobayasi and R. Utiyama, Proc. Phys. Math. Soc. Japan **22**, 882 (1940), has appeared in which bremsstrahlung and pair production cross sections at high energies are calculated by eliminating high frequencies, $k>\hbar c/e^2$, as in this paper.

Booth and Wilson[3] have used the method of virtual quanta to obtain a cross section for bremsstrahlung which, however, is incorrect because they fail to distinguish between a Coulomb field and the actual nuclear electric field near the nuclear radius. Their result does not agree with the cross section in a pure Coulomb field because the method fails completely in that application. In order to refine the conclusions of Oppenheimer, Snyder and Serber, we have calculated by Born approximation, in the limit where the energies are large compared to the rest energy of the mesotron, those terms in the cross sections for bremsstrahlung and pair production of mesotrons which increase most rapidly with the energy. We have in addition, calculated further terms in the cross section for bremsstrahlung by the method of virtual quanta.

The mesotron of unit spin is usually described by Proca's equation which assigns also unit magnetic moment. Corben and Schwinger[4] point out that a consistent theory can be developed for particles of unit spin and arbitrary magnetic moment, but conclude from cosmic-ray data that of these the unit magnetic moment is most likely. In the present paper, also, the theory describing a mesotron of gyromagnetic ratio unity is used since it gives a unique cancellation in the matrix elements of the current and thus leads to cross sections increasing least rapidly with the energy.

Both the Proca wave field and the Kemmer[5] matrix formulation of the theory were used to calculate the differential cross sections. The first method is considerably longer and more tedious but yields the added information that at high energies it is the longitudinal-transverse mesotron spin transitions which are important. The second method requires the use of spin sum and spur techniques which, as their application to mesotron theory is new, will be described in some detail in Section II.

The calculation by Born approximation of the leading terms in the cross sections for bremsstrahlung and pair creation gives the following results. The cross sections in the Coulomb field Ze/r are

$$\sigma = A\alpha Z^2 e^4 E^2/(\mu c^2)^4, \tag{1}$$

where for bremsstrahlung, $A = 11/72$ and E is the initial mesotron energy; and for pair creation, $A = 19/72$ and E is the γ-ray energy. In complete contrast to the Dirac theory in this high energy limit, these impacts involve large angles of scattering and radiation with large momentum transfers of the order E/c. These are associated with high frequency Fourier components of the Coulomb field which are present only at distances $\sim\hbar c/E$, which, for $E \gg \mu c^2$, is much less than the actual nuclear radius where the electric field is certainly not Coulombian. Thus, in order to obtain cross sections with any significance, it is necessary to consider a more exact approximation to the electric field near the nucleus. The atomic screening can be neglected since only close impacts contribute appreciably.

In connection with this treatment of the electric field near the nucleus, it is, of course, important to remember that all specifically nuclear reactions and couplings are being neglected. In fact we have at present no method at all adequate for handling the large couplings presumably involved. The electromagnetic effects we treat are thus not a complete description of the collisions, but constitute a sort of minimum prediction largely independent of the specifically nuclear effects, characterized by different angular distributions, different reaction products and different ranges of the impact parameter.

A closer approximation to the nuclear potential is $(Ze/r)(1-e^{-r/d})$, where d is the nuclear radius and is taken to be $5\hbar Z^{\frac{1}{3}}/6\mu c = 1.82\times 10^{-13} Z^{\frac{1}{3}}$ cm for $\mu = 177$ electron masses. This essentially sets an upper limit of about $\mu c/Z^{\frac{1}{3}}$ on the momentum transfer to the nucleus and gives

$$\sigma = \frac{B\alpha Z^2 e^4 E^2}{(\mu c^2)^4}\frac{\hbar c}{Ed} = \frac{B'\alpha Z^{5/3} e^4 E}{(\mu c^2)^3}, \tag{2}$$

where E has the two meanings stated above, and $B' = \pi/18$ and $\pi/6$, respectively, for bremsstrahlung and pair creation. In contrast to the virtual quanta calculation of these cross sections which cannot take into account the shape of the potential near the nucleus, the constant B can be determined definitely for any assumed shape.

[3] F. Booth and A. H. Wilson, Proc. Roy. Soc. **A175**, 483 (1940).
[4] H. C. Corben and J. Schwinger, Phys. Rev. **58**, 953 (1940).
[5] N. Kemmer, Proc. Roy. Soc. **A173**, 91 (1939).

Since these cross sections are derived by perturbation methods, their validity is limited to energies where the perturbing interactions with the Coulomb field and with the radiation field are small. Oppenheimer, Snyder and Serber[1] show that the more incisive limitation arises from the requirement that the coupling with the radiation field be small which sets an upper limit $\sim 10^{10}$ ev on the validity of the formulae. Under these circumstances, where the leading terms in the cross sections lose their validity before they become dominant, it can be of interest to investigate terms of lower order, which give cross sections increasing only logarithmically with the energy. The impacts responsible for these terms are relatively distant and the method of virtual quanta is thus applicable (see Section IV). One of these terms shows the "infra-red catastrophe," so that their order of magnitude is most conveniently demonstrated by the cross section for fractional energy loss of a mesotron by bremsstrahlung

$$\sigma = \alpha Z^2 \left(\frac{e^2}{\mu c^2}\right)^2 \left[\frac{5\pi}{144}\frac{E}{\mu c^2 Z^{\frac{1}{3}}} + \frac{7}{72}\ln^3\frac{2\pi E}{5\mu Z^{\frac{1}{3}}} - \frac{23}{96}\ln^2\frac{2\pi E}{5\mu Z^{\frac{1}{3}}} + \left(\frac{7\pi^2}{72}+\frac{121}{48}\right)\ln\frac{2\pi E}{5\mu Z^{\frac{1}{3}}}\right]. \quad (3)$$

The first term in this expression is determined by the cross section (2). The other terms must be regarded as having the characteristic uncertainty of the method of virtual quanta: they contain undetermined factors of order unity in the arguments of the logarithms. The last term is, in structure and origin, similar to the dominant term in the corresponding cross section for bremsstrahlung of particles of half integral spin and unit magnetic moment, e.g., electrons. The impacts responsible for it are relatively distant; the couplings are always small, being of the order $(e^2/\hbar c)^{\frac{1}{2}}$. The terms in $\ln^3 E$ and $\ln^2 E$ result from two features not present in calculations based on the Dirac theory. First is the existence of terms in the cross section which depend on the impact parameter as $\ln^2 r$ which weights close impacts and high energies more than for the Dirac particle where the dependence is as $\ln r$. Second is the presence of terms in $1/(1-\epsilon)$, $0 \leqslant \epsilon \leqslant 1-(\mu c^2/E)$, where ϵ is the fractional energy transfer to the γ-ray, which weight large energy transfers. The term in $\ln^2 r$ depends on the frequency of the virtual quanta as $\ln^2 k$ and at high energies, involve high frequencies and correspondingly large couplings. Thus the arguments of Oppenheimer, Snyder and Serber, which limit the validity of the first term proportional to E to frequencies of the order $(\hbar c/e^2)^{\frac{1}{2}}$ in the symmetric coordinate system, or to $2\hbar c/e^2$ in the mesotron rest system in which the virtual quantum calculation is performed, must also be invoked to limit the validity of the $\ln^3 E$ and the $\ln^2 E$ terms arising from this $\ln^2 k$ term in the cross section.

With the leading terms in (3) so limited in validity, it is of interest to calculate at least the lower limit for their contribution to the cross section at energies $>10^{10}$ ev. This is accomplished by making a virtual quantum calculation of all terms in the cross section and cutting off the frequency integral at $k/\mu c^2 = A \leqslant 2\hbar c/e^2$. The cut-off A cannot be assigned exactly but must certainly be greater than 10 if relativistic mesotron theory and the effects due to spin are to have any meaning; there seems to be no *a priori* theoretical reason why A should not be of order 100. Calculations were made with $A = \hbar c/e^2 = 137$. The Born approximation calculations of (1) and (2) are discussed in Section III. The virtual quantum calculations and their modifications of (3) are given in Section IV. The application of these calculations to a discussion of cosmic-ray bursts appears in a separate paper.

II

Kemmer's wave equation for the mesotron of mass μ, charge $\pm e$, spin 1 and magnetic moment 1 is

$$\partial_\rho \beta_\rho \psi + K\psi = 0, \quad (4)$$

where $K = \mu c/\hbar$, $\partial_\rho = \partial/\partial x_\rho$, $x_4 = ict$ and the operators β_ρ are ten-row square matrices obeying the commutation rules

$$\beta_\mu \beta_\nu \beta_\rho + \beta_\rho \beta_\nu \beta_\mu = \beta_\mu \delta_{\nu\rho} + \beta_\rho \delta_{\nu\mu}, \quad (5)$$

the charge and the energy are given by

$$ne = e\int \psi^* \beta_4 \psi d\tau; \quad E = \int \psi^* \beta_4 H \psi d\tau, \quad (6)$$

where H is the Hamiltonian defined by

$$H\psi = -\frac{h}{i}\frac{\partial\psi}{\partial t}. \tag{7}$$

From (4) Kemmer obtains the Hamiltonian

$$H = (hc/i)\partial_k i(\beta_4\beta_k - \beta_k\beta_4) + \mu c^2\beta_4 \tag{8}$$

together with the supplementary condition

$$\partial_k\beta_k\beta_4{}^2\psi + (1-\beta_4{}^2)K\psi = 0. \tag{9}$$

For plane wave solutions $u(p, t)$

$$H^3u = E^2Hu,$$

so that H has the eigenvalues 0 and $\pm E$, but there are no solutions of $Hu_0 = 0$ compatible with the condition (9). The six solutions of $Hu_+ = Eu_+$ and $Hu_- = -Eu_-$ are normalized to unit charge by setting $u_+{}^*\beta_4u_+ = 1$ and $u_-{}^*\beta_4u_- = -1$. To these are adjoined, for mathematical convenience in spur methods, four solutions u_0 of $Hu_0 = 0$ in order to complete the set of ten vectors u to form a matrix which is, apart from a normalization constant, unitary. Kemmer shows that $E = \mu c^2u^*u$ which determines the normalization in agreement with unit charge.

The second quantization is carried through in the usual manner by expanding u in terms of the six solutions for positive and negative charge.

The Hamiltonian (8) is not suitable for the treatment of the interaction with the electromagnetic field since the energy matrix β_4H is not in Hermitian form and this leads to complications in the treatment of the zero states due to the perturbation of the supplementary condition. A satisfactory Hamiltonian can be obtained by using the wave equation (4) and the supplementary condition (9) explicitly in the expression (6) for the energy. There results[6]

$$H = (1/\mu)\int \psi^*\beta_4{}^2[\mu^2c^2 - \hbar^2(\partial_k\beta_k)(\partial_l\beta_l)]\beta_4{}^2\psi d\tau. \tag{10}$$

The interaction with the electromagnetic field is introduced by the usual substitution $\partial_\mu \rightarrow \partial_\mu{}^- = \partial_\mu - (ie/hc)A_\mu$, $A_4 = iV$. The perturbation due to the scalar potential is then

$$H_1 = \int \psi^*\beta_4V\psi d\tau, \tag{11}$$

that linear in the vector potential is

$$H_2 = (ieh/\mu c)\int \psi^*\beta_4{}^2[(A_k\beta_k)(\partial_l\beta_l) + (\partial_k\beta_k)(A_l\beta_l)]\beta_4{}^2\psi d\tau \tag{12}$$

and the term quadratic in A is

$$H_3 = (e^2/\mu c^2)\int \psi^*\beta_4{}^2(A_k\beta_k)(A_l\beta_l)\beta_4{}^2\psi d\tau. \tag{13}$$

In momentum space

$$\begin{aligned} H_1 = \int d\mathbf{k}\int d\mathbf{l}\int d\mathbf{x}\, \exp[(i/h)(\mathbf{k}-\mathbf{l})\cdot\mathbf{x}]V(x)\sum_{i,j=1}^{3}[&a_j{}^*(l)a_i(k)\exp[(i/h)(E_l - E_k)t]u_+{}^{*j}(l)\beta_4u_+{}^i(k) \\ &+ a_j{}^*(l)b_i{}^*(k)\exp[(i/h)(E_l+E_k)t]u_+{}^{*j}(l)\beta_4u_-{}^i(k) \\ &+ b_j(l)a_i(k)\exp[-(i/h)(E_l+E_k)t]u_-{}^{*j}(l)\beta_4u_+{}^i(k) \\ &+ b_j(l)b_i{}^*(k)\exp[-(i/h)(E_l+E_k)t]u_-{}^{*j}(l)\beta_4u_-{}^i(k)]. \end{aligned} \tag{14}$$

The summation over the spin indices is suppressed by writing u^* as a one-row and u as a one-column matrix. a^* creates, while a destroys, a positive mesotron, and b^* creates, while b destroys, a negative mesotron.

[6] We are grateful to Dr. Kemmer for informing us of this result by private communication.

Matrix elements of H_2 for absorption of a quantum of momentum $\mathbf{n}=\mathbf{l}-\mathbf{k}$ and polarization $\mathbf{e}$ are

$$H_2=-\frac{e}{\mu c^2}\left(\frac{2\pi\hbar^2c^2}{n}\right)^{\frac{1}{2}}\int d\mathbf{k}\int d\mathbf{l}\sum_{i,j=1}^{3}[a_j^*(l)a_i(k)\exp[(i/h)(E_l-E_k)t]u_+^{*j}(l)\beta_4^2(k\beta_e\beta_k+l\beta_l\beta_e)\beta_4^2u_-^i(k)$$
$$+a_j^*(l)b_i^*(k)\exp[(i/h)(E_l+E_k)t]u_+^{*j}(l)\beta_4^2(k\beta_e\beta_k+l\beta_l\beta_e)\beta_4^2u_-^i(k)$$
$$+b_j(l)a_i(k)\exp[-(i/h)(E_l+E_k)t]u_-^{*j}(l)\beta_4^2(k\beta_e\beta_k+l\beta_l\beta_e)\beta_4^2u_+^i(k)$$
$$+b_j(l)b_i^*(k)\exp[-(i/h)(E_l-E_k)t]u_-^{*j}(l)\beta_4^2(k\beta_e\beta_k+l\beta_l\beta_e)\beta_4^2u_-^i(k)], \quad (15)$$

where $\beta_p=p_l\beta_l/p$. The matrix elements of H_2 for emission of a quantum are obtained from the above by setting $\mathbf{n}=\mathbf{k}-\mathbf{l}$.

H_3 has matrix elements only for two quanta processes. They are similar to those given above with a different normalization and with $\beta_4^2(\beta_{e_1}\beta_{e_2}+\beta_{e_2}\beta_{e_1})\beta_4^2$ as the matrix operator where $\mathbf{e}_1$ and $\mathbf{e}_2$ are unit vectors in the directions of polarization of the two quanta. In double absorption $\mathbf{n}_1+\mathbf{n}_2=\mathbf{l}-\mathbf{k}$, for double emission $\mathbf{n}_1+\mathbf{n}_2=\mathbf{k}-\mathbf{l}$, for absorption of 1 and emission of 2 $\mathbf{n}_1-\mathbf{n}_2=\mathbf{l}-\mathbf{k}$, and for emission of 1 and absorption of 2 $\mathbf{n}_1-\mathbf{n}_2=\mathbf{k}-\mathbf{l}$. H_3 is not involved in either bremsstrahlung or pair production since these appear as one quantum process in the nuclear rest system.

Let us now refer, in particular, to the creation of a positive mesotron $\mathbf{k}$ and a negative mesotron $\mathbf{l}$ (its actual momentum is $-\mathbf{l}$) by a γ-ray of momentum $\mathbf{n}$ near a nucleus of charge Ze. The conservation of energy gives

$$n=E_k+E_l=(\mu^2c^4+k^2)^{\frac{1}{2}}+(\mu^2c^4+l^2)^{\frac{1}{2}}$$

for time proportional transitions. The transition takes place by means of H_1 and H_2 through an intermediate state; H_2 conserving momentum and H_1 transferring an amount of momentum $\mathbf{q}=\mathbf{n}+\mathbf{l}-\mathbf{k}$ to the nucleus. Indicating the quantum, positive mesotron and negative mesotron in order, we have the following sets of state A: $\mathbf{n}$, $-$, $-$; intermediate state I: $-$, $\mathbf{k}$, $\mathbf{k}-\mathbf{n}$; II: $\mathbf{n}$, $\mathbf{k}-\mathbf{n}$, $\mathbf{l}$; III: $-$, $\mathbf{n}+\mathbf{l}$, $\mathbf{l}$: IV: $\mathbf{n}$, $\mathbf{k}$, $\mathbf{n}+\mathbf{l}$; and finally, F: $-$, $\mathbf{k}$, $\mathbf{l}$. The matrix element $H(FA)$ between the initial and the final states is then given by

$$H(FA)=\sum\left[\frac{H_1(F\mathrm{I})H_2(\mathrm{I}A)}{E_A-E_{\mathrm{I}}}+\frac{H_2(F\mathrm{II})H_1(\mathrm{II}A)}{E_A-E_{\mathrm{II}}}+\frac{H_1(F\mathrm{III})H_2(\mathrm{III}A)}{E_A-E_{\mathrm{III}}}+\frac{H_2(F\mathrm{IV})H_1(\mathrm{IV}A)}{E_A-E_{\mathrm{IV}}}\right],$$

where the summation is to be taken over the polarizations of the intermediate states. On inserting the explicit values on the right, we can make some reduction by combining terms and using the relations

$$\sum_{i=1}^{3}[u_-^i(p)u_-^{*i}(p)-u_+^i(p)u_+^{*i}(p)]=-\frac{H_p}{E_p}\sum_{m=1}^{10}u^m(p)u^{*m}(p)=-\frac{H_p}{\mu c^2}$$

and

$$\sum_{i=1}^{3}[u_+^i(p)u_+^{*i}(p)+u_-^i(p)u_-^{*i}(p)]=\frac{H_p^2}{E_p^2}\sum_{m=1}^{10}u^m(p)u^{*m}(p)=\frac{H_p^2}{\mu c^2E_p},$$

where m goes over $+$, 0, $-$ states and

$$H_p=\mu c^2\beta_4+ip(\beta_4\beta_p-\beta_p\beta_4).$$

The final result is

$$H(FA)=-\frac{e}{(\mu c^2)^2}\left(\frac{2\pi\hbar^2c^2}{n}\right)^{\frac{1}{2}}V(q)\left\{\frac{u_+^{*i}(k)\beta_4^2(a\beta_e\beta_a+k\beta_k\beta_e)\beta_4^2H_a(H_a-E_l)\beta_4u_-^i(l)}{E_l^2-E_a^2}\right.$$
$$\left.+\frac{u_+^{*j}(k)\beta_4H_b(H_b+E_k)\beta_4^2(l\beta_e\beta_l+b\beta_b\beta_e)\beta_4^2u_-^i(l)}{E_k^2-E_b^2}\right\}, \quad (16)$$

where $V(q)$ is the Fourier component of V and $\mathbf{a}=\mathbf{k}-\mathbf{n}$, $\mathbf{b}=\mathbf{n}+\mathbf{l}$. The differential cross section for pair production is

$$d\varphi=\frac{\pi}{\hbar c}\frac{kE_k lE_l d\Omega_k d\Omega_l dE_k}{(2\pi\hbar c)^6}\sum_e\sum_{i,j=1}^{3}|H(FA)|^2.$$

To perform the summations over the spins of positive and negative mesotron, we introduce the annihilation operators $\lambda_+(p)$ and $\lambda_-(p)$ such that $\lambda_+u_+=u_+$, $\lambda_+u_0=0$, $\lambda_+u_-=0$ and $\lambda_-u_+=0$, $\lambda_-u_0=0$, $\lambda_-u_-=u_-$. They are given by

$$\lambda_+(p)=(H_p/2E_p^2)(H_p+E_p),\quad \lambda_-(p)=(H_p/2E_p^2)(H_p-E_p).$$

This gives

$$d\varphi=\frac{e^2}{\hbar c}\frac{(V(q))^2}{8n(\mu c^2)^6}\frac{kld\Omega_k d\Omega_l dE_k}{(2\pi\hbar c)^4}\sum_e\text{Spur}\left\{\frac{P}{(E_l^2-E_a^2)^2}+\frac{2Q}{(E_l^2-E_a^2)(E_k^2-E_b^2)}+\frac{R}{(E_k^2-E_b^2)^2}\right\},$$

where

$$P=\beta_4^2(a\beta_e\beta_a+k\beta_k\beta_e)\beta_4^2H_a(H_a-E_l)\beta_4H_l(H_l-E_l)\beta_4H_a(H_a-E_l)\beta_4^2(k\beta_e\beta_k+a\beta_a\beta_e)\beta_4^2H_k(H_k+E_k),$$

$$Q=\beta_4^2(a\beta_e\beta_a+k\beta_k\beta_e)\beta_4^2H_a(H_a-E_l)\beta_4H_l(H_l-E_l)\beta_4^2(b\beta_e\beta_b+l\beta_l\beta_e)\beta_4^2H_b(H_b+E_k)\beta_4H_k(H_k+E_k),$$

$$R=\beta_4H_b(H_b+E_k)\beta_4^2(l\beta_e\beta_l+b\beta_b\beta_e)\beta_4^2H_l(H_l-E_l)\beta_4^2(b\beta_e\beta_b+l\beta_l\beta_e)\beta_4^2H_b(H_b+E_k)\beta_4H_k(H_k+E_k).$$

In evaluating these spurs, it is convenient to generalize the commutation laws for arbitrary vectors so that

$$\beta_p\beta_q\beta_r+\beta_r\beta_q\beta_p=(\mathbf{p}\cdot\mathbf{q}/pq)\beta_r+(\mathbf{r}\cdot\mathbf{q}/rq)\beta_p,$$

where $\mathbf{p}$, $\mathbf{q}$, $\mathbf{r}$ are space vectors. In particular

$$\beta_p\beta_q\beta_p=(\mathbf{p}\cdot\mathbf{q}/pq)\beta_p,$$

$$\beta_p^2\beta_q+\beta_q\beta_p^2=(\mathbf{p}\cdot\mathbf{q}/pq)\beta_p+\beta_q.$$

Useful relations involving β_4 are:

$$\beta_4\beta_p\beta_4=0,\quad \beta_p\beta_4\beta_p=0,$$

$$\beta_p\beta_4^2+\beta_4^2\beta_p=\beta_p,\quad \beta_4\beta_p^2+\beta_p^2\beta_4=\beta_4.$$

Thus

$$\beta_4H_p\beta_4=\mu c^2\beta_4,$$

$$\beta_4H_p^2\beta_4=\mu c^2\beta_4^2+p^2\beta_4^2\beta_p^2\beta_4^2.$$

Because of the complexity of the differential cross section, we confine ourselves in this paper to energies such that n, k, $l\gg\mu c^2$. The first nonvanishing terms in P, Q, R are proportional to $(\mu c^2)^2$ and consist of two types:

$$\beta_e\beta_a\beta_4\beta_l^2\beta_4\beta_a\beta_e\beta_4\beta_k^2\beta_4$$

and (18)

$$\beta_k\beta_e\beta_4\beta_a^2\beta_4\beta_l^2\beta_4\beta_a^2\beta_4\beta_e\beta_k\beta_4^2.$$

No simple general methods of evaluating spurs of such expressions have been found, the introduction of Kemmer's η matrices often being complicated and difficult to handle without dealing with the separate components, since these η are not vectors. Kemmer's treatment shows immediately that any product containing an odd number of β_4 or β_p will have a vanishing spur.

It was found useful to introduce a new pseudovector matrix $\boldsymbol{\gamma}$, with components $\gamma_1=i\beta_2\beta_4\beta_3$, $\gamma_2=i\beta_3\beta_4\beta_1$, $\gamma_3=i\beta_1\beta_4\beta_2$ which are Hermitian and obey the same commutation rules as the β_k. The principal advantage of this substitution lies in the reduction of the number of matrices to be considered. In addition, the γ_i are actually simpler in form than the β_i which leads to further simplifying properties such as $\gamma_p\beta_q\gamma_r=0$, and $\gamma_i\gamma_j\gamma_k=0$ for j perpendicular to i and k. Further, we can write

$$i\beta_p\beta_4\beta_q=[\mathbf{p}\times\mathbf{q}]_k\gamma_k/pq=r\gamma_r/pq,$$

where $\mathbf{r}=\mathbf{p}\times\mathbf{q}$ and $\gamma_r=r_k\gamma_k/r$.

The product of an odd number of γ has a vanishing spur since it contains an odd number of β_4. It is easily shown that Spur $\gamma_i^2=2$, and Spur $\gamma_p\gamma_q=2\mathbf{p}\cdot\mathbf{q}/pq$. To evaluate Spur $\gamma_p\gamma_q\gamma_r\gamma_s$ which is a general form of the spur of the first of the expressions (18) which we wish to evaluate, we proceed as follows:

$$\text{Spur }\gamma_p\gamma_q\gamma_r\gamma_s=\text{Spur }\gamma_s\gamma_p\gamma_q\gamma_r=\text{Spur }\gamma_r\gamma_q\gamma_p\gamma_s,$$

since it is real, then

$$\text{Spur }\gamma_p\gamma_q\gamma_r\gamma_s=\tfrac{1}{2}\text{ Spur }(\gamma_p\gamma_q\gamma_r\gamma_s+\gamma_r\gamma_q\gamma_p\gamma_s)$$

$$=\tfrac{1}{2}\text{ Spur }[(\mathbf{p}\cdot\mathbf{q}/pq)\gamma_r+(\mathbf{r}\cdot\mathbf{q}/rq)\gamma_p]\gamma_s$$

by using the commutation rules, and finally

$$\text{Spur } \gamma_p\gamma_q\gamma_r\gamma_s=\frac{(\mathbf{p}\cdot\mathbf{q})(\mathbf{r}\cdot\mathbf{s})+(\mathbf{p}\cdot\mathbf{s})(\mathbf{r}\cdot\mathbf{q})}{pqrs}.$$

A useful commutation rule connecting the β and γ is

$$\gamma_p\beta_q\beta_r+\beta_r\beta_q\gamma_p=2((\mathbf{q}\cdot\mathbf{r})/qr)\gamma_p-((\mathbf{p}\cdot\mathbf{r})/pr)\gamma_q.$$

This gives immediately

$$\begin{aligned}\text{Spur } \gamma_p\gamma_q\beta_r\beta_s&=-\text{Spur } \gamma_p\beta_s\beta_r\gamma_q+2(\mathbf{r}\cdot\mathbf{s}/rs)\text{ Spur }\gamma_p\gamma_q\\&\quad-(\mathbf{q}\cdot\mathbf{s}/qs)\text{ Spur }\gamma_p\gamma_r\\&=\frac{2(\mathbf{p}\cdot\mathbf{q})(\mathbf{r}\cdot\mathbf{s})-(\mathbf{p}\cdot\mathbf{r})(\mathbf{q}\cdot\mathbf{s})}{pqrs}.\end{aligned}$$

The spur of the second of the expressions (18) can now be treated by noting that

$$\beta_4\beta_a{}^2\beta_4\beta_l{}^2\beta_4\beta_a{}^2\beta_4=\beta_l{}^2\beta_4\beta_a{}^2\beta_4,$$

since $\beta_a{}^2\beta_l{}^2=\beta_l{}^2\beta_a{}^2$. The resulting expression

$$\beta_4\beta_k\beta_e\beta_l{}^2\beta_4\beta_a{}^2\beta_4\beta_e\beta_k\beta_4$$

can be written

$$\begin{aligned}&-\beta_l\beta_k\beta_4\beta_l{}^2\beta_4\beta_a{}^2\beta_4\beta_l\beta_k\beta_4\\&\qquad+(\mathbf{e}\cdot\mathbf{k}/k)\beta_4\beta_l{}^2\beta_4\beta_a{}^2\beta_4\beta_e\beta_k\beta_4.\end{aligned}$$

The first is of the general form $\gamma_p\gamma_q\gamma_r\gamma_s$ and the second of the form $\gamma_p\gamma_q\beta_r\beta_s$; the spurs of both these expressions have been evaluated. We thus obtain another general formula

$$\text{Spur } \beta_p\beta_q\gamma_r\gamma_s\gamma_t\gamma_u=\frac{(\mathbf{p}\cdot\mathbf{q})(\mathbf{r}\cdot\mathbf{s})(\mathbf{t}\cdot\mathbf{u})+(\mathbf{p}\cdot\mathbf{q})(\mathbf{r}\cdot\mathbf{u})(\mathbf{s}\cdot\mathbf{t})-(\mathbf{p}\cdot\mathbf{r})(\mathbf{q}\cdot\mathbf{u})(\mathbf{s}\cdot\mathbf{t})}{pqrstu}.$$

In concluding this section, we give the spurs of a few simple products of β which enter into problems such as the scattering of mesotrons in a Coulomb field or the scattering of light by mesotrons. They are evaluated by methods similar to those given above.

$$\beta_p\beta_q\beta_4{}^2=-\beta_4\beta_q\beta_p\beta_4+(\mathbf{p}\cdot\mathbf{q}/pq)\beta_4{}^2.$$

Thus

$$\text{Spur } \beta_p\beta_q\beta_4{}^2=\tfrac{1}{2}(\mathbf{p}\cdot\mathbf{q}/pq)\text{ Spur }\beta_4{}^2=3\mathbf{p}\cdot\mathbf{q}/pq.$$

Also

$$\beta_p\beta_q\beta_4{}^2\beta_r\beta_s=-\beta_p\beta_q\beta_4\beta_s\beta_r\beta_4+(\mathbf{r}\cdot\mathbf{s})/rs)\beta_p\beta_q\beta_4{}^2,$$

$$\begin{aligned}\text{Spur } \beta_p\beta_q\beta_4{}^2\beta_r\beta_s&=\frac{2(\mathbf{q}\times\mathbf{s})\cdot(\mathbf{r}\times\mathbf{p})}{pqrs}+\frac{3(\mathbf{p}\cdot\mathbf{q})(\mathbf{r}\cdot\mathbf{s})}{pqrs}\\&=\frac{2(\mathbf{q}\cdot\mathbf{r})(\mathbf{p}\cdot\mathbf{s})+(\mathbf{p}\cdot\mathbf{q})(\mathbf{r}\cdot\mathbf{s})}{pqrs}.\end{aligned}$$

III

In this section, we indicate the manner in which the integration of the differential cross section was carried out. After averaging over the polarizations of the incident γ-ray, the cross section appears in terms of k, θ_+, φ_+ of the positive mesotron and l, θ_-, φ_- of the negative mesotron, referred to the direction of the γ-ray as the polar axis. In place of φ_+ and φ_-, the azimuthal angles, we introduce $(\varphi_+-\varphi_-)$ and $\frac{1}{2}(\varphi_++\varphi_-)$: Only the former has physical significance, integration over the latter yields a factor 2π.

We then introduce $x=1-\cos\theta_+$, $y=1+\cos\theta_-$, $z=\cos(\varphi_+-\varphi_-)$, so that $0\leqslant x\leqslant 2$, $0\leqslant y\leqslant 2$ and we can limit z by $-1\leqslant z\leqslant 1$ by introducing a factor 2. The cross section can then be written

$$d\varphi=\pi\alpha\frac{kldkdxdydz}{2n(\mu c^2)^4(1-z^2)^{\frac{1}{2}}}\frac{(V(q))^2}{(2\pi hc)^4}\{A+bzB+b^2z^2C+b^3z^3D\},\tag{19}$$

where

$$\begin{aligned}A&=\tfrac{1}{4}\{[(6k^4+8k^3l+22k^2l^2)x-(3k^4+4k^3l+11k^2l^2)x^2]\\&\quad+[(22k^2l^2+8kl^3+6l^4)+(4k^3l-32k^2l^2+4kl^3)x+(-2k^3l+14k^2l^2)]y\\&\quad+[-(11k^2l^2+4kl^3+3l^4)+(14k^2l^2-2kl^3)x-6k^2l^2x^2]y^2\},\\B&=-\tfrac{1}{2}\{[(3k^2-4kl+3l^2)+(-k^2+5kl)x]+[(5kl-l^2)-4klx]y\},\\C&=-\tfrac{1}{2}\{2/y+2/x-1\},\\D&=-1/klxy,\end{aligned}$$

$$\begin{aligned}q^2&=2(a-bz),\\a&=k^2x+l^2y+klxy,\\b&=kl\sin\theta_+\sin\theta_-.\end{aligned}$$

For pure Coulomb field, $V(q)=4\pi Ze^2h^2c^2/q^2$ whereas for a field $(Ze/r)(1-e^{-r/d})$

$$V(q)=\frac{4\pi Ze^2h^2c^2}{q^2}\,\frac{(hc/d)}{q^2+(hc/d)^2}.$$

The first integral over z is simple. The integrals over y and x can be shortened by using the symmetry in y and x, but even then they are tedious though elementary. There results for a Coulomb field

$$d\sigma=\frac{\alpha Z^2e^4}{2(\mu c^2)^4}\,\frac{kldk}{n}\left\{-\frac{1}{3}+\frac{9k^2+9kl+8l^2}{12kn}\ln\frac{n^2}{l^2}+\frac{8k^2+9kl+9l^2}{12ln}\ln\frac{n^2}{k^2}\right\} \quad (20)$$

and for the cut-off field

$$d\sigma=\frac{\pi\alpha Z^2e^4hcdk}{48(\mu c^2)^4dn^2}\{7k^2+12kl+7l^2\}. \quad (21)$$

The differential cross section for bremsstrahlung, where a mesotron of momentum **k** is scattered in the electric field of a nucleus, emitting a quantum **n** and leaving the mesotron with momentum **l**, can be obtained from that for pair creation by redefinition of the variables x, y, z, changing the sign of l in the square of the matrix element, and introducing different expressions for the density of states and average over the initial states. Thus the angle integrals are unchanged and the cross sections for bremsstrahlung are simply obtained from (20) and (21) by changing the sign of l in the brackets and changing the density factors outside the brackets. In the Coulomb field,

$$d\sigma=\frac{\alpha Z^2e^4nldn}{3(\mu c^2)^4k}\left\{-\frac{1}{3}+\frac{9k^2-9kl+8l^2}{12kn}\ln\frac{n^2}{l^2}-\frac{8k^2-9kl+9l^2}{12ln}\ln\frac{n^2}{k^2}\right\} \quad (22)$$

and for the cut-off field

$$d\sigma=\frac{\pi\alpha Z^2e^4hcdn}{72(\mu c^2)^4k^2d}\{7k^2-12kl+7l^2\}, \quad (23)$$

where now $n=k-l$.

These integrate to the cross sections given in Section I with E equal to n for pair creation and to k for bremsstrahlung.

IV

We now apply the method of virtual quanta to obtain approximately the radiation emitted by a very fast mesotron in the neighborhood of a nucleus. The method can also be applied to the calculation of pair production, but since only the bremsstrahlung is directly connected with cosmic-ray bursts, we will restrict ourselves to just this effect.

Let the mesotron move with velocity v and energy E past a nucleus of charge Ze. Let us consider the process in the Lorentz frame where the mesotron is initially at rest and is scattered by the nucleus which, in this frame, is passing by the mesotron with velocity v. For $v\sim c$, the Coulomb field of the nucleus is greatly contracted longitudinally so that, at not too small distances, the field is largely transverse and can, by Fourier analysis, be represented by light quanta traveling parallel to the direction of motion of the nucleus: The number N_{k_0} of these quanta per unit area of energy k_0 per unit energy at a distance r from the path is approximately

$$\begin{aligned} N_{k_0}&=\alpha Z^2/\pi^2r^2k_0 \quad \text{for } k_0<Eh/r\mu c,\\ N_{k_0}&=0 \quad \text{for } k_0>Eh/r\mu c. \end{aligned} \quad (24)$$

The lower limit of r is taken to be approximately the size of the larger of the two interacting particles; here it is the nucleus with $r_{\min}\sim d$. The cross section for the scattering of a photon of energy k_0 to one of energy k through an angle θ by a mesotron initially at rest has been calculated by Booth and Wilson[3] and is

$$\sigma(k_0,k,\theta)=\tfrac{1}{2}(e^2/\mu c^2)^2d\Omega(k^2/k_0^2)\{(1+\cos^2\theta)+(1/48(\mu c^2)^2)[kk_0(28-64\cos\theta+12\cos^2\theta)+(k^2+k_0^2)(29-16\cos\theta+\cos^2\theta)]\}. \quad (25)$$

From the scattered quanta we must pick out such k and θ that correspond to a definite energy ϵE, $0\leqslant\epsilon\leqslant 1-(\mu c^2/E)$, in the nuclear rest system. These are determined for $v\sim c$ by $k\sim k_0(1-\epsilon)$,

$$1-\cos\theta=\epsilon\mu c^2/[k_0(1-\epsilon)],$$
$$d\Omega=2\pi\mu c^2d\epsilon/[k_0(1-\epsilon)^2],$$

$k_0 \geqslant \epsilon\mu c^2/[2(1-\epsilon)]$. The cross section for bremsstrahlung $\sigma(\epsilon, E)$ is then given by

$$\sigma(\epsilon, E)d\epsilon = \int_{\epsilon\mu c^2/[2(1-\epsilon)]}^{k_{0\,\max}} dk_0 \int_{fd}^{r_{\max}} 2\pi r dr \times N_{k_0}\sigma(k_0, k(\epsilon, k_0), \theta(\epsilon, k_0)).$$

The uncertainties in both the lower and upper limits of the r integral are here represented by f which is of order unity. If k_0 is written in units of μc^2 and r in units of $\hbar/\mu c$, we have

$$\sigma(\epsilon, E)d\epsilon = \alpha(e^2/\mu c^2)^2 Z^2 d\epsilon \int_{\epsilon/[2(1-\epsilon)]}^{k_{0\,\max}} dk_0 \int_{(5/6)fZ^{\frac{1}{3}}}^{E/\mu c^2 k_0} \times \frac{dr}{r}\left\{\frac{(2-2\epsilon+7\epsilon^2)}{12} + \frac{\epsilon(34-34\epsilon+7\epsilon^2)}{12(1-\epsilon)k_0} + \frac{96(1-\epsilon)^2+\epsilon^2(14-14\epsilon+\epsilon^2)}{24(1-\epsilon)^2 k_0^2} - \frac{4\epsilon}{(1-\epsilon)k_0^3} + \frac{2\epsilon^2}{(1-\epsilon)^2 k_0^4}\right\}. \quad (26)$$

Interchanging the order of integrations and integrating the above, we see the dependence of the various terms on the impact parameter r. These dependences are $1/r$, $\ln^2 r$, and $\ln r$ for the first, second and last three terms, respectively.

In the cut-off electromagnetic field of the nucleus, the neglect of the transverse momentum transfers (and the longitudinal components of the nuclear field) with respect to the longitudinal momentum transfers is justified in the zero momentum system where the mesotron energy is $(\frac{1}{2}\mu c^2 E)^{\frac{1}{2}}$ or in the mesotron rest system, but not in the nuclear rest system. However, the approximation is critical since the first term of (26) is proportional to the highest frequency available and inversely proportional to the smallest impact parameter, so that the ratio of the uncertainties in the upper and lower limits of r as written in (26) enters as a multiplicative constant in the first term, which at sufficiently high energies is dominant. In the other terms, it is the logarithm of the ratio of the upper and lower impact parameters which is an unessential approximation always present in calculations by this method. There is a difference in nature between the two approximations in the limits of the impact parameter r. The upper limit is approximate only as a mathematical convenience in the representation of N_{k_0}. On the other hand, the lower limit d of r is, to a certain extent, conceptually indeterminate since it supplies a cut-off in the space integral which is independent of the shape of the electromagnetic field near d; whereas the actual process depends on the Fourier analysis of this field. These two inaccuracies in the method of virtual quanta could, in principle, be removed by treating initially a suitable model for the field of a moving nucleus which would become constant for $r<d$, and by eliminating the mathematical approximations. This would, however, essentially reduce the calculation to the one we have performed in the previous section, though in a different Lorentz system.

It is for these reasons that the first term in the cross section was calculated by the better approximations of Section III. The factor f which expresses the ratio of uncertainties in the upper and lower limits of r was then taken to be $6/\pi$ to give agreement with the result of Section III. This does not, of course, guarantee that no further uncertainty exists in the logarithmic terms, but since it will be unimportant, it is convenient to omit it. The integration over the impact parameter in (26) then yields the factor

$$\ln \frac{\pi E}{5\mu c^2 Z^{\frac{1}{3}} k_0}.$$

The upper limit of the frequency integral will in general be given by $k_{0\,\max} = \pi E/5\mu c^2 Z^{\frac{1}{3}}$ where the logarithm vanishes. This gives a cross section

$$\sigma = \alpha\left(\frac{e^2}{\mu c^2}\right)^2 Z^2 d\epsilon\left\{\frac{\pi E}{5\mu c^2 Z^{\frac{1}{3}}}\left(\frac{2-2\epsilon+7\epsilon^2}{12}\right) + \frac{\epsilon(34-34\epsilon+7\epsilon^2)}{24(1-\epsilon)}\ln^2\frac{2\pi E(1-\epsilon)}{5\mu c^2 Z^{\frac{1}{3}}\epsilon} + \left[\frac{16(1-\epsilon)}{3\epsilon} + \frac{13\epsilon}{12} - \frac{5\epsilon^3}{24(1-\epsilon)}\right]\ln\frac{2\pi E(1-\epsilon)}{5\mu c^2 Z^{\frac{1}{3}}\epsilon} - \frac{\epsilon(10-10\epsilon+3\epsilon^2)}{8(1-\epsilon)} - \frac{52}{9}\frac{(1-\epsilon)}{\epsilon}\right\}. \quad (27)$$

For very high energies the first two terms which depend on high frequencies and large couplings cannot be right. But neglecting possible reduction of the cross section by nonlinearities in

the theory,[7] a lower limit to σ can be assigned by cutting off the frequency integral at $k_{0\,\max}=A$, some constant less than $2hc/e^2$. There results

$$\sigma=\alpha\left(\frac{e^2}{\mu c^2}\right)^2 Z^2 d\epsilon\left\{\left(A+A\ln\frac{\pi E}{5A\mu c^2 Z^{\frac{1}{3}}}\right)\times\frac{(2-2\epsilon+7\epsilon^2)}{12}+\frac{\epsilon(34-34\epsilon+7\epsilon^2)}{24(1-\epsilon)}\times\left[\ln^2\frac{2\pi E(1-\epsilon)}{5\mu c^2 Z^{\frac{1}{3}}\epsilon}-\ln^2\frac{\pi E}{5A\mu c^2 Z^{\frac{1}{3}}}\right]\right.$$
$$\left.+\left[\frac{16(1-\epsilon)}{3\epsilon}+\frac{13\epsilon}{12}-\frac{5\epsilon^3}{24(1-\epsilon)}\right]\ln\frac{2\pi E(1-\epsilon)}{5\mu c^2 Z^{\frac{1}{3}}\epsilon}-\frac{\epsilon(10-10\epsilon+3\epsilon^2)}{8(1-\epsilon)}-\frac{52}{9}\frac{(1-\epsilon)}{\epsilon}\right\} \quad (28)$$

for $E>(5/\pi)\mu c^2 Z^{\frac{1}{3}}A$. For $E<(5/\pi)\mu c^2 Z^{\frac{1}{3}}A$, we get (27) above, as with no cut-off.

A consideration of cosmic-ray bursts based on these and other calculations is given in another paper.

In conclusion, the authors wish to express their appreciation to Professor J. R. Oppenheimer for continued advice and encouragement.

[7] A rigorous treatment might show that the presence of high Fourier components diminishes the contribution from the low frequencies. We are here ignoring this possibility. See J. R. Oppenheimer, Phys. Rev. **47**, 44 (1935).

MARCH 1, 1941 PHYSICAL REVIEW VOLUME 59

Burst Production by Mesotrons

R. F. CHRISTY AND S. KUSAKA
Department of Physics, University of California, Berkeley, California

(Received December 31, 1940)

Assuming that, under great absorbing thicknesses, cosmic-ray bursts are cascade showers from high energy soft secondaries produced in the shielding matter by mesotron-electron collisions and by mesotron bremsstrahlung, we have calculated the frequency of burst production as a function of burst size. For the mesotron of spin 1 and moment $eh/2\mu c$, we have used the previously calculated knock-on formulae, supplemented by our own calculations of the bremsstrahlung; for the latter, the cross section has terms, significant for our work, in E, $\ln^2 E$, and $\ln E$. Up to energies close to 10^{11} ev, only slight modifications are introduced by omitting altogether those processes which cannot be treated by the Born approximation, and the *minimum* cross sections we used differ little from those given directly by the Born approximation. Using these cross sections, the cascade theory of showers, and a modified form of the Furry model to take into account the fluctuations, the frequency of burst production was calculated. The sea-level data of Schein and Gill give for the number of bursts of size greater than S, $N_S \backsim S^{-\gamma}$, with $\gamma=1.8$. Our calculations give for spin 1, $\gamma\sim1.5$ and numerically too many by a factor of 20. Similar calculations for the mesotron of spin 0 give $\gamma\sim1.8$ and the same in number as the observations within an uncertainty of about a factor 1.5. For spin $\frac{1}{2}$ and moment $eh/2\mu c$, the bursts are approximately twice as numerous as for spin 0. This evidence thus favors spin 0, or possibly spin $\frac{1}{2}$, but tends to exclude spin 1.

I

COSMIC-RAY bursts, insofar as they involve high energies of order 10^9–10^{11} ev, provide a feasible test of relativistic mesotron theory. Experiments have shown that the ionization in bursts does not show the characteristic high initial recombination of that due to slow heavy particles. Furthermore, bursts frequently appear simultaneously in ionization chambers one of which is above the other, and sometimes are larger in the lower chamber.[1] This appears to be conclusive evidence that at least the majority of bursts are not due to several slow heavy particles resulting from a nuclear explosion or evaporation but, rather, are due to many fast electrons resulting from the cascade multiplication of a high energy soft ray in the material above the chamber. Now the transition curves of Nie, and Steinke and Schmidt[2] for bursts in lead show a maximum at ~4 cm but no apparent decrease for thicknesses greater than 10 cm; bursts have also been observed at great depths underground.

[1] H. Nie, Zeits. f. Physik **99**, 776 (1936); H. Euler, Zeits. f. Physik **116**, 73 (1940).

[2] H. Nie, Zeits. f. Physik **99**, 453 (1936); E. C. Steinke and H. Schmidt, Zeits. f. Physik **115**, 740 (1940).

Since at these great thicknesses of absorber, and at great depths, the primary soft radiation is entirely absorbed out, the energetic soft rays which initiate bursts must be secondary to the mesotronic or penetrating component. Experiments on the size and frequency of large bursts (>100 particles) under thick absorbers can thus measure the cross sections for the production of energetic soft secondaries by mesotrons. Since these cross sections at high energies $\sim 10^{10}$ ev are markedly spin dependent, we see that accurate burst experiments can be used to decide between the various possible relativistic theories of the mesotron.

For these purposes the experiment must have a good (calculable) geometry, the absorber must be sufficiently thick to absorb out all primary soft radiation, and it must have statistically reliable data involving the energy range 10^{10}–10^{11} ev where spin effects become really prominent. In lead this means bursts of size 100 to 1000 particles. An examination of the experimental material on bursts shows that the sea-level data of Schein and Gill[3] alone satisfy these requirements.

In limiting the data to those experiments in which the cascade soft radiation from the air is ineffective in producing large bursts, we seriously restrict the useful experiments. This seems necessary since that part of the initial soft radiation which can be effective in making large bursts must arise from the degradation of primary rays with energy of order 10^{15}–10^{18} ev. Now the absorption coefficient in the cascade theory is critically dependent on the exact shape of the energy distribution curve: In this effective energy range both the number and energy distribution of the primaries are practically unknown. Thus it appears impossible at present to calculate to better than an order of magnitude the number of large bursts due to this source, and, in consequence, we must restrict ourselves to those experiments where it is clear that only mesotron secondaries are responsible for the bursts. At sea level, the necessary shielding matter must be the equivalent in shower units of 11 cm of lead; at high altitudes the absorber should be increased by the equivalent of 1.5 or 2 cm of lead per 1000 m elevation because of the rapid increase in the soft component with altitude.

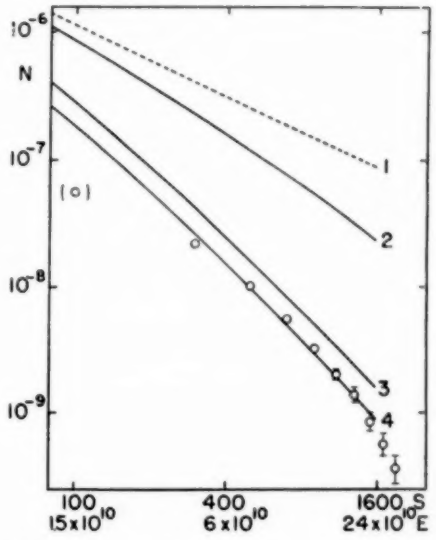

FIG. 1. Plot of burst frequency per sec. per cm² against minimum burst size given in terms of both the number of particles, S, and the energy, E, of the burst. Curve 1 is for spin 1 without cut-off, 2 for spin 1 with cut-off, 3 for spin ½, and 4 for spin 0. The circles indicate the experimental points of Schein and Gill.

The apparatus of Schein and Gill, in the experiment to which we refer, consisted of a Carnegie model C cosmic-ray ionization meter. The spherical steel bomb forming the ionization chamber had walls 1.25 cm thick,[4] volume 19.3 liters, radius 18 cm, and contained argon at 50 atmospheres. Surrounding the ionization chamber was lead shot, the equivalent of 10.7 cm solid lead. A plot of their data, the frequency of bursts N_S containing more than S ionizing particles as a function of S from $S=100$ to 2000 appears in Fig. 1.[5]

[3] M. Schein and P. S. Gill, Rev. Mod. Phys. **11**, 267 (1939).

[4] We are indebted to Dr. Schein for correcting this value.

[5] In plotting the experimental data we have departed slightly from the quoted burst sizes by considering the first group of size 1 actually to refer to size between 0.5 and 1.5 as stated. The experiments give the number of bursts between 100 and 300, then 300–500, etc., particles and in totaling to obtain the number of bursts of more than S particles we then have the points for $S=100$, 300, 500, etc., rather than for 200, 400, 600, etc., as given by Schein and Gill. This change is significant only for small S and results in flattening the curves near $S=100$. There is some reason to believe that some small bursts were missed because of the difficulty of distinguishing small bursts from background, and that the point for $S=100$ is somewhat low. In both the sea-level and high altitude results the point $S=100$ falls out of line with the curve from the remaining points.

II

Two distinct processes are important in the production of soft secondaries by mesotrons: the elastic collisions of mesotrons with atomic electrons (knock on), and the emission of γ-rays by mesotrons in the electric field of the nucleus (bremsstrahlung). The cross sections[6] for the former process are, in units of the *radiation* cross section $\bar{\varphi}=(e^2/\mu c^2)^2\alpha Z^2$, which is convenient for this work:

spin 0, moment 0

$$\sigma(E_0,\epsilon)=\frac{2\pi}{\alpha Z}\frac{\mu}{m}\frac{\mu c^2}{E_0}\frac{d\epsilon}{\epsilon^2}\left(1-\frac{\epsilon}{\epsilon_m}\right),$$

spin $\frac{1}{2}$, moment $eh/2\mu c$

$$\sigma(E_0,\epsilon)=\frac{2\pi}{\alpha Z}\frac{\mu}{m}\frac{\mu c^2}{E_0}\frac{d\epsilon}{\epsilon^2}\left(1-\frac{\epsilon}{\epsilon_m}+\frac{\epsilon^2}{2}\right),$$

spin 1, moment $eh/2\mu c$

$$\sigma(E_0,\epsilon)=\frac{2\pi}{\alpha Z}\frac{\mu}{m}\frac{\mu c^2}{E_0}\frac{d\epsilon}{\epsilon^2}\times\left[1-\frac{\epsilon}{\epsilon_m}+\frac{\epsilon^2}{3}+\frac{mE_0\epsilon}{3\mu^2c^2}\left(1-\frac{\epsilon}{\epsilon_m}+\frac{\epsilon^2}{2}\right)\right],$$

where $\epsilon_m\approx[1+(\mu^2c^2/2mE_0)]^{-1}$ is the maximum fractional energy transfer from a mesotron of energy E_0 to an electron, and μ is the mesotron mass. The bremsstrahlung cross sections,[7] in units $\bar{\varphi}$, for spin 0 and spin $\frac{1}{2}$ are

spin 0, moment 0

$$\sigma(E_0,\epsilon)=\frac{16}{3}\frac{(1-\epsilon)}{\epsilon}\left[\ln\frac{2(1-\epsilon)E_0}{(5/6)\mu c^2Z^{\frac{1}{3}}\epsilon}-\frac{1}{2}\right],$$

spin $\frac{1}{2}$, moment $eh/2\mu c$

$$\sigma(E_0,\epsilon)=\frac{16}{3}\left(\frac{3\epsilon}{4}+\frac{1-\epsilon}{\epsilon}\right)\left[\ln\frac{2(1-\epsilon)E_0}{(5/6)\mu c^2Z^{\frac{1}{3}}\epsilon}-\frac{1}{2}\right].$$

The bremsstrahlung cross section for spin 1, moment $eh/2\mu c$ has been evaluated by the authors in the previous paper. It is important to note, as was pointed out by Corben and Schwinger[6] that for the spins discussed above, the magnetic moment we associate with each is just that magnetic moment which gives *minimum* electromagnetic effects.

The bremsstrahlung cross sections depend on the mesotron mass as $1/\mu^2$ whereas, except for the high energy term for spin 1, the knock-on cross sections are essentially independent of μ. The appearance of $(5/6)\mu c^2Z^{\frac{1}{3}}$ in the logarithm is an approximate expression for the lower limit of the impact parameter, the nuclear radius, and is really independent of μ. Experiments seem to indicate that μ lies between 150 and 200 electron masses; in our calculations we have used $\mu/m=177$ but we must expect some uncertainty, $\sim$20 percent in $1/\mu^2$ and in our results, from this source.

The bremsstrahlung cross sections for spins 0 and $\frac{1}{2}$ are probably correct up to energies such that $E_0\hbar/\mu^2c^3\approx\hbar^2Z^{-\frac{1}{3}}/me^2$ or $E_0\approx5\times10^{11}$ ev in lead, where the screening of the nuclear field by the atomic electrons becomes important. Above this energy the cross sections are essentially constant.

In contrast, the bremsstrahlung cross section for spin 1 is but little affected by the atomic screening since it derives its most important contribution from small impact parameters even at high energies. Oppenheimer, Snyder and Serber[8] have shown, however, that the perturbation treatment leading to (2) of the previous paper is open to serious doubt for $E_0>2\times10^{10}$ ev because of the large coupling energies associated with the dominant high frequencies. Neglecting the possibility[9] that the presence of the very high frequencies might materially reduce the contribution from lower frequencies, we have obtained a *minimum* estimate of the cross section by eliminating the contribution of frequencies which cannot be correctly treated by perturbation methods. We have accordingly used the cross section (28) of the previous paper in which frequencies $>137\mu c^2$ have been eliminated and which includes additional terms, important

[6] H. S. W. Massey and H. C. Corben, Proc. Camb. Phil. Soc. **35**, 463 (1939); H. C. Corben and J. Schwinger, Phys. Rev. **58**, 953 (1940); H. J. Bhabha, Proc. Roy. Soc. **A164**, 257 (1938).

[7] The cross section for spin 0 was calculated by us. That for spin $\frac{1}{2}$ was obtained from W. Heitler, *The Quantum Theory of Radiation* (Oxford, 1936). p. 168, with the appropriate modification made for the finite size of the nucleus.

[8] J. R. Oppenheimer, H. Snyder and R. Serber, Phys. Rev. **57**, 75 (1940).

[9] J. R. Oppenheimer, Phys. Rev. **47**, 44 (1935).

for $E_0 \sim 10^{10}$ ev, in $\ln E_0$. The effect of this frequency cut off at $137\mu c^2$, which is one-half the limiting frequency suggested by Oppenheimer, Snyder and Serber, is to diminish the cross section for $E_0 > 8\times10^{10}$ ev; the decrease is only of order 10 percent at 10^{11} ev. The use of this cross section diminishes the burst probability by ~ 20 percent for $S=100$ and by ~ 80 percent for $S=1000$.

III

The number of mesotrons at these high energies has been determined, for energies up to $\sim 10^{11}$ ev, by the observations of Clay and his coworkers, and Wilson[10] on the cosmic-ray intensity at great depths below sea level. They find the number of mesotrons at depth h below the top of the atmosphere decreases as $h^{-\gamma}$ with $\gamma=1.8$ or 1.9 up to 300 m water equivalent and $\gamma=2.4$ for 300 m $< h <$ 1000 m water equivalent. Observations at ~ 1500 m depth indicate an even more rapid decrease in the intensity. If ionization is the most important mechanism of energy loss up to $E_0 \sim 10^{12}$ ev these measurements can be immediately translated into an integral energy spectrum at sea level. There results that the number of mesotrons at sea level of energy greater than E_0 is approximately $(E_0+1.8\times10^9)^{-\gamma}$ with $\gamma=1.9$ up to $E_0=6\times10^{10}$ ev and $\gamma=2.4$ for $6\times10^{10} < E_0 < 2\times10^{11}$. The corresponding differential spectrum would begin to deviate from a power law of -2.9 at $E_0 \sim 10^{11}$ ev. If this is the case, the cross section for fractional energy loss per atom must be less than 2×10^{-28} cm^2 in earth. If the actual spectrum at sea level were represented by $\gamma=1.9$ up to $E_0=2\times10^{11}$ ev, the cross section 2×10^{-28} cm^2 could account for the additional absorption at high energies represented by the increase in γ with depth. Now the cross section for radiative energy loss in earth of mesotrons of spin 0 or $\frac{1}{2}$ is considerably less than 2×10^{-28} cm^2 and in these cases we may assume, neglecting specifically nuclear energy loss, that γ increases for high energies at sea level. On the other hand, for mesotrons of spin 1 the cross section for fractional energy loss by bremsstrahlung is $\sim 2\times10^{-28}$ cm^2 so that we may take $\gamma=1.9$ up to the highest measured energies ($\sim 2\times10^{11}$ ev) in the appropriate sea level spectrum. For $E_0 > 2\times10^{11}$ ev, there is no direct evidence on the mesotron spectrum.

We have taken the total mesotron intensity at sea level to be 0.01 mesotron per unit solid angle near the vertical, per cm^2 per sec. as suggested by Nordheim and Hebb, and Johnson.[11] Wilson's readings with a slanted counter telescope and the observations on the angular distribution of mesotrons at sea level are both in agreement with the hypothesis that where produced, near the top of the atmosphere, the mesotrons are hemispherically isotropic, the angular distribution at and below sea level being the result of the increased absorption thickness at angles from the vertical. Thus we take for the differential mesotron spectrum at sea level

$$N(E_0)dE_0d\Omega = \frac{0.02(E_c)^{1.9}dE_0d\Omega}{(E_0+1.8\times10^9 \sec\theta)^{2.9}},$$

where the exponent in the denominator increases to 3.4, with the appropriate change in normalization, at $E_0=10^{11}$ ev in the cases of spin 0 and $\frac{1}{2}$. The effect of mesotron decay is to reduce the number of low energy mesotrons which are ineffective in burst production; there results a deviation from the power law at low energies. In order to give correctly the total number of mesotrons with a power law spectrum which is correct at high energies, the spectrum must be cut off at $E_0 \sim 0.6\ 10^9$ ev. This is effected by setting $E_c=(1.8+0.6)\times10^9=2.4\times10^9$ in the differential spectrum. This spectrum gives a total intensity $\sim\cos^2\theta$ as observed but for $E_0 \gg 1.8\times10^9$ ev the distribution is hemispherically isotropic.

Experimental data on bursts are not concerned with the average ionization under thick absorbers or even with the average ionization due to the cascade multiplication of a single soft ray. On the contrary, they are a body of information on a series of *individual* showers. Thus, in discussing the cascade multiplication of a high energy soft secondary in the shielding material, we cannot content ourselves with calculating the average number of ionizing particles in the shower but

[10] P. H. Clay, A. van Gemert and J. Clay, Physica **6**, 184 (1939); J. Clay and A. van Gemert, Physica **6**, 497 (1939); V. C. Wilson, Phys. Rev. **53**, 337 (1938).

[11] L. W. Nordheim and M. H. Hebb, Phys. Rev. **56**, 494 (1939); T. H. Johnson, Rev. Mod. Phys. **10**, 208 (1938).

must investigate individual cases or fluctuations around this average and the probability of finding a particular number of particles as observed. This situation is accentuated by the fact that the number of high energy secondaries will, like the number of mesotrons, decrease rapidly with increasing energy. This means that fluctuations in which more than the average number of particles are found will be heavily weighted, whereas the reverse fluctuations, producing fewer than average, will be relatively unimportant. Not merely the breadth of the probability distribution but also its asymmetry is thus of some importance. We do not know the actual probability law $P(E, S, x)$ that there will be S ionizing particles at a distance x from the beginning of a shower initiated by a soft ray of energy E. For the approximate Furry[12] model which neglects ionization (and is thus independent of E) and treats electrons and γ-rays in the same way, $P=e^{-x}(1-e^{-x})^{S-1}$, $S_{Av}(x)=e^{x}$, and $\langle S^2\rangle_{Av}-(S_{Av})^2=(S_{Av})^2-S_{Av}$ or $\sigma=S_{Av}(1-1/S_{Av})^{\frac{1}{2}}$. Although we cannot use this explicit form for P and S_{Av}, this model gives formally an expression for the dispersion $\sigma\sim S_{Av}$ which is of the right order of magnitude, and near the beginning of the shower, is certainly correct. Near the maximum of the shower, where the largest contributions arise, the detailed calculations of Nordsieck, Lamb and Uhlenbeck[13] show that $\sigma\sim\frac{1}{2}S_{Av}$. In this region the actual fluctuations are certainly much better approximated by the Furry model than those, $\sigma\sim(S_{Av})^{\frac{1}{2}}$ of the Poisson formula. We have, in accordance, used a modification of the Furry formula which gives the same expression for the fluctuations and can be written

$$P(E, S, x)=\frac{1}{S_{Av}(E, x)}\left[1-\frac{1}{S_{Av}(E, x)}\right]^{S-1}$$

where $S_{Av}(E, x)$ is chosen to fit the calculated[14] average multiplication of a soft ray of energy E. Actually since P is asymmetric in the direction of emphasizing small S, its effect is smaller than would be expected from the large value of σ: it gives about twice as many bursts as calculations based on the assumption of no fluctuations. To express the fact that the actual fluctuations are intermediate between S_{Av} and 0, we have so corrected P as to reduce the burst probability by $\sim\sqrt{2}$.

In addition to the above general features, the number of mesotrons, the cross sections for production of soft secondaries, and the multiplication of these secondaries, which are common to any similar description of bursts, there are some features peculiar to the experimental arrangement. The spherically symmetric geometry of Schein and Gill is certainly the most desirable but their steel ionization chamber inside the lead absorber was of sufficient thickness $\sim$1.3 cm to introduce important transition effects in the passage of the shower from the lead to the interior of the chamber.[15] The effective thickness, in view of the effects of scattering and oblique incidence can be taken to be $\sim$1.5 cm or 0.8 shower units of iron. The essential effect of the iron is to reduce the number of particles in the shower to a value intermediate between the numbers normally expected in lead and in iron. The number of particles in a shower is measured by the number at maximum which is $\sim E/9\beta$ for $E\sim10^{10}$ ev where β is the energy, characteristic of the material, where multiplication stops. For iron $\beta=22.4$ Mev, whereas for lead, refinements[16] of the usual theory give $\beta\sim8$ Mev; in general β varies roughly as $1/Z$. The transition effects can be represented by using an effective β between 8 and 22 Mev. Different estimates of this indicate that about $\frac{1}{3}$ of the shower particles in lead are removed by the iron so that $\beta\approx12$ Mev. We have chosen $\beta=13$ Mev and do not think this value is in error by more than 15 percent.

In some burst experiments the scattering of the shower particles in the absorber, which results in their angular divergence, is an important consideration; we will see, however, that in this experiment scattering is not serious and the resulting cross-sectional area of a burst emerging from the absorber is small compared to the size of the ionization chamber for all burst sizes. The angles involved in the multiplicative acts themselves are always small, except

[12] W. H. Furry, Phys. Rev. **52**, 569 (1937).
[13] A. Nordsieck, W. E. Lamb, Jr. and G. E. Uhlenbeck, Physica **4**, 344 (1940).
[14] R. Serber, Phys. Rev. **54**, 317 (1938).
[15] We are indebted to Professor H. A. Bethe for calling our attention to the effect of the thick steel wall.
[16] Dr. Corben has kindly communicated to us the results of his refinements of the cascade theory for heavy elements.

at the lowest energies, and can be neglected here. The theory of multiple scattering gives $\langle\theta^2\rangle_{Av}\sim tZ^2/E^2$ so that the scattering is important only at low energies which occur near the end of the path of the burst in the absorber. Large and small bursts are alike in the energies involved in this region, differing only in the number of particles. The only essential difference between large and small bursts is that the large one starts earlier in the absorber and undergoes additional high energy multiplicative processes which involve extremely small angles. Thus the mean scattering angle is independent of burst size. We can in fact confine our attention to the scattering in the last few cm of absorber which is, here, iron. The mean scattering angle $\langle\theta^2\rangle_{Av}^{\frac{1}{2}}\sim 20°$ for $E\sim\beta=13$ Mev which, occurring in the last cm of material, corresponds to a burst about 1 cm in diameter having half its particles confined to a cone of vertical angle $\sim 40°$. Tending to counteract the decrease in burst size due to the increased path length in iron is the scattering back into the ionization chamber of particles which have traversed it once. Thus, with a spherical ionization chamber immediately surrounded by dense absorber, the corrections due to scattering appear to be small and can be treated as slightly augmenting the transition effects. This is not the case for those experiments which are performed with only a flat plate of absorber above the chamber, especially if it is separated any considerable distance from the chamber. Then the scattering can result only in some of the burst particles missing the chamber. This may be a considerable fraction of the burst if the absorber is lead. In particular, there may then be a differentiation against large bursts and a distortion of the burst curve. These considerations will be important in discussing the experiments of Nie, Steinke and Schmidt.

IV

In calculating the number of bursts, it is simplest to find the number of bursts of size greater than S. On the modified Furry model the probability formula for this is then

$$P'(E, x, S)=\sum_{r=S+1}^{\infty}P(E, x, r)=\left(1-\frac{1}{S_{Av}(E, x)}\right)^{S}.$$

In approximating to $S_{Av}(E, x)$ we have taken

$$S_{Av}(E, x)=\left\{1-\left(1-\frac{9\beta}{E}\right)\left(\frac{x}{7}\right)^{58\beta/E}\times\exp\left[\frac{58\beta}{E}\left(1-\frac{x}{7}\right)\right]\right\}^{-1},$$

where x is measured in shower units of length

$$x_0=\left[4\alpha Z^2\left(\frac{e^2}{mc^2}\right)^2 N\ln\frac{191}{Z^{\frac{1}{3}}}\right]^{-1}$$

and the numerical constants were chosen to approximate to Serber's calculation of cascade multiplication. This form for S_{Av} is good for E in the range $10^{10}-10^{11}$ ev for our purposes which merely require a good approximation to the height and width of the maximum. The expression has compensating errors in that for small bursts it underestimates the height of the maximum and overestimates its breadth. The total probability P'' of getting a burst greater than S from an initial ray of energy E is then obtained by integrating P' over the thickness of the absorber. This integral may be extended to ∞ since the major contribution comes near the maximum of S_{Av}. Then

$$P''(E, S)=x_0\int_0^{\infty}P'(E, x, S)dx$$

$$=x_0\int_0^{\infty}\left(1-\frac{9\beta}{E}\right)^{S}\left(\frac{x}{7}\right)^{58\beta S/E}\times\exp\left[\frac{58\beta S}{E}\left(1-\frac{x}{7}\right)\right]dx$$

or

$$P''(E, S)=7x_0(E/9\beta S)^{\frac{1}{2}}e^{-9\beta S/E}.$$

We can estimate how to correct the error introduced by the somewhat large fluctuations of the Furry model by calculating $I=\int_0^{\infty}P''(E, S)\times(dE/E^3)$ which is closely connected with the number of bursts of size greater than S. With the above formula, $I=0.077x_0/(\beta S)^2$, the maximum of the integrand occurring at $E=3.6\beta S$ and the effective distance in the absorber or burst range being $\sim x_0$. If we assume no fluctuations and integrate the effective length, weighted as $1/E^3$, where there are more than S particles, there results $I=0.035x_0/(\beta S)^2$. Here the most probable energy is $10\beta S$ and the effective burst range $3.5x_0$.

For $\sigma \sim \frac{1}{2}S_{Av}$ we take the most probable energy and the effective range to be the harmonic means of the respective quantities for $\sigma = S_{Av}$ and $\sigma = 0$; thus we take the most probable energy to be $6\beta S$ and the effective range $1.9x_0$. The modified probability law is

$$P'''(E, s) = 13.5x_0(E/15\beta S)^{\frac{1}{2}}e^{-15\beta S/E}$$

which we use in the remaining calculations. For this law, $I = 0.053x_0/(\beta S)^2$.

We must now integrate this probability over all secondary energies with the appropriate weights given by the number of mesotrons and the cross section for production of secondaries. The number of bursts of size greater than S per cm² per sec. due to any particular cross section for secondary production is then

$$N_i(S) = \bar{\varphi}N\int_0^\infty dE\int_0^{\epsilon_m}\frac{d\epsilon}{\epsilon}\int d\Omega \times F\left(\frac{E}{\epsilon}, \theta\right)\sigma_i\left(\frac{E}{\epsilon}, \epsilon\right)P'''(E, S),$$

where E is the energy of the secondary and ϵ the fractional energy transfer, the energy of the primary mesotron being E/ϵ; $F(E/\epsilon, \theta)$ is the number of mesotrons at sea level per unit solid angle per unit energy per cm² per sec. of energy E/ϵ at an angle θ with the vertical; and σ_i is a cross section, measured in units $\bar{\varphi}$, for the creation of a secondary of energy E by a primary of energy E/ϵ in the absorber. If we introduce P''', x_0, and F explicitly and express E in units $15\beta S$ there results

$$N_i(S) = \frac{13.5}{4\ln(191/Z^{\frac{1}{3}})}\frac{m^2}{\mu^2}\times 0.02\times\left(\frac{2.4\times10^9}{15\beta S}\right)^{1.9} \times\int_0^\infty\frac{e^{-1/E}dE}{E^{2.4}}\int_0^{\epsilon_m(15\beta SE)}\epsilon^{1.9}d\epsilon \times\int\frac{d\Omega\sigma_i(15\beta SE'\epsilon, \epsilon)}{(1+1.8\times10^9\epsilon\sec\theta/15\beta S)^{2.9}}.$$

where it is understood that the spectrum and integrals are to be appropriately modified at high energies in the cases spin 0 and $\frac{1}{2}$. For the knock-on cross sections, which are proportional to $1/Z$ in these units, the last two integrals were carried out exactly with the exponent 2.9 being replaced by 3 in the θ integral. This is unimportant since $1.8\times10^9\epsilon\sec\theta/(15\beta S)$ is small for most angles for $S > 100$. The resulting quantity, which may be called a modified burst production cross section, was plotted, the corrections to the mesotron spectrum above $E_0 = 10^{11}$ ev introduced in the graph, and the remaining integral carried out by approximate methods. The corresponding burst frequencies are tabulated in Table I for different values of βS for lead. To make estimates for other elements, these burst probabilities due to *knock on* must be multiplied by $82/Z$.

TABLE I. *Number of bursts per cm² per sec. with more than S particles produced in great thicknesses of lead by different processes.*

	Knock on			Bremsstrahlung		
βS	Spin 0	Spin $\frac{1}{2}$	Spin 1	Spin 0	Spin $\frac{1}{2}$	Spin 1
10^9	$6.8\cdot10^{-8}$	$8.7\cdot10^{-8}$	$1.2\cdot10^{-7}$	$2.0\cdot10^{-7}$	$3.2\cdot10^{-7}$	$1.0\cdot10^{-6}$
2.10^9	$1.3\cdot10^{-8}$	$1.8\cdot10^{-8}$	$3.2\cdot10^{-8}$	$7.3\cdot10^{-8}$	$1.2\cdot10^{-7}$	$4.8\cdot10^{-7}$
4.10^9	$2.3\cdot10^{-9}$	$3.3\cdot10^{-9}$	$8.1\cdot10^{-9}$	$2.2\cdot10^{-8}$	$3.8\cdot10^{-8}$	$2.1\cdot10^{-7}$
8.10^9	$3.5\cdot10^{-10}$	$5.4\cdot10^{-10}$	$2.1\cdot10^{-9}$	$6.0\cdot10^{-9}$	$1.0\cdot10^{-8}$	$8.7\cdot10^{-8}$
16.10^9	$5.1\cdot10^{-11}$	$8.1\cdot10^{-11}$	$5.5\cdot10^{-10}$	$1.4\cdot10^{-9}$	$2.5\cdot10^{-9}$	$3.3\cdot10^{-8}$
32.10^9	$7.1\cdot10^{-12}$	$1.2\cdot10^{-11}$	$1.5\cdot10^{-10}$	$2.9\cdot10^{-10}$	$5.1\cdot10^{-10}$	$1.2\cdot10^{-8}$
64.10^9	$9.7\cdot10^{-13}$	$1.6\cdot10^{-12}$	$3.9\cdot10^{-11}$	$5.0\cdot10^{-11}$	$9.0\cdot10^{-11}$	$3.7\cdot10^{-9}$

The bremsstrahlung cross sections are more complicated functions of ϵ and it was necessary to approximate slightly by calculating

$$\int_0^{\epsilon_m}\epsilon^2\sigma d\epsilon,$$

the burst production cross section, and correcting it at low energies by multiplying by

$$\int\frac{d\Omega}{(1+1.8\times10^9\bar{\epsilon}\sec\theta/15\beta S)^3}$$

with $\bar{\epsilon} = \frac{3}{4}$. This modified burst production cross section was then treated as before and tabulated. These burst frequencies depend on Z only through β.

The total burst frequency for any mesotron spin and any element for βS in the range given, can be found by adding $82/Z$ N(knock on) to N(bremsstrahlung) and substituting an appropriate value of β which varies roughly as $1/Z$. These calculations cannot with any certainty be extended beyond $\beta S = 16\times10^9$ ev because of the lack of *a priori* knowledge of the mesotron spectrum above $E_0 \sim 2\times10^{11}$ ev. In Fig. 1 we have plotted $N(S)$ against (S) on a double logarithmic scale for spins 0, $\frac{1}{2}$, and 1, together with the experimental results of Schein and Gill.

V

The principal sources of error or uncertainty in these calculations are the values of μ/m and β; both of which enter quadratically. We limit our error in β to 15 percent and in its effect to 30 percent. Errors in the number of mesotrons and in our treatment of cascades should not be greater than 15 percent. Except for the mass uncertainty we would limit errors to ~ 40 percent. We believe $\mu/m = 177$ is probably correct to within 15 percent and would thus assign an over-all limit of error of about 60 percent.

In view of these possible errors, we see that the experimentally observed burst frequency is consistent with either spin 0 or spin $\frac{1}{2}$ and moment $e\hbar/2\mu c$. Any appreciably different moment for spin $\frac{1}{2}$ would result in a burst frequency comparable to that from spin 1 moment $e\hbar/2\mu c$. Our calculations give slightly greater weight to the spin 0 hypothesis but do not justify an absolute distinction. On the other hand, spin 1 and moment $e\hbar/2\mu c$ (which gives the minimum electromagnetic effects for this spin) gives more bursts than are observed by at least a factor ten. Furthermore, this discrepancy becomes larger for large bursts where the data shows a more rapid decrease of burst frequency with burst size. Thus the experiments tend to exclude the possibility of spin 1 but are consistent with either spin 0 or spin $\frac{1}{2}$.

Further confirmation of this conclusion is given by Bhabha's calculation of the bursts produced in clay and his comparison with the experiments of Carmichael and Chou.[17] He found that the knock-on formula for spin 1 gave good agreement with observation. If he had then included the bremsstrahlung which must accompany a particle of spin 1, he would have found far too many large bursts. However it is apparent from our tables that the total burst frequency in clay for spin 0 or $\frac{1}{2}$ is roughly equal to that given by the spin 1 knock-on formula. With the conclusions from the data of Schein and Gill, this is significant, although the data of Carmichael and Chou do not involve sufficiently high energies alone to justify a sure conclusion.

We have already indicated that in Nie's experiments the geometry was such as to preclude the possibility of exact calculation. The experiments have, however, contributed some doubt as to the Z dependence of bursts. Our calculations give Z^2 dependence for large bursts ($S>500$) where bremsstrahlung is dominant; this is reduced to Z dependence in the neighborhood of $S=100$ where knock on becomes important. For much smaller bursts Z independence may be expected since the mesotron spectrum flattens out at low energies.[18] Now Nie worked primarily with small bursts and appeared to find as many in iron as in lead although the transition curve for iron was not carried as far as the plateau. However, the effects of scattering, which was probably an important factor in decreasing the apparent burst size with his geometry, increase as Z^2—which would tend to decrease the difference between lead and iron. There is still a real need for a good experiment on burst production in a light element such as water.

The immediate conclusions to be drawn from the experiment of Schein and Gill are that the exponent in the mesotron spectrum at sea level must increase by several units in the range $10^{11} < E_0 < 10^{12}$ ev, and that the burst production cross section,

$$\int_0^{\epsilon_m} \epsilon^2 \sigma d\epsilon < 10^{-27} \text{ cm}^2$$

at $E \approx 5 \times 10^{10}$ ev. The burst frequencies calculated either with spin 0 or spin $\frac{1}{2}$ agree with experiment; those calculated with spin 1 do not. In critically examining the possibility of spin 1 we see that two points are perhaps questionable. In the first place, our calculations for bremsstrahlung of spin 1 which has been intended to give the minimum effect possible for this case, can, of course, be fully justified only by a more complete theory than we have at present. In the second place, if the mesotron mass were several times as great as here supposed, the experiments of Schein and Gill would no longer exclude this case.

In conclusion we wish to express our appreciation of the invaluable assistance of Professor J. R. Oppenheimer, with whom all parts of this work have been discussed.

[17] H. J. Bhabha, H. Carmichael and C. N. Chou, Proc. Ind. Acad. Sci. **10**, 221 (1939); H. Carmichael and C. N. Chou, Nature **144**, 325 (1939).

[18] The essence of this discussion is to be found in Oppenheimer, Snyder and Serber, reference 8, and J. R. Oppenheimer, Rev. Mod. Phys. **11**, 264 (1939).

Radiative X-Ray Transitions Within the L Shell

D. H. TOMBOULIAN AND WILLOUGHBY M. CADY
Cornell University, Ithaca, New York

(January 17, 1941)

Whereas N–N and M–M lines have been observed in the x-ray spectra of several elements, L–L lines have not been identified. However, isolated lines of sodium (375A), magnesium (317A) and aluminum (290A) reported by Skinner are here designated as L_I–$L_{II,III}$. Thus the L_I term in these elements may now be evaluated, and reliable predictions of L_I may be made for the elements silicon to chromium.

THE x-ray lines most easily observed are those for which the initial and final states differ in the quantum number n. Many transitions have been observed, however, in which $\Delta n=0$. Thus Magnusson[1] has identified as N–N transitions the lines of several elements in the ultra-soft region, and Siegbahn and Magnusson[2] cite several M–M lines. Transitions within the L shell have apparently not been reported, although two are allowed: L_I–L_{II} and L_I–L_{III}.

Among the competing processes whereby a missing L_I electron may be replaced, the radiative L–L transitions should be very weak in heavy elements, since the energy released by L_I–M is so much greater than that released by L_I–$L_{II,III}$, that an L_I ionization is almost always followed by the former process instead of the latter. In light elements, however, this inequality is less emphatic. We are therefore led to seek the L–L radiation in the spectra of the lightest elements having completed L shells.

The wave-length of such transitions can be predicted with the aid of the screening-doublet law. This law, as relating the term values T of L_I and L_{II}, may be written either in the form

$$(T_{LI}/R)^{\frac{1}{2}}-(T_{LII}/R)^{\frac{1}{2}}=\text{constant} \qquad (1)$$

or in the form

$$(T_{LI}/R)-(T_{LII}/R)=\text{linear function of } Z. \qquad (2)$$

Table I illustrates the application of (1) and (2) to the prediction of the transition L_I–L_{II}. Here the known terms for elements $Z\geqslant 26$ are as evaluated by Siegbahn;[3] the remaining term values are based on the observations of Skinner.[4] Column 2 of Table I gives in parentheses predictions of L_I, made with the aid of column 4 (cf. Eq. (1)). Similarly, predictions in column 5 are based on column 7, where $\Delta T/R$ is estimated by graphical extrapolation (cf. Eq. (2)). Column 8 presents the final prediction of L_I, in which column 2 has been weighted twice as heavily as column 5. In column 9 is listed the wave-length of the L_I–L_{II} transition, predicted from columns 6 and 8.

Skinner,[4] in his exhaustive description of the L spectra of Na, Mg and Al, lists as unidentified one line for each of these elements. These lines are listed in the last column of Table I. The wave-length agreement is excellent, and strongly points to the identification of Skinner's lines as the L–L transitions. One of these lines appears on two of our own sodium spectrograms;[5] our value for the wave-length is 376.5A, the half-width at half-maximum being some 3A.

The line L_I–L_{III} should lie very close to L_I–L_{II}, and should be the brighter of the two. Indeed Skinner's lines are more correctly designated L_I–L_{III}.

With this identification one can now for the first time evaluate the level L_I of Na, Mg and Al. This evaluation is presented in Table II. The values of $\Delta(T/R)^{\frac{1}{2}}$ are also given, the parentheses indicating interpolated values for the elements $14\leqslant Z\leqslant 25$. The last column gives the L_I–L_{III} line as observed and rough predictions for the elements in which it has not been observed.

The width of the Na L_I–L_{III} transition implies

[1] T. Magnusson, Zeits. f. Physik **79**, 161 (1932).
[2] M. Siegbahn and T. Magnusson, Zeits. f. Physik **88**, 559 (1934).
[3] M. Siegbahn, *Spektroskopie d. Röntgenstrahlen* (Springer, Berlin, 1931).
[4] H. W. B. Skinner, Phil. Trans. Roy. Soc. **239**, 95 (1940).
[5] W. M. Cady and D. H. Tomboulian, Phys. Rev. **59**, 381 (1941).

TABLE I. *Prediction of the line $L_I - L_{II}$ for* Na, Mg *and* Al.

1 Z	2 $\left(\frac{T}{R}\right)^{\frac{1}{2}}(L_I)$	3 $\left(\frac{T}{R}\right)^{\frac{1}{2}}(L_{II})$	4 $\Delta\left(\frac{T}{R}\right)^{\frac{1}{2}}$	5 $\frac{T}{R}(L_I)$	6 $\frac{T}{R}(L_{II})$	7 $\Delta\frac{T}{R}$	8 $\frac{T}{R}(L_I)$	9 $\lambda(L_I-L_{II})$ CALC. (A)	10 λ OBS. (A)
50	18.09	17.46	0.63	327.4	304.9	22.5			
45	15.83	15.21	0.62	250.7	231.2	19.5			
40	13.66	13.04	0.62	186.6	170.0	16.6			
33	10.61	10.00	0.61	112.6	100.0	12.6			
30	9.40	8.78	0.62	88.4	77.1	11.3			
28	8.65	8.04	0.61	74.8	64.6	10.2			
26	7.91	7.29	0.62	62.5	53.2	9.3			
13	(2.92)	2.318	(0.60)	(9.0)	5.372	(3.6)	(8.68)	(275)	290
12	(2.51)	1.913	(0.60)	(6.9)	3.658	(3.2)	(6.50)	(321)	317
11	(2.10)	1.504*	(0.60)	(5.0)	2.263*	(2.7)	(4.61)	(388)	375

* Estimated from L_{III} by the spin doublet law.

TABLE II. *The L terms and L−L lines of light elements.*

Z	$\left(\frac{T}{R}\right)^{\frac{1}{2}}(L_I)$	$\left(\frac{T}{R}\right)^{\frac{1}{2}}(L_{II})$	$\Delta\left(\frac{T}{R}\right)^{\frac{1}{2}}$	$\frac{T}{R}(L_I)$	$\frac{T}{R}(L_{II})$	$\frac{T}{R}(L_{III})$	(A)
26 Fe	7.91	7.29	0.62	62.5	53.2	52.2	88†
25 Mn	(7.56)	6.95	(0.61)	(57.2)	48.3	47.4	(93)
24 Cr	(7.17)	6.56	(0.61)	(51.4)	43.0	42.3	(100)
23 V	(6.81)	6.20	(0.61)	(46.4)	38.5	37.9	(107)
22 Ti	(6.44)	5.83	(0.61)	(41.5)	34.0	33.6	(115)
21 Sc	(6.10)	5.50	(0.60)	(37.2)	30.3	30.0	(126)
20 Ca	(5.68)	5.08	(0.60)	(32.3)	25.8	25.5	(134)
19 K	(5.26)	4.66	(0.60)	(27.7)	21.7	21.5	(147)
17 Cl	(4.45)	3.86	(0.59)	(19.8)	14.9	14.8	(182)
16 S	(4.06)	3.480	(0.58)	(16.5)	12.11	12.02	(203)
15 P	(3.69)	3.112	(0.58)	(13.6)	9.68	9.60	(228)
14 Si	(3.31)	2.716	(0.59)	(11.0)	7.378	7.325	(248)
13 Al	2.913	2.318	0.595	8.485	5.372	5.343	290
12 Mg	2.552	1.913	0.639	6.513	3.658	3.638	317
11 Na	2.163	1.504*	0.659	4.678	2.263*	2.248	375

* Estimated from L_{III} by the spin doublet law.
† Not observed.

a voltage spread of nearly one-half electron volt. Since L_{III} is known to be sharp, this width must inhere almost wholly in L_I.

An objection to the proposed identification of L_I–L_{III} may be raised: the value of $\Delta(T/R)^{\frac{1}{2}}$ rises suddenly at low Z if the identification is correct. This is, however, not surprising, for $\Delta(T/R)^{\frac{1}{2}}$ is proportional to the difference between two screening constants, and it is known that screening constants vary irregularly with Z in the region of low energies; the value of $\Delta(T/R)^{\frac{1}{2}}$ for the $M_I M_{II}$ screening doublet, calculated for the elements[6] K to Co shows a somewhat similar behavior.

[6] M. Siegbahn and T. Magnusson, Zeits. f. Physik **95**, 133 (1935).

The Extreme Ultraviolet Spectra of Ne IV, V and VI

FRED W. PAUL AND HARRY D. POLSTER
University of Rochester, Rochester, New York

(Received December 18, 1940)

An electrical discharge suitable for the excitation of high stages of ionization in gases has been developed. This discharge has been used to excite neon gas and the resulting emission has been recorded with a 3-meter grazing incidence vacuum spectrograph. One hundred and seventeen lines have been identified in the spectrum of Ne IV; fifty-six lines in Ne V, and twenty-five in Ne VI. It has been possible to make fairly accurate calculations of the ionization potentials of Ne IV and Ne V as 96.43 volts and 125.8 volts, respectively. The ionization potential of Ne VI is estimated to be 157 volts.

THIS investigation is the outgrowth of an attempt to develop a light source which would yield the spectra of highly ionized atoms of gaseous elements. Although the past few years have brought extensive advances in the knowledge of the spectra of highly ionized atoms of elements that can be fixed in a solid electrode, there have been no corresponding additions to the knowledge of the spectra of ions that can be handled only as gases.[1] Boyce in his investigations of neon[2] and argon[3] found the greatest excitation provided by the electrodeless discharge to correspond to the lowest excited levels of Ne IV and A V. Neon was selected as the most suitable subject for investigation because the spectra of the ions of neon can be predicted very accurately by interpolation among the data of Edlén for boron, carbon, nitrogen and oxygen,[4] of Bowen[5] and Edlén[6] for fluorine and those of Soderquist for sodium, magnesium and aluminum[7] and because the excitation required to produce a given stage of ionization for neon is greater than that for any other rare gas except helium. That this is the case is readily seen from a diagram such as Fig. 1 in which the position of the lowest level of each ion relative to the ground state of the normal atom is plotted as ordinate and various rare gas ions are located in separate columns.

[1] In a note published while this investigation was in progress Parker and Phillips (Phys. Rev. **58**, 93(L) (1940) have described the excitation of A VI, VII and VIII.
[2] J. C. Boyce, Phys. Rev. **46**, 378 (1934).
[3] J. C. Boyce, Phys. Rev. **48**, 396 (1935).
[4] B. Edlén, Nova Acta Regiae Soc. Scient. Upsaliensis, [IV] **9**, No. 6, 3 (1934).
[5] I. S. Bowen, Phys. Rev. **45**, 82 (1934).
[6] B. Edlén, Zeits. f. Physik **94**, 47 (1935).
[7] J. Soderquist, Nova Acta Regiae Soc. Scient. Upsaliensis, [IV] **9**, No. 7, 3 (1934).

EXPERIMENTAL

Two general types of discharge tubes were used as sources. The first was very similar in design and performance to the capillary tubes used to produce short wave-length continuous radiation. A tungsten wire inserted part way into a Pyrex or quartz capillary of about 2-mm bore served as one electrode for a highly condensed electrical discharge which took place inside the bore of the capillary. This discharge could be viewed by looking end-on at the capillary, or by drilling a hole in the side of the capillary and viewing transversely. Neon was admitted to the region of the discharge by letting it flow in along the tungsten wire. This type of tube proved quite successful in producing highly ionized atoms, and some results from this tube were given in a preliminary report.[8] However, the spectra from the capillary tubes showed very broad, diffuse lines.

The second type of discharge tube employed was very similar in design to the usual Geissler tube for observing the spectra of gases. A ring electrode of heavy tungsten wire was placed at each end of a central Pyrex tube of about 10-mm bore and 150-mm length, which was surrounded by a water-cooling jacket. The central tube was then fitted with replaceable quartz inner tubes with bores ranging from 3 mm to 7 mm. Neon was introduced to the tube at the end remote from the spectrograph and allowed to flow through the tube and through the slit of the spectrograph. The electrical discharge took place periodically between the tungsten electrodes. The larger bore tubes proved to be successful in

[8] F. W. Paul, Phys. Rev. **56**, 1067(L) (1939).

eliminating most of the fuzziness of the lines, while by suitable adjustments of the electrical circuit greater excitation could be obtained with these tubes than with the capillary tubes. The reason for this last observation was that the capillary tubes more frequently failed at the higher voltages and capacitances.

The rate of flow of gas through the discharge tubes was made steady by a reservoir system and adjusted by means of a series of external capillaries of various bores and lengths.

The electrical circuit consisted of a transformer, a rectifier tube, and a bank of condensers. The voltage applied to the tubes was varied from 5 kv to 105 kv and the capacitance connected in parallel with the discharge tubes was varied from 0.1 μf to 1.8 μf. The rate at which discharges occurred and the voltage across the tube was adjusted by means of a spark gap in series with the tube, as well as by varying the output and voltage of the transformer.

The spectrograms were obtained in the recently constructed 3-meter grazing incidence vacuum spectrograph at the Ohio State University. The angle of incidence was set at about 84°. The dispersion at 500A was approximately 1 A/mm. Ilford type Q-2 and Eastman special ultraviolet sensitive plates were used. Exposure times of five minutes to two hours with about two discharges per second gave a good range of blackening of the plates.

Although the gas system was reasonably free of leaks and efforts were made to obtain pure gas (purified neon in Pyrex flasks was used and was passed through liquid-air cooled, activated charcoal before it entered the discharge tube), the spectra were always contaminated with many strong lines of carbon, nitrogen and oxygen. In the discharge tubes of smaller bore the lines of silicon were also observed. Although these impurities were bothersome in that they obscured parts of some multiplets, they served as very convenient wave-length standards.

Many spectrograms of the discharge were taken in the region from 96 to 1010A with various discharge conditions. From these, six were selected which showed the sharpest lines and the best variation in the spectrum with changing discharge conditions. Each of these has been measured twice on various comparators including the one at the Ohio State University, the large measuring engine at Massachusetts Institute of Technology and a smaller comparator at the University of Rochester.

Results

All of the spectrograms show quite strongly the lines of Ne III, IV and V. The spectrum of Ne II shows up only very faintly, except at the lower voltages and capacitances, and the spectrum of Ne VI appears faintly on the spectrograms obtained with the highest excitation conditions. Under no conditions were even the strongest lines of Ne I observed. Changing the discharge conditions changes the distribution of intensity among these spectra. As was expected, the use of greater voltages or greater capacitances, or both, resulted in the production of higher excitation spectra. The use of smaller bores in the discharge tubes also produced higher excitations. The effect of varying the pressure in the discharge could not be well established, as the discharge was somewhat critical to pressure variations, and failed to

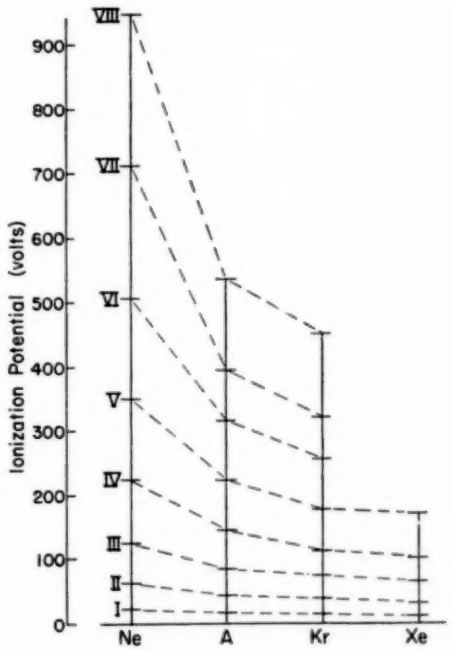

FIG. 1. The positions of various rare gas ions relative to the lowest level of the normal atom. All intervals above Ne V, A IV, Kr III and Xe III are estimated from isoelectronic sequence data. The broken lines connect the same stage of ionization in different gases. From this diagram one can predict that if a source produces the spectrum of Ne VI it will almost certainly produce that of A VII and probably some of A VIII.

TABLE I. *Lines identified as belonging to the spectrum of* Ne IV.

INT.	λ A.U.	ν CM^{-1}	TRANSITION
1	786.141	127,204	$2p^5\,{}^2P^0_{1/2}-2s^22p^2(^1D)3d^2P_{3/2}$
3*h*	780.250	128,164	$2p^5\,{}^2P^0_{3/2}-2s^22p^2(^1D)3d^2P_{3/2}$
	763.959	calc.	$2p^5\,{}^2P^0_{1/2}-2s^22p^2(^1D)3d^2S_{1/2}$
3*h*	758.317	131,871	$2p^5\,{}^2P^0_{3/2}-2s^22p^2(^1D)3d^2S_{1/2}$
1	609.168	164,158	$2s2p^4\,{}^2P_{1/2}-2p^5\,{}^2P^0_{3/2}$
5	606.527	164,873	$2s2p^4\,{}^2P_{3/2}-2p^5\,{}^2P^0_{3/2}$
2	605.595	165,127	$2s2p^4\,{}^2P_{1/2}-2p^5\,{}^2P^0_{1/2}$
2	602.999	165,838	$2s2p^4\,{}^2P_{3/2}-2p^5\,{}^2P^0_{1/2}$
150	543.891	183,860	$2s^22p^3\,{}^4S^0_{3/2}-2s2p^4\,{}^4P_{5/2}$*
100	542.073	184,477	$2s^22p^3\,{}^4S^0_{3/2}-2s2p^4\,{}^4P_{3/2}$*
80	541.127	184,799	$2s^22p^3\,{}^4S^0_{3/2}-2s2p^4\,{}^4P_{1/2}$*
3	539.731	185,277	$2s2p^4\,{}^2S_{1/2}-2p^5\,{}^2P^0_{3/2}$
1	536.965	186,232	$2s2p^4\,{}^2S_{1/2}-2p^5\,{}^2P^0_{1/2}$
25	521.813	191,640	$2s^22p^3\,{}^2P^0_{3/2}-2s2p^4\,{}^2D_{5/2}$*
25	521.742	191,666	$2s^22p^3\,{}^2P^0_{1/2}-2s2p^4\,{}^2D_{3/2}$*
200	469.865	212,827	$2s^22p^3\,{}^2D^0_{3/2}-2s2p^4\,{}^2D_{5/2}$*
200	469.817	212,849	$\left\{\begin{matrix}2s^22p^3\,{}^2D^0_{3/2}-2s2p^{42}\,D_{3/2}\\ 2s^22p^3\,{}^2D^0_{5/2}-2s2p^{42}\,D_{5/2}\end{matrix}\right\}$*
50	433.237	230,821	$2s2p^4\,{}^2D-2p^5\,{}^2P^0_{3/2}$
25	431.472	231,765	$2s2p^4\,{}^2D_{3/2}-2p^5\,{}^2P^0_{1/2}$
150	421.609	237,187	$2s^22p^3\,{}^2P^0-2s2p^4\,{}^2S_{1/2}$*
100	388.218	257,587	$2s^22p^3\,{}^2P^0-2s2p^4\,{}^2P_{3/2}$*
125	387.141	258,304	$2s^22p^3\,{}^2P^0-2s2p^4\,{}^2P_{1/2}$*
200*w*	358.721	278,768	$2s^22p^3\,{}^2D^0-2s2p^4\,{}^2P_{3/2}$* Blend C III
50	357.831	279,461	$2s^22p^3\,{}^2D^0_{3/2}-2s2p^4\,{}^2P_{1/2}$
3	294.390	339,686	$2s2p^4\,{}^4P_{1/2}-2s^22p^2(^3P)3p^4P^0_{1/2}$
3	294.100	340,020	$2s2p^4\,{}^4P_{3/2}-2s^22p^2(^3P)3p^4P^0_{1/2}$
1	293.947	340,197	$2s2p^4\,{}^4P_{3/2}-2s^22p^2(^3P)3p^4P^0_{3/2}$
5	293.649	340,543	$2s2p^4\,{}^4P_{3/2}-2s^22p^2(^3P)3p^4P^0_{5/2}$
10	293.429	340,798	$2s2p^4\,{}^4P_{5/2}-2s^22p^2(^3P)3p^4P^0_{3/2}$
15	293.123	341,154	$2s2p^4\,{}^4P_{5/2}-2s^22p^2(^3P)3p^4P^0_{5/2}$
10	287.206	348,182	$2s2p^4\,{}^4P_{1/2}-2s^22p^2(^3P)3p^4S^0_{3/2}$
15	286.934	348,512	$2s2p^4\,{}^4P_{3/2}-2s^22p^2(^3P)3p^4S^0_{3/2}$
15	286.688	349,104	$2s2p^4\,{}^4P_{5/2}-2s^22p^2(^3P)3p^4S^0_{3/2}$
8	248.004	403,219	$2s2p^4\,{}^4P_{1/2}-2s2p^3(^5S)3s^4S^0_{3/2}$
8	247.807	403,540	$2s2p^4\,{}^4P_{3/2}-2s2p^3(^5S)3s^4S^0_{3/2}$
10	247.422	404,168	$2s2p^4\,{}^4P_{5/2}-2s2p^3(^5S)3s^4S^0_{3/2}$
25	234.701	426,074	$2s^22p^3\,{}^2P^0-2s^22p^2(^3P)3s^2P_{1/2}$
25	234.316	426,774	$2s^22p^3\,{}^2P^0-2s^22p^2(^3P)3s^2P_{3/2}$
25	223.605	447,217	$2s^22p^3\,{}^2D^0_{3/2}-2s^22p^2(^3P)3s^2P_{1/2}$
25	223.241	447,946	$2s^22p^3\,{}^2D^0_{5/2}-2s^22p^2(^3P)3s^2P_{3/2}$
40	222.600	449,236	$2s^22p^3\,{}^2P^0-2s^22p^2(^1D)3s^2D_{5/2,3/2}$
5	218.766	457,109	$2s2p^4\,{}^4P_{1/2}-2s^22p^2(^3P)4p^4D^0_{1/2}$
25	218.643	457,367	$\left\{\begin{matrix}2s2p^4\,{}^4P_{3/2}-2s^22p^2(^3P)4p^4D^0_{1/2}\\ 2s2p^4\,{}^4P_{1/2}-2s^22p^2(^3P)4p^4D^0_{3/2}\end{matrix}\right\}$
20*db*	218.483	457,702	$2s2p^4\,{}^4P_{3/2}-2s^22p^2(^3P)4p^4D^0_{3/2}$
15	218.343	457,995	$2s2p^4\,{}^4P_{3/2}-2s^22p^2(^3P)4p^4D^0_{5/2}$
(10)	218.184	458,329	$2s2p^4\,{}^4P_{5/2}-2s^22p^2(^3P)4p^4D^0_{3/2}$
(20)	218.131	458,440	$2s2p^4\,{}^4P_{1/2}-2s^22p^2(^3P)4p^4P^0_{1/2}$
(25)	217.830	459,074	$2s2p^4\,{}^4P_{5/2}-2s^22p^2(^3P)4p^4D^0_{7/2}$
(15)	217.777	459,185	$2s2p^4\,{}^4P_{3/2}-2s^22p^2(^3P)4p^4P^0_{3/2}$
15	217.640	459,474	$\left\{\begin{matrix}2s2p^4\,{}^4P_{5/2}-2s^22p^2(^3P)4p^4P^0_{3/2}\\ 2s2p^4\,{}^4P_{3/2}-2s^22p^2(^3P)4p^4P^0_{5/2}\end{matrix}\right\}$
15	217.337	460,115	$2s2p^4\,{}^4P_{5/2}-2s^22p^2(^3P)4p^4P^0_{5/2}$
15	215.843	463,300	$2s2p^4\,{}^4P_{1/2}-2s^22p^2(^3P)4p^4S^0_{3/2}$
3	215.711	463,583	$2s2p^4\,{}^4P_{3/2}-2s^22p^2(^3P)4p^4S^0_{3/2}$
(5)	215.396	464,261	$2s2p^4\,{}^4P_{5/2}-2s^22p^2(^3P)4p^4S^0_{3/2}$
150	212.556	470,464	$2s^22p^3\,{}^2D^0-2s^22p^2(^1D)3s^2D$
80	208.899	478,701	$2s^22p^3\,{}^4S^0_{3/2}-2s^22p^2(^3P)3s^4P_{1/2}$
100	208.734	479,079	$2s^22p^3\,{}^4S^0_{3/2}-2s^22p^2(^3P)3s^4P_{3/2}$
100	208.485	479,651	$2s^22p^3\,{}^4S^0_{3/2}-2s^22p^2(^3P)3s^4P_{5/2}$
5	204.908	488,024	$2s2p^4\,{}^4P_{1/2}-2s2p^3(^5S)3d^4D^0$
15	204.786	488,315	$2s2p^4\,{}^4P_{3/2}-2s2p^3(^5S)3d^4D^0$
25	204.531	488,923	$2s2p^4\,{}^4P_{5/2}-2s2p^3(^5S)3d^4D^0$
15	204.270	489,548	$2s^22p^3\,{}^2P^0-2s^22p^2(^1S)3s^2S_{1/2}$
50	194.623	513,814	$2s^22p^3\,{}^2P^0-2s^22p^2(^3P)3d^2P_{3/2}$
40	194.477	514,200	$2s^22p^3\,{}^2P^0-2s^22p^2(^3P)3d^2P_{1/2}$
100	194.276	514,732	$2s^22p^3\,{}^2P^0-2s^22p^2(^1S)3d^2D$
15	190.645	524,535	$2s^22p^3\,{}^2P^0-2s^22p^2(^3P)3d^2D_{3/2}$
25	190.565	524,755	$2s^22p^3\,{}^2D^0_{3/2}-2s^22p^2(^3P)3d^2D_{5/2}$
15	186.915	535,003	$2s^22p^3\,{}^2D^0-2s^22p^2(^3P)3d^2P_{3/2}$
5	186.787	535,369	$2s^22p^3\,{}^2D^0-2s^22p^2(^3P)3d^2P_{1/2}$
150	186.575	535,977	$2s^22p^3\,{}^2D^0-2s^22p^2(^1S)3d^2D$
( )	185.370	538,416	$2s^22p^3\,{}^2D^0-2s^22p^2(^3P)3d^2F_{5/2}$ (O V)
20	185.479	539,145	$2s^22p^3\,{}^2D^0_{5/2}-2s^22p^2(^3P)3d^2F_{7/2}$
12	183.247	545,712	$2s^22p^3\,{}^2D^0-2s^22p^2(^3P)3d^2D_{3/2}$
15	183.165	545,956	$2s^22p^3\,{}^2D^0-2s^22p^2(^3P)3d^2D_{5/2}$
( )	182.829	calc.	$2s^22p^3\,{}^2P^0-2s^22p^2(^1D)3d^2D$ (O IV)
20	181.691	550,506	$2s^22p^3\,{}^2P^0-2s^22p^2(^1D)3d^2P_{1/2}$
20	181.614	550,618	$2s^22p^3\,{}^2P^0-2s^22p^2(^1D)3d^2P_{3/2}$
15	180.402	554,318	$2s^22p^3\,{}^2P^0-2s^22p^2(^1D)3d^2S_{1/2}$
80	177.161	564,458	$2s^22p^3\,{}^2D^0-2s^22p^2(^1D)3d^2F$
50	176.007	568,159	$2s^22p^3\,{}^2D^0-2s^22p^2(^1D)3d^2D$
8	174.920	571,690	$2s^22p^3\,{}^2D^0_{3/2}-2s^22p^2(^1D)3d^2P_{1/2}$
10	174.880	571,821	$2s^22p^3\,{}^2D^0-2s^22p^2(^1D)3d^2P_{3/2}$
3	174.303	573,714	$2s^22p^3\,{}^2P^0-2s^22p^2(^3P)4s^2P_{1/2}$
( )	174.120	calc.	$2s^22p^3\,{}^2P^0-2s^22p^2(^3P)4s^2P_{3/2}$ (O IV)
80	172.620	579,307	$2s^22p^3\,{}^4S^0_{3/2}-2s^22p^2(^3P)3d^4P_{5/2}$
50	172.525	579,626	$2s^22p^3\,{}^4S^0_{3/2}-2s^22p^2(^3P)3d^4P_{3/2}$ Resolved
40	172.492	579,737	$2s^22p^3\,{}^4S^0_{3/2}-2s^22p^2(^3P)3d^4P_{1/2}$ in third
2	168.101	594,880	$2s^22p^3\,{}^2D^0_{3/2}-2s^22p^2(^3P)4s^2P_{1/2}$ order
5	167.921	595,518	$2s^22p^3\,{}^2D^0-2s^22p^2(^3P)4s^2P_{3/2}$
( )	166.113	calc.	$2s^22p^3\,{}^2P^0-2s^22p^2(^1D)4s^2D$ (O V)
(2)	163.602	611,239	$2s^22p^3\,{}^2P^0-2s^22p^2(^3P)4d^2D_{3/2}$
12	163.562	611,389	$2s^22p^3\,{}^2P^0_{3/2}-2s^22p^2(^3P)4d^2D_{5/2}$
10	160.471	623,165	$2s^22p^3\,{}^2D^0-2s^22p^2(^1D)4s^2D$
15	158.822	629,636	$2s^22p^3\,{}^2D^0-2s^22p^2(^3P)4d^2F_{5/2}$
15	158.646	630,302	$2s^22p^3\,{}^2D^0_{5/2}-2s^22p^2(^3P)4d^2F_{7/2}$
(2)	158.105	632,491	$2s^22p^3\,{}^2D^0-2s^22p^2(^3P)4d^2D_{3/2}$
5	158.063	632,659	$2s^22p^3\,{}^2D^0-2s^22p^2(^3P)4d^2D_{5/2}$
2	157.862	633,465	$2s^22p^3\,{}^4S^0_{3/2}-2s^22p^2(^3P)4s^4P_{1/2}$
3	157.781	633,790	$2s^22p^3\,{}^4S^0_{3/2}-2s^22p^2(^3P)4s^4P_{3/2}$
5	157.626	634,413	$2s^22p^3\,{}^4S^0_{3/2}-2s^22p^2(^3P)4s^4P_{5/2}$
3	156.873	637,458	$2s^22p^3\,{}^2P^0-2s^22p^2(^1D)4d^2D$
5*h*	156.480	639,059	$2s^22p^3\,{}^2P^0-2s^22p^2(^1D)4d^2P$
5	154.488	647,299	$2s^22p^3\,{}^2P^0-2s^22p^2(^1S)4d^2D$
15	152.231	656,896	$2s^22p^3\,{}^2D^0-2s^22p^2(^1D)4d^2F$
15	151.817	658,662	$2s^22p^3\,{}^2D^0-2s^22p^2(^1S)4d^2D$
( )	151.456	calc.	$2s^22p^3\,{}^2D^0-2s^22p^2(^1S)4d^2P$ (O V)
1	150.931	662,554	$2s^22p^3\,{}^2P^0-2s^22p^2(^1D)5s^2D$
2	149.589	668,498	$2s^22p^3\,{}^2D^0-2s^22p^2(^1S)4d^2D$
4	148.942	671,402	$2s^22p^3\,{}^4S^0_{3/2}-2s^22p^2(^3P)4d^4P_{5/2}$
3	148.787	672,102	$2s^22p^3\,{}^4S^0_{3/2}-2s^22p^2(^3P)4d^4P_{3/2}$
1	148.660	672,676	$2s^22p^3\,{}^4S^0_{3/2}-2s^22p^2(^3P)4d^4P_{1/2}$
2*db*	146.262	683,704	$2s^22p^3\,{}^2D^0-2s^22p^2(^1D)5s^2D$
1	144.288	693,106	$2s^22p^3\,{}^4S^0_{3/2}-2s^22p^2(^3P)5s^4P_{1/2}$
2	144.151	693,717	$2s^22p^3\,{}^4S^0_{3/2}-2s^22p^2(^3P)5s^4P_{3/2}$
2	144.019	694,353	$2s^22p^3\,{}^4S^0_{3/2}-2s^22p^2(^3P)5s^4P_{5/2}$
3	142.929	699,648	$2s^22p^3\,{}^2D^0-2s^22p^2(^1D)5d^2F$
3	140.127	713,638	$2s^22p^3\,{}^2D^0-2s^22p^2(^1D)6s^2D$

* Identified by Boyce.

operate at higher pressures. However, quadrupling the pressure appeared to make the discharge brighter so that shorter exposures were needed, without changing the degree of excitation appreciably.

Ne IV

The spectrum of Ne IV was very well developed, the strongest lines on the plates being due usually to Ne IV. The identifications by Boyce were corroborated and the analysis extended to include 117 lines which arise from transitions among 70 levels. The lines identified as Ne IV are given in Table I. The intensities and characteristics of the lines are given in the first column; in the second the wave-lengths in angstroms; in the third the wave numbers in reciprocal centimeters, and in the fourth the assignment. An *h* after the intensity indicates that the line was not sharp. Parentheses, ( ), around the intensity or in place of an intensity estimate indicated that the line was partially or completely obscured by neighboring lines. The symbol *db* after an intensity indicates that the line appeared double but unresolved. A *w* indicates that the line was very wide. The abbreviation calc. in place of a wave number in the second column indicates that the wave-length

was calculated from the position of the levels concerned as determined by experimental evidence and that the emission line was not observed.

Most of the assignments seem to be quite certain from their agreement with the predicted positions of the levels, and with the predicted multiplet separations, the intensities of the lines relative to neighboring lines, and the consistency of the assignments with each other.

The lowest configurations of Ne IV are the $2s^22p^3$, giving rise to the lowest terms of both the doublet and the quartet systems; the $2s2p^4$ and the $2p^5$. The higher even terms are due to the configurations $2s^22p^2ns$ and $2s^22p^2nd$. These have been fairly well established for $n=3$, 4. A few levels for which $n=5$ have been found and in the doublet spectrum one identification for $n=6$ is made. The line identified as arising from a transition between the $2p^2(^1D)6s^2D$ levels and the low $^2D^0$ level fits well in a Ritz series formula for the $2s^22p^3\ ^2D^0-2s^22p^2(^1D)ns^2D$ series and is probably correctly assigned.

It is surprising that so little evidence as to the positions of the higher odd levels in the doublet system can be found. Although several transitions between high odd levels and lower even levels should give lines of considerable strength in the region investigated, none of these has been certainly identified in the doublet spectrum.

Although special efforts were made to resolve the groups of lines at λλ469.8 and 521.8, no resolution beyond that obtained by Boyce resulted. The assignments of values in these groups are accordingly those given by Boyce as are the wave-lengths of the λ469 group which appeared as a single very broad band on our plates. The intensities and the wave-lengths of the 521 group are those determined in this investigation. The average value obtained from eleven pairs of lines for the separation of the $2s^22p^3\ ^2D^0$ levels from the $2s^22p^3\ ^2P^0$ levels is 21,205 cm^{-1}. This is taken as the separation of the centers of gravity and the positions of the levels are given accordingly, with separations according to Boyce's estimates. The term table for the doublet system is given in Table II. The position of the $2s^22p^3\ ^2D^0$ levels relative to the ground state of Ne V is determined from the limit of the $2s^22p^3\ ^2D^0-2s^22p^2(^1D_2)ns\ ^2D$ series as determined with a Ritz formula, and the observed $^1D_2-{}^3P_0$ separation in Ne V. The limit of the series is 773,459 cm^{-1}. The $^1D_2$ level is found to be 30,294 cm^{-1} above the $^3P_0$ level. The value 743,165 cm^{-1} thus arrived at is taken to be the position of the center of gravity of the $2s^22p^3\ ^2D^0_{5/2,3/2}$ pair. No combinations between the doublet and quartet systems have been observed.

In the quartet system the transitions from high levels of even parity to the low $^4S^0$ are well established. The positions of the $2p^2(^3P)nd\ ^4D$ and ^4F levels are still undetermined. Here the positions of the high odd levels seem quite

TABLE II. *Term table for the doublet system of* Ne IV.

CONFIG.	TERM	CM^{-1}	CONFIG.	TERM	CM^{-1}	CONFIG.	TERM	CM^{-1}	CONFIG.	TERM	CM^{-1}
$2s^22p^3$	$^2D^0_{5/2}$	38,540	$2p^5$	$^2P^0_{1/2}$	483,275	$2s^22p^2(^3P)3d$	$^2D_{3/2}$	584,508	$2s^22p^3(^3P)4d$	$^2F_{7/2}$	668,842
	$^2D^0_{3/2}$	38,565	$2s^22p^3(^3P)3s$	$^2P_{1/2}$	485,805	$2s^22p^2(^1D)3d$	^2F	603,007		$^2D_{3/2}$	671,017
	$^2P^0_{1/2}$	59,747		$^2P_{3/2}$	486,507		^2D	606,708		$^2D_{5/2}$	671,177
	$^2P^0_{3/2}$	59,757	$2s^22p^2(^1D)3s$	$^2D_{5/2,3/2}$	509,001		$^2P_{1/2}$	610,258	$2s^22p^2(^1D)4d$	^2F	695,445
$2s2p^4$	$^2D_{5/2}$	251,397	$2s^22p^2(^1S)3s$	$^2S_{1/2}$	549,302		$^2P_{3/2}$	610,371		^2D	697,212
	$^2D_{3/2}$	251,413	$2s^22p^2(^3P)3d$	$^2P_{3/2}$	573,558		$^2S_{1/2}$	614,072		^2P	698,813
	$^2S_{1/2}$	296,941		$^2P_{1/2}$	573,943	$2s^22p^2(^3P)4s$	$^2P_{1/2}$	633,456	$2s^22p^2(^1S)4d$	^2D	707,050
	$^2P_{3/2}$	317,341	$2s^22p^2(^1s)3d$	^2D	574,505		$^2P_{3/2}$	634,065	$2s^22p^2(^1D)5s$	^2D	722,280
	$^2P_{1/2}$	318,042		$^2F_{5/2}$	576,965	$2s^22p^2(^1D)4s$	^2D	661,714	$2s^22p^2(^1D)5d$	^2F	738,197
$2p^5$	$^2P^0_{3/2}$	482,213		$^2F_{7/2}$	577,685	$2s^22p^2(^3P)4d$	$^2F_{5/2}$	668,185	$2s^22p^2(^1D)6s$	^2D	752,187
				$^2D_{3/2}$	584,275						

TABLE III. *Term table for the quartet system of* Ne IV.

CONFIG.	TERM	CM^{-1}	CONFIG.	TERM	CM^{-1}	CONFIG.	TERM	CM^{-1}	CONFIG.	TERM	CM^{-1}
$2s^22p^3$	$^4S^0_{3/2}$	0	$2s^22p^2(^3P)3p$	$^4P^0_{5/2}$	524,676	$2s^22p^2(^3P)4s$	$^4P_{5/2}$	633,790	$2s^22p^3(^3P)4p$	$^4P^0_{5/2}$	643,975
$2s2p^4$	$^4P_{5/2}$	183,860		$^4P^0_{3/2}$	525,017		$^4P_{3/2}$	634,413		$^4S^0_{3/2}$	648,060
	$^4P_{3/2}$	184,477		$^4S^0_{3/2}$	532,978	$2s^22p^2(^3P)4p$	$^4D^0_{1/2}$	641,908	$2s^22p^3(^3P)4d$	$^4P_{5/2}$	671,402
	$^4P_{1/2}$	184,799	$2s^22p^2(^3P)3d$	$^4P_{5/2}$	579,307		$^4D^0_{3/2}$	642,184		$^4P_{3/2}$	672,102
$2s^22p^3(^3P)3s$	$^4P_{1/2}$	478,701		$^4P_{3/2}$	579,626		$^4D^0_{5/2}$	642,472		$^4P_{1/2}$	672,676
	$^4P_{3/2}$	479,079		$^4P_{1/2}$	579,737		$^4D^0_{7/2}$	642,934	$2s2p^3(^4S)3d$	$^4D^0$	672,799
	$^4P_{5/2}$	479,651	$2s2p^3(^4S)3s$	$^4S^0_{3/2}$	588,021	$2s^22p^2(^3P)4p$	$^4P^0_{1/2}$	643,239	$2s^22p^2(^3P)5s$	$^4P_{1/2}$	693,106
$2s^22p^2(^3P)3p$	$^4P^0_{1/2}$	524,391	$2s^22p^2(^3P)4s$	$^4P_{1/2}$	633,465		$^4P^0_{3/2}$	643,672		$^4P_{3/2}$	693,717
										$^4P_{5/2}$	694,353

TABLE IV. *Lines identified as belonging to the spectrum of* Ne V.

INT.	λ A.U.	ν CM^{-1}	TRANSITION
80	572.336	174,722	$2s^22p^2\ ^3P_2-2s2p^3\ ^3D^0_3$
25	572.106	174,793	$2s^22p^2\ ^3P_2-2s2p^3\ ^3D^0_2$
50	569.830	175,491	$2s^22p^2\ ^3P_1-2s2p^3\ ^3D^0_2$
25	569.759	175,513	$2s^22p^2\ ^3P_1-2s2p^3\ ^3D^0_1$
40	568.418	175,927	$2s^22p^2\ ^3P_0-2s2p^3\ ^3D^0_1$
( )	488.940	calc.	$2s^22p^3\ ^3P^0_{2,1,0}-2p^4\ ^3P_2$ (Ne III)
3*w*	487.070	205,309	$2s2p^3\ ^3P^0_{2,1}-2p^4\ ^3P_1$
50	482.987	207,045	$2s^22p^2\ ^3P_2-2s2p^3\ ^3P^0_{2,1}$
25	481.361	207,744	$2s^22p^2\ ^3P_1-2s2p^3\ ^3P^0_{2,1}$
15	481.281	207,779	$2s^22p^2\ ^3P_1-2s2p^3\ ^3P^0_0$
25	480.406	208,157	$2s^22p^2\ ^3P_0-2s2p^3\ ^3P^0_1$
5	422.347	236,772	$2s2p^3\ ^5D^0_{2,1}-2p^4\ ^3P_2$
15	422.214	236,847	$2s2p^3\ ^3D^0_3-2p^4\ ^3P_2$
15	420.951	237,557	$2s2p^3\ ^3D^0_{2,1}-2p^4\ ^3P_1$
10	420.386	237,876	$2s2p^3\ ^3D^0_1-2p^4\ ^3P_0$
25	416.834	239,904	$2s^22p^2\ ^1S_0-2s2p^3\ ^1P^0_1$
80	416.198	240,270	$2s^22p^2\ ^1D_2-2s2p^3\ ^1D^0_2$
100	365.594	273,526	$2s^22p^2\ ^1D_2-2s2p^3\ ^1P^0_1$
50	359.385	278,253	$2s^22p^2\ ^3P_2-2s2p^3\ ^3S^0_1$ Blend O III
50	358.472	278,962	$2s^22p^2\ ^3P_1-2s2p^3\ ^3S^0_1$ Blend N III
40	357.955	279,365	$2s^22p^2\ ^3P_0-2s2p^3\ ^3S^0_1$
2	195.621	511,193	$2s2p^3\ ^3P^0_1-2s2p^2(^4P)3s^3P_0$
3	195.553	511,370	$2s2p^3\ ^3P^0_{2,1}-2s2p^2(^4P)3s^3P_1$
5	195.368	511,854	$2s2p^3\ ^3P^0_{2,1}-2s2p^2(^4P)3s^3P_2$
10	184.730	541,331	$2s^22p^2\ ^1S_0-2s^22p(^2P)3s^1P^0_1$
50	173.932	574,937	$2s^22p^2\ ^1D_2-2s^22p(^2P)3s^1P^0_1$
5	167.921	595,518	$2s^22p^2\ ^3P_2-2s^22p(^2P)3s^3P^0_1$
5	167.837	595,816	$2s^22p^2\ ^3P_1-2s^22p(^2P)3s^3P^0_0$
25	167.670	596,410	$2s^22p^2\ ^3P_2-2s^22p(^2P)3s^3P^0_2$ $2s^22p^2\ ^3P_1-2s^22p(^2P)3s^3P^0_1$
3	167.610	596,623	$2s^22p^2\ ^3P_0-2s^22p(^2P)3s^3P^0_1$
15	167.483	597,076	$2s^22p^2\ ^3P_1-2s^22p(^2P)3s^3P^0_2$
8	164.294	608,665	$2s^22p^2\ ^5S^0_2-2s^22p(^4P)3s^5P_1$
10	164.145	609,217	$2s^22p^2\ ^5S^0_2-2s^22p(^4P)3s^5P_2$ (O V)
10	164.023	609,670	$2s^22p^2\ ^5S^0_2-2s^22p(^4P)3s^5P_3$
2	156.610	638,529	$2s^22p^2\ ^1S_0-2s^22p(^2P)3d^1P^0_1$
12	151.424	660,397	$2s^22p^2\ ^1D_2-2s^22p(^2P)3d^1D^0_2$(O V, Ne IV)
3	148.787	672,102	$2s^22p^2\ ^1D_2-2s^22p(^2P)3d^1P^0_1$
15	147.132	679,662	$2s^22p^2\ ^1D_2-2s^22p(^2P)3d^1F^0_3$
15	143.344	697,623	$2s^22p^2\ ^3P_2-2s^22p(^2P)3d^3D^0_3$
10	143.273	697,968	$2s^22p^2\ ^3P_1-2s^22p(^2P)3d^3D^0_2$
5	143.219	698,231	$2s^22p^2\ ^3P_0-2s^22p(^2P)3d^3D^0_1$
15	142.724	700,653	$2s^22p^2\ ^3P_2-2s^22p(^2P)3d^3P^0_2$
4	142.661	700,962	$2s^22p^2\ ^3P_2-2s^22p(^2P)3d^3P^0_1$
10	142.503	701,746	$2s^22p^2\ ^3P_{1,0}-2s^22p(^2P)3d^3P^0_{2,1,0}$
10	142.441	702,045	$2s^22p^2\ ^3P_1-2s^22p(^2P)3d^3P^0_0$
15	140.791	710,273	$2s2p^3\ ^5S^0_2-2s2p^2(^4P)3d^5P_3$
15	140.757	710,444	$2s2p^3\ ^5S^0_2-2s2p^2(^4P)3d^5P_2$
5	140.716	710,651	$2s2p^3\ ^5S^0_2-2s2p^2(^4P)3d^5P_1$
2	136.215	734,134	$2s^22p^3\ ^5S^0_2-2s2p^2(^4P)4s^5P$
5	129.034	774,990	$2s^22p^2\ ^1D_2-2s^22p(^2P)4s^1P^0_1$
1	128.793	776,440	$2s2p^3\ ^5S^0_2-2s2p^2(^4P)4d^5P?$
2	125.830	794,723	$2s^22p^2\ ^3P-2s^22p(^2P)4s^3P^0$
3	123.712	808,329	$2s^22p^2\ ^1D_2-2s^22p(^2P)4d^1D^0_2$
20*db*	122.520	816,913	$2s^22p^2\ ^1D_2-2s^22p(^2P)4d^1F^0_3$ Also Ne VI
1	118.841	841,460	$2s^22p^2\ ^3P-2s^22p(^2P)4d^3D^0$
5	118.715	842,354	$2s^22p^2\ ^3P-2s^22p(^2P)4d^3P^0$

certainly determined by the transitions into the $2s2p^4\ ^4P$ levels. However, the transitions from the $3p\ ^4D^0$ levels seem to be covered by impurity lines, and the exact positions of the $4p\ ^4D^0_{5/2}$ and $^4P^0_{1/2}$ are somewhat doubtful due to overlapping by neighboring lines. Table III gives the term table for the quartet system. A Ritz formula fitted to the $2s^22p^3\ ^4S^0_{3/2}-2s^22p^2(^3P_2)ns\ ^4P_{5/2}$ series gives the limit 782,826 cm^{-1}. This locates the $^4S^0_{3/2}$ level 781,714 cm^{-1} below the $2s^22p^2\ ^3P_0$ level of Ne V, giving an ionization potential of 96.43 volts for Ne IV.

Ne V

The spectrum of Ne V was much weaker than that of Ne IV. Table IV includes 56 lines which have been assigned to transitions among 47 levels. The arrangement and notation of the table are the same as for Table I. The notations after the assignments indicate that the line is classified in two spectra and that the lines of another spectrum partially obscure the present line. Although many of the levels are determined from only one line the assignments appear fairly safe, with a few exceptions. The $2s^22p^2\ ^1D_2-2s^22p(^2P)4d\ ^1F^0_3$ assignment is that line of a pair which gives best agreement with the predicted value. The relative intensities of the two groups of lines identified as $2s^22p^2\ ^3P-2s^22p(^2P)4d\ ^3D^0$ and $^3P^0$ appear out of proportion. It may be that the shorter wave-length group is in coincidence with some other lines.

Certain lines which should be included in this spectrum are missing because overlapping lines make their accurate identification impossible. In this group are the transitions from the $2p^4\ ^1D_2$ and $^1S_0$ levels to the $2s2p^3\ ^1D^0_2$ and $^1P^0_1$ levels, which are covered by second-order O III lines, and the $2s2p^3\ ^3P^0-2s2p^2(^4P)3d\ ^3P$ lines which are obscured by the strong O V lines at λ166A.

The term scheme of the singlet system is given in Table V; that of the triplet system in Table VI, and that of the quintet system in Table VII. The absolute value of the $2s^22p^2\ ^3P_0$ level relative to the $2s^22p\ ^2P^0_{1/2}$ level of Ne VI is estimated from the $2s^22p^2\ ^3P_2-2s^22p(^2P_{3/2})nd\ ^3P^0$ and $^3D^0$ series, for each of which two members are observed, to be 1,019,950 cm^{-1}. This corresponds to an ionization potential of 125.8 volts. From the intersystem combinations $^3P_1-{}^1D_2$, $^3P_2-{}^1D_2$ ob-

TABLE V. *Term table for the singlet system of* Ne V.

CONFIG.	TERM	CM^{-1}	CONFIG.	TERM	CM^{-1}
$2s^22p^2$	$^1D_2$	30,294	$2s^22p(^2P)3d$	$^1D^0_2$	690,691
	$^1S_0$	63,900		$^1P^0_1$	702,412
$2s2p^3$	$^1D^0_2$	270,564		$^1F^0_3$	709,956
	$^1P^0_1$	303,812	$2s^22p(^2P)4s$	$^1P^0_1$	805,284
$2s^22p(^2P)3s$	$^1P^0_1$	605,231	$2s^22p(^2P)4d$	$^1D^0_2$	838,623
				$^1F^0_3$	847,207?

TABLE VI. *Term table for the triplet system of* Ne V.

CONFIG.	TERM	CM^{-1}	CONFIG.	TERM	CM^{-1}	CONFIG.	TERM	CM^{-1}	CONFIG.	TERM	CM^{-1}
$2s^22p^2$	$^3P_0$	0	$2s2p^3$	$^3P^0_0$	208,193	$2s^22p(^3P)3s$	$^5P^0_2$	597,492	$2s2p^2(^4P)3s$	$^3P_0$	719,350
	$^3P_1$	414		$^3P^0_1$	279,365	$2s^22p(^3P)3d$	$^3D^0_1$	698,231		$^3P_1$	719,527
	$^3P_2$	1112	$2p^4$	$^3P_2$	412,681		$^3D^0_2$	698,382		$^3P_2$	720,011
$2s2p^3$	$^5D^0_0$	175,834		$^3P_1$	413,466		$^3D^0_3$	698,735	$2s2p(^3P)4s$	$^3P^0$	795,279
	$^3D^0_2$	175,905		$^3P_0$	413,803		$^5P^0_2$	701,765	$2s^22p(^3P)4d$	$^3D^0$	842,020
	$^3D^0_1$	175,927	$2s^22p(^3P)3s$	$^3P^0_2$	596,230		$^5P^0_1$	702,074		$^3P^0$	842,914
	$^3P^0_2$	208,157		$^3P^0_1$	596,626		$^5P^0_0$	702,459			
	$^3P^0_1$										

TABLE VII. *Term table for the quintet system of* Ne V.

CONFIG.	TERM	CM^{-1}	CONFIG.	TERM	CM^{-1}
$2s2p^3$	$^5S^0_2$	86,700	$2s2p^2(^4P)3d$	$^5P_2$	797,144
$2s2p^2(^4P)3s$	$^5P_1$	695,365		$^5P_1$	797,351
	$^5P_2$	695,917	$2s2p^2(^4P)4s$	^5P	820,834
	$^5P_3$	696,370	$2s2p^2(^4P)4d$	^5P	863,140
$2s2p^2(^4P)3d$	$^5P_3$	796,973			

served in the spectra of gaseous nebulae as given by Bowen,[9] the $2s^22p^2\ ^1D_2$ level is located 30,294 cm^{-1} above the $2s^22p^2\ ^3P_0$ level, giving the value 989,656 cm^{-1} for its position relative to the $2s^22p^2P^0_{1/2}$ level of Ne VI. From isoelectronic sequence data the $2s2p^3\ ^5S^0_2$ level is estimated to be 86,700±300 cm^{-1} above the $2s^22p^2\ ^3P_0$ level. No intersystem combinations have been identified in the extreme ultraviolet.

Ne VI

A few of the stronger lines of Ne VI have been identified and are recorded in Table VIII. These make possible the location of the levels of lower excitation relative to the ground state $^2P^0$. The positions of the levels and the fine structure separations are in good agreement with the predicted values. Two unresolved groups of lines have been identified as belonging to the quartet system. It is unfortunate that the $2p^3\ ^4S^0_{3/2}$ level was not located. Transitions between this level and the low $2s2p^2\ ^4P$ should produce lines at about 220,000 cm^{-1} and from this group the splitting of the ^4P could be evaluated.

The resulting term table for the doublet system is given in Table IX and for the quartet system in Table X. The value of the $2s^22p^2P^0_{1/2}$ is estimated from isoelectronic sequence data to be 1,274,000±1000 cm^{-1}. This gives an ionization potential of 157 volts for Ne VI. The $2s2p^2\ ^4P_{1/2}$

TABLE IX. *Term table for the doublet system of* Ne VI.

CONFIG.	TERM	CM^{-1}	CONFIG.	TERM	CM^{-1}
$2s^22p$	$^2P^0_{1/2}$	0	$2s^2(^1S_0)3s$	$^2S_{1/2}$	722,610
	$^2P^0_{3/2}$	1316	$2s^2(^1S_0)3p$	$^2P^0_{1/2}$	763,096
$2s2p^2$	$^2D_{5/2}$	178,998		$^2P^0_{3/2}$	763,385
	$^2D_{3/2}$	179,020	$2s^2(^1S_0)3d$	^2D	816,405
	$^2S_{1/2}$	232,587	$2s2p(^3P)3p$	^2P	878,852
	$^2P_{1/2}$	249,292		^2S	900,408
	$^2P_{3/2}$	250,112		^2D	906,373

TABLE X. *Term table for the quartet system of* Ne VI.

CONFIG.	TERM	CM^{-1}
$2s2p^2$	^4P	99,300
$2s2p(^3P)3s$	$^4P^0$	834,113
$2s2p(^3P)3d$	$^4D^0$	924,791

[9] I. S. Bowen, Rev. Mod. Phys. **8**, 55 (1936.)

TABLE VIII. *Lines identified as belonging to the spectrum of* Ne VI.

INT.	λ A.U.	ν CM^{-1}	TRANSITION	INT.	λ A.U.	ν CM^{-1}	TRANSITION
15	562.805	177,682	$2s^22p^2P^0_{3/2}-2s2p^2\ ^2D_{5/2}$	2	171.212	584,071	$2s2p^2\ ^2D_{3/2}-2s^2(^1S_0)3p^2P^0_{1/2}$
1	562.735	177,704	$2s^22p^2P^0_{3/2}-2s2p^2\ ^2D_{3/2}$	5*w*	171.114	584,405	$2s2p^3\ ^2D_{5/2,3/2}-2s^2(^1S_0)3p^2P^0_{3/2}$
5	558.595	179,021	$2s^22p^2P^0_{1/2}-2s2p^2\ ^2D_{3/2}$	3	138.630	721,344	$2s^22p^2P^0_{3/2}-2s^2(^1S_0)3s^2S_{1/2}$
5	432.393	231,271	$2s^22p^2P^0_{3/2}-2s2p^2\ ^2S_{1/2}$	3	138.397	722,559	$2s^22p^2P^0_{1/2}-2s^2(^1S_0)3s^2S_{1/2}$
( )	429.947	calc.	$2s^22p^2P^0_{1/2}-2s2p^2\ ^2S_{1/2}$ (O II)	4	136.089	734,813	$2s2p^3\ ^4P-2s2p(^3P)3s^4P^0$
10	403.262	247,978	$2s^22p^2P^0_{3/2}-2s2p^2\ ^2P_{1/2}$	10*w*	122.686	815,089	$2s^22p^2P^0_{3/2}-2s^2(^1S_0)3d^2D$
25	401.939	248,794	$2s^22p^2P^0_{3/2}-2s2p^2\ ^2P_{3/2}$	20*db*	122.520	816,913	$2s^22p^2P^0_{1/2}-2s^2(^1S_0)3d^2D$ (also Ne V)
15	401.138	249,291	$2s^22p^2P^0_{1/2}-2s2p^2\ ^2P_{1/2}$	5*h*	121.140	825,491	$2s2p^3\ ^4P-2s2p(^3P)3d^4D^0$
5	399.820	250,113	$2s^22p^2P^0_{1/2}-2s2p^2\ ^2P_{3/2}$	1	113.870	878,194	$2s2p^2\ ^2P^0-2s2p(^3P)3p^2P$
2	194.936	512,989	$2s2p^2\ ^2P_{3/2}-2s^2(^1S_0)3p^2P^0_{1/2}$	1	111.142	899,750	$2s2p^2\ ^2P^0-2s2p(^3P)3p^2S$
2	194.839	513,244	$2s2p^2\ ^2P_{3/2}-2s^2(^1S_0)3p^2P^0_{3/2}$	2	110.410	905,715	$2s2p^2\ ^2P^0-2s2p(^3P)3p^2D$
25*db*	194.625	513,808	$2s2p^2\ ^2P_{1/2}-2s^2(^1S_0)3p^2P^0_{1/2}$ (O V)				
3	188.424	530,718	$2s2p^2\ ^2S_{1/2}-2s^2(^1S_0)3p^2P^0_{3/2}$ (O ?)				
	188.498	calc.	$2s2p^2\ ^2S_{1/2}-2s^2(^1S_0)3p^2P^0_{1/2}$				

level is estimated to be 99,300±500 cm^{-1} above the $2s^22p\ ^2P^0_{1/2}$ level.

In conclusion the authors wish to thank Professor J. C. Boyce for much helpful advice during the course of this work, and Professor G. R. Harrison for the use of the measuring engines in the Massachusetts Institute of Technology laboratory.

MARCH 1, 1941 PHYSICAL REVIEW VOLUME 59

A New Mass Spectrograph and the Isotopic Constitution of Nickel

HENRY A. STRAUS
Ryerson Physical Laboratory, University of Chicago, Chicago, Illinois
(Received January 9, 1941)

A new double focusing mass spectrograph which has a 90° electric field and a 60° magnetic field has been constructed and used to determine the isotopic constitution of nickel. The instrument and the null method of measurement are described. The isotopic constitution of nickel is found to be Ni^{58}—62.8 percent Ni^{60}—29.5 percent, Ni^{61}—1.7 percent, Ni^{62}—4.7 percent, Ni^{64}—1.3 percent.

INTRODUCTION

THE published values of the abundance ratios among the isotopes of nickel have for some time shown considerable discrepancies. Aston[1] found Ni^{61} to be 1.7 percent of the total and failed to find Ni^{64}. De Gier and Zeeman,[2] who used the parabola method of positive ion analysis, failed to find Ni^{61}, probably because of the low resolving power of their instrument, but found Ni^{64} to constitute 0.9 percent of the total. Lub,[3] using a similar apparatus, also found Ni^{64} to be 0.9 percent of the total, but found Ni^{61}, which he estimated to be 0.1 percent of the total. Dempster[4] published a photograph of the mass spectrum of nickel in which it appeared that the abundance of Ni^{61} was approximately equal to the abundance of Ni^{64}.

These results were all obtained from photographic observations. Dempster used an oscillating spark between nickel electrodes as an ion source. The others all used a discharge tube containing nickel carbonyl. The organic compounds of the C_5 group, present in the latter case, may lead to erroneous estimates of the relative intensities of the nickel lines by their superposition on the nickel lines.

[1] F. W. Aston, Proc. Roy. Soc. **149**, 396 (1935).
[2] J. de Gier and P. Zeeman, Proc. K. Akad. Amst. **38.8**, 810 (1935).
[3] W. A. Lub, Proc. K. Akad. Amst. **42.3**, 253 (1939).
[4] A. J. Dempster, Phys. Rev. **50**, 98 (1936).

APPARATUS

A new double focusing mass spectrograph has been constructed. The design of this instrument is based on the theory published by R. Herzog.[5] A radial electric field is used as an energy analyzer in this instrument. The mean orbit radius in this field is ten cm and the deflection of the beam is 90°. Guard plates, which are applied at the ends of the field to reduce the stray field, are cut so that they do not interfere with the passage of the beam. A magnetic field serves as a momentum analyzer and gives the mass dispersion. The mean radius of the orbits in this field is 16.6 cm and the beam is deflected 60°.

In Herzog's paper the fundamental focusing condition is given by

$$(l'-g')(l''-g'')=f^2. \qquad (1)$$

Here l' is the distance from the source slit to the edge of the field, measured along the orbit, and g'' is the distance beyond the field at which an originally parallel bundle of rays meet; l'' is the distance beyond the field at which the orbits intersect or focus. g' is the distance from the field to the point from which diverge orbits that are parallel after passing through the field. f is the focal length. Continuing in Herzog's notation, we

[5] R. Herzog, Zeits. f. Physik **89**, 447 (1934).

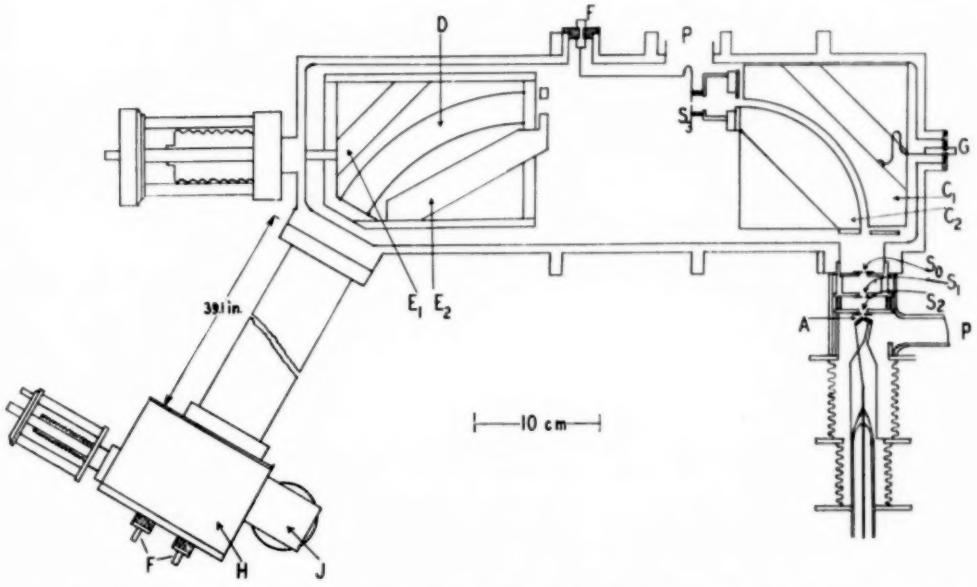

FIG. 1. Plan of mass spectrograph including section through deflection chamber and source. The yoke and core of the magnet are omitted. The parts are labeled as follows: S_0, S_1, S_2, S_3 are slits. P refers to pumping lines. A is the spark and C_1 and C_2 are the electric field plates. G is the lead for the deflecting potential. F are electrometer leads. D is the pole piece and E_1 and E_2 the pole piece spacers. H is the collector chamber and J the secondary electron magnet.

have for the radial electric field,

$$f_e = a_e/\sqrt{2}\,\sin\sqrt{2}\Phi_e, \tag{2}$$

$$g_e = a_e\cot\sqrt{2}\Phi_e. \tag{3}$$

In these equations a_e is the radius of the orbit in the electric field and Φ_e is the deflection in the field. For the dimensions chosen, f_e is 8.89 cm and g_e is -5.38 cm. The source slit, S_0 in Fig. 1, is at a distance 3.50 cm from the entrance to the electric field. Equation (1) thus shows that the image produced by the electric field is at $l''=3.5$ cm. In the magnetic field the corresponding equations are

$$f_m = a_m/\sin\Phi_m, \tag{4}$$

$$g_m = a_m\cot\Phi_m, \tag{5}$$

where a_m is the orbit radius in the magnetic field and Φ_m is the angle of deflection. For the dimensions given, f_m is 19.17 cm and g_m is 9.58 cm.

To obtain velocity focusing, it is necessary that the velocity dispersion in the two fields be equal. For the electric field this quantity is measured by $K_e=a_e[1+f_e/(l_e'-g_e)]=20$. Thus $K_m=a_m[1+f_m/(l_m''-g_m)]=20$. This fixes l_m'', the distance from the magnetic field to the collector, as 103.1 cm. The fundamental equation for a focus now determines the last dimension of the apparatus.

When g_m, l_m'' and f_m are substituted in $(l_m'-g_m)(l_m''-g_m)=f_m^2$, l_m', the distance from S_3 to the magnetic field is 13.5 cm. The dispersion, as calculated from Herzog's theory, is 4.9 mm for 1 percent mass difference, agreeing approximately with 5.05 mm observed.

As mentioned above, the electric field forms an energy spectrum 3.5 cm beyond the field. A two-millimeter slit, S_3 is placed here to select a range of energy from the ion beam to be passed into the magnetic field. At a distance of 13.5 cm beyond this slit the ions effectively enter the magnetic field. The effective magnetic field was used in calculating the orbits. The effective field includes the integrated effect of the stray field which was calculated by the Schwartz transformation. The final image is formed 103 cm from the point at which the ions effectively leave the magnetic field.

In the instrument, as used, the source slit, S_0, was 0.15 mm wide. Between it and the source were two other slits. S_1 was 2 cm from S_0 and was 2.0 mm wide. It was at ground potential with S_0. S_2 was just in front of the spark A, and was maintained at a positive potential with

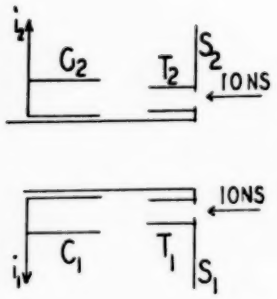

FIG. 2. The collector system in cross section. S_1T_1 and S_2T_2 are the shields and C_1 and C_2 are the collectors. The charges collected are measured by the circuit indicated in Fig. 3.

the source. This slit system greatly impeded the flow of gas from the source into the spectrograph chamber. Pumping the source independently of the chamber thus made it possible to maintain a good vacuum while the source was running.

The ions to be studied were produced in a spark between electrodes of the metal. The spark was maintained at a positive potential with respect to ground by a half-wave rectifier set with condensers whose potential was indicated by a resistance and a milliameter. The spark was energized by a Tesla circuit.

The potential applied to the plates of the electric field was supplied by a high voltage lead battery on trickle charge in some runs and by a stabilized source[6] of 950 volts for the rest of the observations.

The magnet consisted of a pair of pole pieces separated by 0.157 inch which were mounted as a unit inside the spectrograph chamber and an external double yoke on which were mounted the core pieces. Each core piece was wound with 750 turns of number twelve wire. Between alternate layers of the windings, sheets of copper with exposed fins were interposed to reduce the time required for the magnet to come to thermal equilibrium. The magnet current was observed by means of a potentiometer. The magnet current, which was controlled manually with slide wire rheostats, was supplied by a twelve-volt lead battery.

The chamber which held the field assemblies was a bronze casting which had been dipped in tin to make it vacuum tight. The lid was removable to permit access to the field assemblies. Steel inserts were included in the top and the bottom of the chamber to reduce the power required to attain the magnetic field intensity required and to reduce the stray field.

The collector system, whose essential features are shown in Fig. 2, consisted of a pair of Faraday chambers, C_1 and C_2, connected through amber bushings to the electrometers. The shields were equipped with tubes, T_1 and T_2, back of the openings, which were somewhat wider than the focused beam of an isotope. The whole assembly was placed in a magnetic field so the secondary electrons from the openings would not reach the collectors. One of the collectors was fixed in position. The other could be varied in position, which could be observed, by a micrometer screw acting through a sylphon bellows.

Each collector was connected to an electrometer and to one side of a condenser whose other plate was mounted on split insulation and connected to a source of potential, as in Fig. 3. As the collectors receive charge, the two electrometers are maintained at zero potential by adjusting R_1, R_2, and R_3. R_1 and R_2 are dial boxes and R_3 is a potentiometer. After charge has been collected, the ratio of the charges on the two systems when the electrometers show a null reading can be found from the equation

$$(Q_1/Q_2)=kR_1/(R_1+R_2). \qquad (6)$$

Here $k=C_1/C_2$ and is determined by a capacity bridge measurement. The method is similar to that developed by V. A. Bailey[7] and Vanderberg.[8]

OBSERVATIONS

The observations on the abundance ratios in nickel were made with the null method described

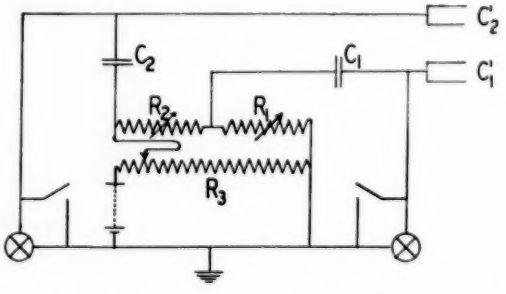

FIG. 3. The circuit used to make the charge comparisons. C_1' and C_2' are the collectors.

[6] R. D. Evans, Rev. Sci. Inst. **5**, 371 (1934).

[7] V. A. Bailey, Phil. Mag. **50**, 381 (1929).

[8] R. M. Vanderberg, Phys. Rev. **59**, 114A (1941).

above. The pressure in the spectrograph, as indicated by an ionization gauge, was less than 5×10^{-6} mm during all the final measurements and was usually about 1 or 2×10^{-6} mm. These pressures were maintained to avoid excessive scattering and loss of charge in the ion beams. The magnet and the voltage stabilizer were allowed to come to equilibrium before any readings were taken.

The collectors were set to a separation corresponding to two mass units to obtain the ratios $Ni^{58} : Ni^{60}$, $Ni^{60} : Ni^{62}$, $Ni^{62} : Ni^{64}$. The background was measured by comparing the background at mass numbers 59 and 63 with the current at Ni^{61}. With the collectors set at a separation corresponding to three mass numbers, the ratio $Ni^{61} : Ni^{64}$ was obtained, as well as a comparison of the background at mass numbers 59 and 65 with Ni^{62}.

Readings were taken of the ratio of the charges collected by the two electrometers at each of a series of different positions as the beams were moved simultaneously by small steps across the respective collectors. Figure 4 shows the behavior of the ratio during a set of observations. On the plateau the ratio remained constant within a few percent. The ratio observed was found to be insensitive to variations of the electric deflecting field. This indicates that there was no systematic weighting of the ratios due to a partial separation of the isotopes in the electric field, caused by a stray magnetic field.

The means of the measurement are:

$$Ni^{60} : Ni^{58} = 0.470 \pm 0.020;$$
$$Ni^{62} : Ni^{60} = 0.158 \pm 0.007;$$
$$Ni^{64} : Ni^{62} = 0.272 \pm 0.01;$$
$$Ni^{61} : Ni^{61} = 0.662 \pm 0.015.$$

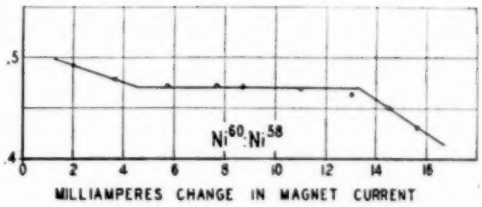

FIG. 4. Results of a set of observations on the ratio $Ni^{60} : Ni^{58}$.

Each of these values is the average of approximately 100 electrometer comparisons.

The correction for background is important only for the weak isotope at 61 which is adjacent to the very strong line at 60 and to the strong line at 62. The corrections to 61 were obtained from the measured background at 59 and 63 by assuming that the background at these mass numbers could be ascribed to the neighboring isotopes in the ratio of their abundance. The measured backgrounds were: $59 : Ni^{61} = 0.20$; $59 : Ni^{62} = 0.09$; $63 : Ni^{61} = 0.06$; $65 : Ni^{62} = 0.007$. With the background correction the ratio $Ni^{64} : Ni^{61}$ is 0.745. The isotopic constitution of nickel calculated on this basis is: Ni^{58}—62.8 percent, Ni^{60}—29.5 percent, Ni^{61}—1.7 percent, Ni^{62}—4.7 percent, Ni^{64}—1.3 percent.*

The author wishes to express his appreciation to Professor A. J. Dempster, who suggested this problem, for his advice concerning this investigation.

* *Note added in proof.*—This isotopic constitution, combined with the isotopic weights published by T. Okuda, K. Ogata, H. Kuroda, S. Shima and S. Shindo, Phys. Rev. **59**, 104 (1941), gives 58.84 as the chemical atomic weight of nickel.

On the Magnitude of Electronic Charges

ALFRED LANDÉ
Mendenhall Laboratory, Ohio State University, Columbus, Ohio

(Received November 25, 1940)

A charged point particle is characterized first by its classical rest energy $\epsilon_0=mc^2$, second by the characteristic wave period $t_0=4\pi e^2/3mc^3$ that occurs in the classical formula $\phi_\tau/\phi_\infty=[1+(t_0/\tau)^2]^{-1}$ for the ratio of the scattering cross section for light of period τ compared with the Thomson cross section ϕ_∞ for light of period ∞. Quantum theory asks that the product $\epsilon_0 t_0$ be as small as $h/210$ as the smallest eigenvalue of a proper value problem. The classical values of ϵ_0 and t_0 together with their quantum product yield the value $\alpha\approx 1/140$ for Sommerfeld's fine-structure constant. The discrepancy may be due to our *classical* treatment of the interaction between light and charged matter. The Lorentz invariance of the energy transmission coefficient $R_\tau=\phi_\tau/\phi_\infty$ makes R_τ apt to serve as a reduction factor in the theory of radiation for avoiding the usual infinities. As a first example, the energy reduction R_τ leads to a modified Coulomb energy together with a finite electrostatic self-energy corresponding to an electrostatic mass $m_{\text{stat}}=m$.

THE velocity of a particle can be found in two ways; first, by measuring the energy ϵ and the momentum p so that

$$v/c=pc/\epsilon \quad \text{whereby} \quad \epsilon^2-(pc)^2=\epsilon_0^2, \qquad (1)$$

if ϵ_0 stands for the rest energy; and second, by measuring the path r during a time interval t so that

$$v/c=r/ct \quad \text{whereby} \quad t^2-(r/c)^2=t_0^2, \qquad (2)$$

if t_0 stands for the rest value of the interval t.

The quantities p and ϵ can be measured optically if the particle is charged. The Compton scattering effect yields p and ϵ within certain margins of accuracy since p and ϵ change during the observation. The universal rest energy ϵ_0 which also is the critical photonic energy for the pair production, has a definite value $\epsilon_0=mc^2$ without uncertainty.

The quantities r and t can also be measured optically by means of light waves scattered by the particle. The Lorentz rest system in which the scattering process takes place is defined by the system of interference fringes of the incident and reflected light and matter waves that move through the distance r during t. The position of the maxima cannot be measured exactly at any time. Therefore r and t are determined within a certain margin only, although the rest period t_0 has a definite universal value (see (7)).

The two uncertainties (corpuscular p and ϵ, wave r and t) are reciprocal in the sense of quantum theory. The probability amplitudes $\psi(r, t)$ and $\chi(p, \epsilon)$ comply with the quantum rule (for free particles) that they are Fourier expansions of one another. At the same time ϵ is determined by p and ϵ_0, and t is determined by r and t_0 by virtue of (1) and (2). The Fourier integrals[1] read

$$\chi(p)=h^{-\frac{1}{2}}\int\psi(r) \times\exp\left[i/\hbar(p\cdot r-\epsilon t)\right]dxdydz(t_0/t)^{\frac{1}{2}},$$
$$\psi(r)=h^{-\frac{1}{2}}\int\chi(p) \times\exp\left[-i/\hbar(p\cdot r-\epsilon t)\right]dp_x dp_y dp_z(\epsilon_0/\epsilon)^{\frac{1}{2}}. \qquad (3)$$

The square roots on the right provide for invariant volume elements. The factors $h^{-\frac{1}{2}}$ are chosen so that the two integral equations are mere inversions of one another in the non-relativistic limit. The integrals are carried over positive and negative values of the square roots; they are soluble only for certain proper values of the quantity

$$\epsilon_0 t_0/\hbar=\mu. \qquad (4)$$

[1] The integrals are modifications of Born's integrals. Born modified the writer's original wrong integrals. See A. Landé, J. Frank. Inst. **228**, 459 (1939). M. Born, Proc. Roy. Soc. Edinburgh **59**, 219 (1939). The proper value theory of Born and Fuchs, Proc. Roy. Soc. Edinburgh **60**, 100, 141 (1940) starts from a different background and arrives at different results.

The smallest proper value of μ turns out to be[2]

$$\mu = 0.02985037\cdots \tag{4'}$$

as the smallest root of the transcendental equation $2\pi\mu[Y_0(\mu)]^2 = 1$.

The smallness of the product $\epsilon_0 l_0$ in terms of h, namely $\epsilon_0 l_0/h \approx 1/210$ must be considered as the chief reason for the smallness of the Sommerfeld fine-structure constant α. Indeed, the latter is

$$\alpha = \frac{e^2}{ch} = \frac{e^2}{ct_0\epsilon_0}\cdot\frac{t_0\epsilon_0}{h} = \frac{e^2}{ct_0mc^2}\cdot\mu = \frac{\mu}{\gamma}, \tag{5}$$

if γ is the numerical factor expressing t_0 in terms of e^2/mc^2 by the formula

$$ct_0 = \gamma e^2/mc^2. \tag{6}$$

A tentative value of γ is obtained by identifying t_0 with the characteristic period t_0 that occurs in the scattering cross section ϕ_τ for light of period τ, as compared with the Thomson cross section ϕ_∞ for light of period ∞. The classical theory of the scattering of infinitely weak light waves yields the formula

$$\phi_\tau = \phi_\infty\cdot[1+(\tau/t_0)^2]^{-1} \text{ where } t_0 = 4\pi e^2/3mc^3. \tag{7}$$

From identifying t_0 of (2) with t_0 of (7) we learn that γ is $4\pi/3$, hence

$$\alpha = \mu/\gamma = 0.0298\cdot(3/4\pi) \approx 1/140 \tag{8}$$

instead of the experimental value $\approx 1/137$. The discrepancy may be due partly to the value of ϕ_τ which was obtained from the *classical* scattering of infinitely weak light waves, as against quantized waves of zero-point energy. A uniform theory is wanted in order to replace the two incoherent sections of computing $\alpha = \mu/\gamma$ from a quantum calculation of μ and a classical calculation of γ. The not quite convincing classical reasons for choosing $\gamma = 4\pi/3$ will be discussed in a paper, Part III, in the *Journal of the Franklin Institute* (1941) to which we also refer for the following remarks.

[2] A. Landé, J. Frank. Inst. **229**, 767 (1940). Part I.

The ratio $R_\tau = \phi_\tau/\phi_\infty$ is apt to serve as a reduction factor to rid the radiation theory of infinities. *R is Lorentz-invariant* since ϕ_∞ is a universal constant, and ϕ_τ depends on the scattered period τ and the speed of the scattering particle in the following way. The light may have the period τ for an observer who is at rest together with the particle. If the observer moves with velocity v' relative to the former rest system he will observe a different period τ'. But the scattering cross section, that is, the ratio of the scattered to the incident intensity per unit area will be the same as in the rest system namely R_τ rather than $R_{\tau'}$. Indeed, the scattering cross section can be thought of as the cross section of a (missing) column of light cut out of the incident parallel light rays, the walls of the column being light rays.

A first application of this reduction factor for the energy transmission is offered by the Dirac-Fermi wave theory of the electrostatic interaction between particles and light. This theory leads to the Coulomb energy e_je_k/r_{jk} and to an infinite self-energy. If one assumes, however, that the energy contribution of the waves of period τ is reduced by the invariant factor $R_\tau = \phi_\tau/\phi_\infty$ of (7), then one obtains a modified Coulomb energy

$$(e_je_k/r_{jk})\cdot[1-\exp(-r_{jk}3mc^2/2e^2)] \tag{9}$$

and a finite electrostatic self-energy of value $E_{\text{stat}} = \frac{3}{4}\ mc^2$. This corresponds to an electrostatic mass

$$m_{\text{stat}} = m, \tag{9'}$$

since, according to Abraham, any spherical electric field of energy E_{stat} has an inertia $m_{\text{stat}} = E_{\text{stat}}\cdot(4/3c^2)$. The reduction of the infinite self-energy through radiation damping is preferable to an arbitrary cutting-off process, and perhaps also to those theories (Born-Infeld and Born's reciprocity) that yield the correct finite self-energy only with a certain selection of an adjustable parameter r_0 called "electronic radius" (determination of the factor γ *a posteriori*).

On the Neutron-Proton Interaction*

WILLIAM RARITA† AND JULIAN SCHWINGER
Department of Physics, University of California, Berkeley, California

(Received January 7, 1941)

Field theories of nuclear forces predict the existence of a spin dependent interaction similar in character to the coupling energy between two dipoles. The purpose of this paper is to study the influence of such spin-spin forces on the behavior of the neutron-proton system. A phenomenological theory is developed in which are adopted simplified rectangular well potentials whose constants are determined to fit the binding energy and quadripole moment of the deuteron, and the scattering of slow neutrons in hydrogen. The range of the forces is chosen to be that deduced from proton-proton scattering. The effects investigated include the magnetic moment of the deuteron, the scattering of neutrons in hydrogen, the radiative capture of slow neutrons, and the photo-disintegration of the deuteron. Most of the effects considered can be understood as a simple consequence of the reduced amount of the $^3S_1$ ground state of the deuteron occasioned by the admixture of a small percentage of a $^3D_1$ state. The phenomenological theory here employed adequately represents the experimental data, with the exception of the photomagnetic disintegration of the deuteron which would seem to require a detailed knowledge of the charge-bearing field.

INTRODUCTION

QUANTUM mechanical concepts have been remarkably successful in providing qualitative interpretations of nuclear phenomena. Attempts to obtain quantitative correlations of nuclear data have proceeded by the heuristic introduction of novel interactions with exchange properties. Several field theories have been proposed to supply a physical foundation for the particular forms of these empirical interaction energies. Although these theories have been beset by divergence difficulties, so that no reliance can be placed on the detailed form of the interactions they predict, the field theories do constitute suggestive models for the understanding of the general nature of nuclear forces.

Current nuclear theories postulate equal interaction energies between all pairs of nuclear particles. There are six such types of interactions, satisfying the physical requirement of invariance under the rotation-reflection group and not explicitly involving the momenta of the interacting particles.[1] In terms of the isotopic spin formalism, the exchange properties of these six interactions are symbolized by

$$1, \quad \boldsymbol{\sigma}_1\cdot\boldsymbol{\sigma}_2, \quad S_{12}, \quad \boldsymbol{\tau}_1\cdot\boldsymbol{\tau}_2, \quad \boldsymbol{\tau}_1\cdot\boldsymbol{\tau}_2\boldsymbol{\sigma}_1\cdot\boldsymbol{\sigma}_2, \quad \boldsymbol{\tau}_1\cdot\boldsymbol{\tau}_2 S_{12}$$

$$S_{12}=\frac{3\boldsymbol{\sigma}_1\cdot\mathbf{r}_{12}\boldsymbol{\sigma}_2\cdot\mathbf{r}_{12}}{r_{12}^2}-\boldsymbol{\sigma}_1\cdot\boldsymbol{\sigma}_2. \qquad (1)$$

The interaction potential constructed from the four operators not containing S_{12} is a linear combination of the conventional Majorana, Heisenberg, Wigner and Barlett forces. The additional S_{12} interaction terms are not only possible *a priori*, but appear naturally in any field theory constructed to yield a spin dependence of nuclear forces. It is the purpose of this and a subsequent paper, to investigate the influence of interaction terms of the type S_{12} and $\boldsymbol{\tau}_1\cdot\boldsymbol{\tau}_2 S_{12}$ on the properties of the two particle neutron-proton system.

GENERAL FORMULAE

The generalization of the interaction operator produces, essentially, a modification of the symmetry properties of the Hamiltonian, which in the usual theory is evidently invariant under rotations of the spin coordinates and space coordinates separately, corresponding to the existence of stationary states characterized by the quantum numbers L, S, m_L, m_S. Interaction terms of the type S_{12}, however, are invariant only under the coupled rotation of the spin and space coordinates. The rotational invariance of the Hamiltonian with the more general interaction yields, therefore, only the total angular momentum quantum numbers J and m for the description of stationary states.

Although spin and orbital angular momentum are not in general conserved individually, the total spin of a *two*-particle system is a constant of the motion. The possibility of describing stationary states by the quantum number S in

* A preliminary report of this work was presented at the November, 1938 meeting of the American Physical Society. Cf. J. Schwinger, Phys. Rev. **55**, 235 (1939).

† On sabbatical leave from Brooklyn College, Brooklyn, New York.

[1] E. Wigner, Phys. Rev. **51**, 106 (1937).

this case is a consequence of the symmetry of the Hamiltonian in the spins of the two particles. By virtue of this symmetry, stationary state wave functions may be chosen to be either symmetrical or anti-symmetrical in the spin coordinates of the particles. The well-known fact that symmetrical spin wave functions correspond to triplet states while anti-symmetrical spin wave functions correspond to singlet states demonstrates the validity of this theorem. The fourth quantum number, in addition to S, J and m, necessary to completely describe the stationary states of the neutron-proton system is provided by the parity, the eigenvalue of the reflection operator.

The singlet states of the neutron-proton system exhibit no novel features in consequence of the easily demonstrable fact that S_{12} has the eigenvalue zero in a singlet state. This is necessarily true since the conservation of total angular momentum becomes the conservation of orbital angular momentum in singlet states. In triplet states, however, new phenomena may be expected to originate in the nonconservation of orbital angular momentum.

A triplet state of definite total angular momentum J is conveniently regarded as a mixture of all possible states of orbital angular momentum L consistent with the rules for compounding angular momenta. Thus a state with $J=1$ is a mixture of ${}^3S_1$, ${}^3P_1$ and ${}^3D_1$ states. The existence of the parity quantum number permits a further classification into even and odd states based upon the theorem that a state of orbital angular momentum L has the parity quantum number $(-1)^L$. The state $J=1$, for example, decomposes into an even state which is a mixture of ${}^3S_1$ and ${}^3D_1$, and an odd ${}^3P_1$ state. We obtain in this way a complete classification of all triplet states, which is illustrated in Table I for the first few values of J.

The investigation of the properties of these states is facilitated by expressing the $SLJm$ eigenstates in terms of the eigenstates of SLm_Lm_S. It is not necessary, however, to utilize the general formulae, for only the properties of the state ${}^3S_1+{}^3D_1$ are of interest in this paper, and in this case special methods are available. That part of the wave function of the ${}^3S_1$ state with magnetic quantum number m which involves angular and spin coordinates is clearly $(4\pi)^{-\frac{1}{2}}\chi_1{}^m$, where $\chi_1{}^m$ denotes the spin wave function appropriate to a triplet state with magnetic quantum number m. The factor $(4\pi)^{-\frac{1}{2}}$ is introduced for normalization purposes. The corresponding part of the ${}^3D_1$ wave function is proportional to $S_{12}\chi_1{}^m$. That this represents a triplet state with $J=1$ is evident from the rotational invariance and spin symmetry of S_{12}. To prove that it represents a D state, we need merely note that $\nabla^2(r^2S_{12}\chi_1{}^m)=0$. The normalized part of the ${}^3D_1$ wave function involving angular and spin coordinates is thus $\frac{1}{4}(2\pi)^{-\frac{1}{2}}S_{12}\chi_1{}^m$. Introducing the symbols $u(r)/r$ and $w(r)/r$ for the radial wave functions of the S and D states, respectively, we then obtain for the wave function of the ${}^3S_1+{}^3D_1$ state the expression

$$\psi=(4\pi)^{-\frac{1}{2}}\left\{\frac{u}{r}+2^{-\frac{1}{2}}\left(\frac{3\boldsymbol{\sigma}_1\cdot\mathbf{r}\boldsymbol{\sigma}_2\cdot\mathbf{r}}{r^2}-1\right)\frac{w}{r}\right\}\chi_1{}^m. \quad (2)$$

In stating that only the ${}^3S_1+{}^3D_1$ state need be considered in detail for the interpretation of the experimental data relevant to the triplet state, we have restricted consideration to energies so small that only S states, and therefore the ${}^3D_1$ state through its coupling with the ${}^3S_1$ state, will be influenced by the neutron-proton interaction. This restriction will be removed in the sequel to this paper. Since these states are symmetrical in the space coordinates of the neutron and the proton, it is sufficient for our purposes to regard the interaction operator as a mixture of ordinary interactions, spin exchange interactions and interactions of the type S_{12}. The inclusion of space exchange operators would be a luxury of no consequence. These remarks find their mathematical expression in the following formula for the interaction operator:

$$V=-\{1-\tfrac{1}{2}g+\tfrac{1}{2}g\boldsymbol{\sigma}_1\cdot\boldsymbol{\sigma}_2+\gamma S_{12}\}J(r). \quad (3)$$

TABLE I. *Classification of triplet states.*

J	PARITY	
	EVEN	ODD
0		${}^3P_0$
1	${}^3S_1+{}^3D_1$	${}^3P_1$
2	${}^3D_2$	${}^3P_2+{}^3F_2$
3	${}^3D_3+{}^3G_3$	${}^3F_3$

The quantities g and γ will in general involve the distance between the two particles.

In the singlet state the interaction assumes a particularly simple form,

$$V_{\text{singlet}} = -(1-2g)J(r),$$

which is readily obtained by replacing $\boldsymbol{\sigma}_2$ with $-\boldsymbol{\sigma}_1$. The corresponding wave equation for the relative motion of the neutron and the proton

$$E\psi = (\hbar^2/M)\nabla^2\psi - (1-2g)J(r)\psi, \tag{4}$$

is of standard Schrödinger type and deserves no further consideration.

Upon insertion of the wave function (2) into the triplet state wave equation,

$$E\psi = \frac{\hbar^2}{M}\nabla^2\psi - \left[1+\gamma\left(\frac{3\boldsymbol{\sigma}_1\cdot\mathbf{r}\boldsymbol{\sigma}_2\cdot\mathbf{r}}{r^2}-1\right)\right]J(r)\psi, \tag{5}$$

we obtain the following differential equations for the ${}^3S_1$ and ${}^3D_1$ radial wave functions:

$$\begin{aligned}\frac{d^2u}{dr^2}+\frac{M}{\hbar^2}[E+J]u &= -2^{\frac{1}{2}}\gamma\frac{M}{\hbar^2}Jw,\\ \frac{d^2w}{dr^2}-\frac{6w}{r^2}+\frac{M}{\hbar^2}[E+(1-2\gamma)J]w &= -2^{\frac{1}{2}}\gamma\frac{M}{\hbar^2}Ju.\end{aligned} \tag{6}$$

The discussion, with the aid of these equations, of the ground state of the deuteron, the scattering of neutrons by protons, the radiative capture of slow neutrons, and the photo-disintegration of the deuteron forms the content of the remainder of this paper.

The Ground State of the Deuteron

Of the radial dependence of the neutron-proton interaction, little is known but that it is of short range. To facilitate the determination of the effects of the postulated interaction, we shall make the simplifying assumption that the quantities g and γ be constants and that $J(r)$ be a rectangular potential well of depth V_0 and range r_0.

Table II. *Quadrupole moments.*

V_0/E_0	$\gamma V_0/\lvert E_0\rvert$	$Q(10^{-27}$ cm$^2)$
9.779	0	0
6.60	4.79	2.67
6.40	4.96	2.73
6.00	5.30	2.84
5.50	5.72	2.95
3.57	7.14	3.34
0	9.42	3.71
−4.00	12.0	4.05
−6.81	13.6	4.26

The wave function of the deuteron ground state satisfies the simultaneous differential equations (6), with $-E=|E_0|=2.17$ Mev. Outside the range of interaction these equations are readily integrable, yielding

$$\begin{aligned}u(r>r_0) &= Ae^{-\alpha(r-r_0)}, \quad \alpha=(M|E_0|/\hbar^2)^{\frac{1}{2}},\\ w(r>r_0) &= Be^{-\alpha(r-r_0)}(1+3/\alpha r+3/(\alpha r)^2).\end{aligned} \tag{7}$$

The differential equations descriptive of the ground state wave function at distances less than r_0 are:

$$\begin{aligned}(d^2/dr^2+\kappa^2)u(r) &= -\lambda^2 w(r),\\ (d^2/dr^2-6/r^2+\kappa'^2)w(r) &= -\lambda^2 u(r),\end{aligned} \tag{8}$$

with the abbreviations:

$$\begin{aligned}\kappa^2 &= (M/\hbar^2)(V_0-|E_0|),\\ \kappa'^2 &= (M/\hbar^2)((1-2\gamma)V_0-|E_0|),\\ \lambda^2 &= 2^{\frac{1}{2}}\gamma(M/\hbar^2)V_0.\end{aligned} \tag{9}$$

Although more elegant methods of treating these equations undoubtedly exist, the procedure adopted was the expansion of u and w in infinite power series,

$$\begin{aligned}u(r) &= \sum_0^\infty A_n x^{n+1} + \ln x \sum_0^\infty C_n x^{n+2},\\ w(r) &= \sum_0^\infty B_n x^{n+3} + \ln x \sum_0^\infty D_n x^{n+3},\\ x &= r/r_0,\end{aligned} \tag{10}$$

which provide solutions of the differential equations if the constants satisfy the recursion formulae:

$$\begin{aligned}&(n+1)(n+2)A_{n+1}\\ &\quad+(2n+3)C_n+(\kappa r_0)^2A_{n-1} = -(\lambda r_0)^2B_{n-3},\\ &(n+1)(n+2)C_n+(\kappa r_0)^2C_{n-2} = -(\lambda r_0)^2D_{n-3},\\ &n(n+5)B_n+(2n+5)D_n\\ &\quad+(\kappa' r_0)^2B_{n-2} = -(\lambda r_0)^2A_n,\\ &n(n+5)D_n+(\kappa' r_0)^2D_{n-2} = -(\lambda r_0)^2C_{n-1}.\end{aligned} \tag{11}$$

The solutions of these recursion relations may be expressed linearly in terms of the two arbitrary constants A_0 and B_0. The reader will be spared the sight of these solutions, for numerical values of the constants are more conveniently obtained by successive solution of the recursion relations than by numerical substitution into an explicit formula.

The continuity of the logarithmic derivatives of u and w provides two equations,

$$\left(\frac{r_0}{u}\frac{du}{dr}\right)_{r=r_0} = -\alpha r_0,$$
$$\left(\frac{r_0}{w}\frac{dw}{dr}\right)_{r=r_0} = -\left(2+\frac{(\alpha r_0)^2(1+\alpha r_0)}{(\alpha r_0)^2+3\alpha r_0+3}\right), \tag{12}$$

which suffice to determine B_0/A_0 and V_0 for a given choice of r_0 and γ. The continuity of u and w then permit the constants A and B of (7) to be expressed in terms of A_0, which in turn may be derived from the normalization condition:

$$1=\int_0^\infty (u^2+w^2)dr$$
$$=\int_0^{r_0}(u^2+w^2)dr+\frac{A^2}{2\alpha}+\frac{B^2}{2\alpha}\left(1+6\frac{(1+\alpha r_0)^2}{(\alpha r_0)^3}\right), \tag{13}$$

thus completing the solution of the ground state problem.

This procedure provides a relation between V_0 and γ for a fixed r_0. To obtain a unique set of constants γ and V_0, it is necessary to employ some additional property of the neutron-proton system, sensitive to the magnitude of the spin-spin interaction term (S_{12}). Such a property is embodied in the recently discovered electric quadripole moment of the deuteron. A non-spherical distribution of charge is a consequence of the ${}^3D_1$ state adjoined to the ${}^3S_1$ state by the spin-spin forces. Conversely, the experimental existence of an unsymmetrical charge distribution in the ground state demands the introduction of a noncentral force, for otherwise the ground state would be pure S in character. The quadripole moment Q is defined as the value of $\frac{1}{4}(3z^2-r^2)$ averaged over the asymmetrical charge distribution obtained from the wave function (2), in the magnetic sub-state $m=1$.

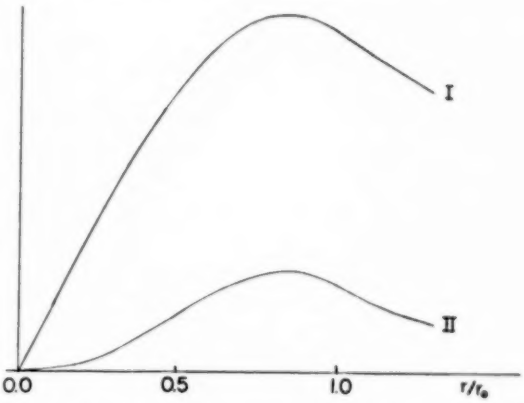

FIG. 1. S and D radial wave functions. I: $u(r)$; II: $w(r)$

$$Q=\frac{2^{\frac{1}{2}}}{10}\int_0^\infty r^2(uw-2^{-\frac{1}{2}}w^2)dr. \tag{14}$$

Nordsieck's evaluation[2] of the experiments of Rabi[3] and his co-workers gives for the value of the quadripole moment of the deuteron: $Q=+(2.73\pm0.05)\times10^{-27}$ cm^2. The positive sign indicates that the charge distribution is prolate with respect to the direction of the deuteron spin. Inspection of the interaction operator (3) shows that the condition necessary for the potential energy to be a minimum with the relative position vector $\mathbf{r}$ aligned parallel to the spin is that γV_0 be positive. Some sets of values for γ and V_0, consistent with this condition, were determined to fit the observed binding energy; and the quadripole moment was computed for each set. The results of these calculations for $r_0=2.80\times10^{-13}$ cm are summarized in Table II. The final set of constants, consistent with both binding energy and quadripole moment, is thus:

$$V_0/|E_0|=6.40, \quad \gamma=0.775, \quad r_0=2.80\times10^{-13}\text{ cm}.$$

The S and D radial functions appropriate to these constants are plotted in Fig. 1. The uncertainty in these values, arising from the 2-percent limit of error in the interpretation of the quadripole moment measurements, is estimated as 3 percent for V_0 and 6 percent for γ.

[2] A. Nordsieck, Phys. Rev. **58**, 310 (1940).
[3] J. M. B. Kellogg, I. I. Rabi, N. F. Ramsey and J. R. Zacharias, Phys. Rev. **57**, 677 (1940).

In principle, a test of this assignment of constants is provided by the measured magnetic moment of the deuteron. The magnetic moment associated with the ${}^3S_1+{}^3D_1$ state is no longer the sum of the intrinsic neutron and proton moments, for the ${}^3D_1$ state introduces an orbital contribution proportional to the probability of observing the deuteron in the ${}^3D_1$ state, i.e., $\int_0^\infty w^2dr$. To justify this statement let us consider the magnetic moment operator of the neutron-proton system, expressed in units of the nuclear magneton, $eh/2Mc$; *viz.*,

$$\mathbf{M}=\mu_n\boldsymbol{\sigma}_n+\mu_p\boldsymbol{\sigma}_p+\tfrac{1}{2}\mathbf{L}, \tag{15}$$

where μ_n and μ_p denote the magnetic moments of the neutron and proton in magneton units, and $\mathbf{L}$ represents the internal orbital angular momentum of the system in units of $\hbar$. The factor of $\frac{1}{2}$ occurring in (15) stems from the fact that, although two particles contribute to the orbital angular momentum $\mathbf{L}$, only one possesses a charge. The expression for $\mathbf{M}$ is conveniently rewritten as follows:

$$\mathbf{M}=\tfrac{1}{2}\mathbf{J}+(\mu_n+\mu_p-\tfrac{1}{2})\mathbf{S}+\tfrac{1}{2}(\mu_n-\mu_p)(\boldsymbol{\sigma}_n-\boldsymbol{\sigma}_p), \tag{16}$$

where to $\mathbf{S}$ and $\mathbf{J}$ we attribute their usual significance. The magnetic moment of the deuteron is then obtained by calculating the average value of M_z in the magnetic sub-state of the deuteron with unit magnetic quantum number. This evaluation may be simplified by noting that all triplet state matrix elements of $(\boldsymbol{\sigma}_n-\boldsymbol{\sigma}_p)$ vanish, and that $\mathbf{S}$ may be replaced by its component in the direction of $\mathbf{J}$, i.e.,

$$\mathbf{S}\rightarrow\mathbf{J}\frac{\mathbf{S}\cdot\mathbf{J}}{\mathbf{J}^2}=\mathbf{J}\frac{\mathbf{J}^2+\mathbf{S}^2-\mathbf{L}^2}{2\mathbf{J}^2}=\mathbf{J}\frac{4-\mathbf{L}^2}{4},$$

substituting for $\mathbf{J}^2$ and $\mathbf{S}^2$ their eigenvalue 2. Hence, for the purpose of determining μ_D, the magnetic moment of the deuteron, the magnetic moment operator may be replaced by

$$\mathbf{J}[\mu_n+\mu_p-\tfrac{1}{4}(\mu_n+\mu_p-\tfrac{1}{2})\mathbf{L}^2]. \tag{17}$$

From the evident fact that the average value of $\mathbf{L}^2$ is $6\int_0^\infty w^2dr$, we obtain immediately the desired formula for the magnetic moment of the deuteron; *viz.*,

$$\mu_D=\mu_n+\mu_p-\tfrac{3}{2}(\mu_n+\mu_p-\tfrac{1}{2})\int_0^\infty w^2dr, \tag{18}$$

or

$$\mu_n=\frac{\mu_D-\frac{3}{4}\int_0^\infty w^2dr}{1-\frac{3}{2}\int_0^\infty w^2dr}-\mu_p. \tag{19}$$

The wave functions of Fig. 1 imply a D state probability

$$\int_0^\infty w^2dr=0.039.$$

The neutron magnetic moment inferred from Eq. (19) combined with the measurements of μ_p and μ_D, $\mu_p=2.785\pm0.02$, $\mu_D=0.855\pm0.006$, namely, $\mu_n=-1.908\pm0.02$, differs but slightly from that obtained by simple subtraction: -1.930 ± 0.02. The direct measurement of the moment of a free neutron by Bloch and Alvarez[4] gives $\mu_n=-1.935\pm0.02$. Presumably the discrepancy between these two results is not significant, in view of the overlapping errors of the direct measurements. Should increased accuracy in the measurements reveal a definite divergence, the concept of unperturbed intrinsic moments implicit in these calculations, would have to be abandoned. However, it should be remembered that the possibility still exists that a different radial dependence of the interactions would yield a smaller D state probability. The only information available on this question is furnished by Bethe's calculations[5] on the "cut-off" neutral mesotron potential which predicts

$$\int_0^\infty w^2dr=0.06.$$

Further evidence for the nonconservation of orbital angular momentum, manifest in the orbital contribution to the deuteron magnetic moment, is provided by the small, but real, difference between the magnetic moments of the deuteron and ${}_3Li^6$. The slight difference between the ground states of the two nuclei contemplated in the usual theory is quite insufficient to account for more than a negligible fraction of the difference between $\mu({}_1H^2)=0.854$ and $\mu({}_3Li^6)$

[4] L. W. Alvarez and F. Bloch, Phys. Rev. **57**, 111 (1940).
[5] H. A. Bethe, Phys. Rev. **57**, 390 (1940).

$=0.820$. Indeed, according to current theory, the magnetic moments of all the odd-odd nuclei should be equal; whereas, in actuality, they form a monotonically decreasing sequence;[6] *viz.*, $\mu({}_1H^2)=0.854$, $\mu({}_3Li^6)=0.820$, $\mu({}_5B^{10})=0.597$, $\mu({}_7N^{14})=0.402$. The explanation of this anomalous behavior is to be sought in the increasing admixture of states with higher orbital angular momentum to the fundamental state ${}^3S_1$. To admit the validity of this interpretation, one need merely note that the magnetic moment of a member of this nuclear class is represented by

$$\mu=(\mu_n+\mu_p)-(\mu_n+\mu_p-\tfrac{1}{2})\times[(\mathbf{L}^2)_{Av}-(\mathbf{S}^2)_{Av}+2]/4. \quad (18')$$

Further, with increasing nuclear complexity, one may anticipate a progressive relaxation of the prohibition of singlet-triplet mixing, so rigidly enforced in the deuteron, thus introducing an additional nuclear moment variation with atomic weight of the character demanded by experiment.

Neutron-Proton Scattering

The scattering of neutrons by protons has proved a fruitful source of information concerning the neutron-proton interaction. Slow neutron scattering experiments in paraffin, and ortho- and para-hydrogen have demonstrated the existence of spin dependent interactions which do not yield a bound singlet state of the deuteron. An exacting test of any interaction designed to produce these results is provided by the experimental values of scattering cross sections at higher energies. The most accurate measurements available at present are those of Zinn, Seely and Cohen,[7] and Aoki[8] who obtain a scattering cross section of $(2.40\pm0.10)\times10^{-24}$ cm^2 for a neutron energy of 2.8 Mev. The current theoretical value depends upon the range of interaction in the triplet state, which is not known with certainty. Calculations on the binding energies of light nuclei indicate an interaction range somewhat greater than 2×10^{-13} cm. Similar results have been obtained from experiments on proton-proton scattering, although these experiments, in reality, are pertinent only to the interaction of the ${}^1S$ state. The theoretical value of the cross section at 2.8 Mev, calculated from the interaction ranges thus obtained, is apparently larger than the experimental value. The first question which presents itself, therefore, is whether the inclusion of the S_{12} interaction term will serve to decrease the theoretical value of the scattering cross section.

The interdependence of spin and orbital motion expressed by the interaction operator (3) complicates the calculation of scattering cross sections. The orbital part of the incident wave corresponds to a state with zero orbital magnetic quantum number in the direction of wave propagation. The total component of angular momentum in this direction is consequently equal to the spin magnetic quantum number of the initial beam. Although total angular momentum is conserved, spin angular momentum alone is not, and one will therefore find scattered waves with altered values of the spin magnetic quantum number associated with corresponding nonvanishing values of the orbital magnetic quantum number. A natural consequence of this nonconservation of spin angular momentum is a dependence of the scattering cross section upon the spin magnetic quantum number of the incident beam.

Confining our attention to the triplet state, which alone exhibits these phenomena, we may write for the wave function of an incident wave propagated in the $\mathbf{k}$ direction with magnetic quantum number $m=1, 0, -1$:

$$\exp[i\mathbf{k}\cdot\mathbf{r}]\chi_1{}^m=\left\{\sum_{L=0}^{\infty}(2L+1)i^L\frac{g_L(kr)}{kr}P_L(\cos\vartheta)\right\}\chi_1{}^m, \quad (20)$$

where

$$g_L(\rho)=(\pi\rho/2)^{\frac{1}{2}}J_{L+\frac{1}{2}}(\rho)\sim\sin(\rho-\tfrac{1}{2}\pi L), \quad (21)$$

[6] S. Millman, P. Kusch and I. I. Rabi, Phys. Rev. **56**, 165 (1939); M. Phillips, Phys. Rev. **57**, 160 (1940).
[7] W. H. Zinn, S. Seely and V. W. Cohen, Phys. Rev. **56**, 260 (1939).
[8] H. Aoki, Proc. Phys.-Math. Soc. Jap. **21**, 232 (1939).

and k is related to E, the energy of relative motion, by

$$k=(ME)^{\frac{1}{2}}/\hbar. \tag{22}$$

To simplify the calculations, we shall assume that only the even state in the continuum with $J=1$ is perturbed by the neutron-proton interaction. The justification of this approximation has already been presented. The wave function of this state is of the general form (2) with the S and D radial functions determined by the simultaneous differential equations (6). Within the range of interaction these equations assume the form (8) encountered in the solution of the ground state problem, save that $-|E_0|$ must be replaced by E in the definitions of κ^2 and κ'^2. Methods identical with those presented in the previous section may be employed for their solution. In the region $r>r_0$, the differential equations (6) may be integrated explicitly, *viz*:

$$\begin{gathered}u(r)=\sin(kr+\delta_0),\\ w(r)=\eta\{-\sin(kr+\delta_2)-(3/kr)\cos(kr+\delta_2)+[3/(kr)^2]\sin(kr+\delta_2)\}.\end{gathered} \tag{23}$$

Two relations between δ_0, δ_2 and B_0/A_0 are provided by the continuity of the logarithmic derivatives of u and w. The third necessary relation can only be obtained from an examination of the conditions necessary for the existence of a solution to the scattering problem.

In consequence of the hypothesis that only the even state with unit angular momentum is perturbed by the neutron-proton interaction, the wave function representing the scattering of the two particles will be obtained by replacing that part of the incident wave (20) which is of unit angular momentum and even parity by a suitable multiple of the ${}^3S_1+{}^3D_1$ wave function we have just discussed. The requisite part of the incident wave is evidently of the form (2) with u and w proportional to $g_0(kr)$ and $g_2(kr)$, respectively. Inasmuch as the entire S part of the incident wave must be included therein, we write the desired wave function as

$$\left[\frac{g_0(kr)}{kr}+\beta\left(\frac{3\boldsymbol{\sigma}_1\cdot\mathbf{r}\boldsymbol{\sigma}_2\cdot\mathbf{r}}{r^2}-1\right)\frac{g_2(kr)}{kr}\right]\chi_1{}^m. \tag{24}$$

The constant β may be determined by demanding that (18) be orthogonal to the remainder of the incident wave. Values of β thus obtained depend upon the manner in which the total angular momentum is quantized with respect to the direction of propagation of the incident beam. It is easily verified that

$$\beta=-\frac{1}{8}\left(m\left|\frac{3\boldsymbol{\sigma}_1\cdot\mathbf{k}\boldsymbol{\sigma}_2\cdot\mathbf{k}}{k^2}-1\right|m\right) \tag{25}$$

and thus $\beta=-\frac{1}{4}$ for $m=\pm1$ and $\beta=\frac{1}{2}$ for $m=0$.

Consider first those scattering processes for which $m=\pm1$. In accordance with our previous remarks, the wave function describing this type of scattering is:

$$\exp[i\mathbf{k}\cdot\mathbf{r}]\chi_1{}^{\pm1}-\left[\frac{g_0(kr)}{kr}-\frac{1}{4}S_{12}\frac{g_2(kr)}{kr}\right]\chi_1{}^{\pm1}+A^{(1)}\left[\frac{u^{(1)}(r)}{kr}+2^{-\frac{1}{2}}S_{12}\frac{w^{(1)}(r)}{kr}\right]\chi_1{}^{\pm1}, \tag{26}$$

where the superscript (1) is employed to distinguish quantities from the analogous, but different, quantities encountered in the scattering process with $m=0$. The constants $A^{(1)}$, and $\eta^{(1)}$ of (23) are specified by requiring that (26) satisfy the boundary conditions of containing only diverging spherical waves at infinity in addition to the incident wave. Utilizing the asymptotic formulae:

$$\begin{gathered}g_0(kr)\sim\sin kr,\quad g_2(kr)\sim-\sin kr,\\ u^{(1)}(r)\sim\sin(kr+\delta_0{}^{(1)}),\quad w^{(1)}(r)\sim-\eta^{(1)}\sin(kr+\delta_2{}^{(1)}),\end{gathered} \tag{27}$$

the desired asymptotic form of (26) is realized with the choice of constants:

$$A^{(1)}=e^{i\delta_0{}^{(1)}}, \quad \eta^{(1)}=-2^{-\frac{1}{2}}e^{i(\delta_2{}^{(1)}-\delta_0{}^{(1)})}. \tag{28}$$

This value of $\eta^{(1)}$ provides the third equation of continuity necessary to completely specify the wave function of the ${}^3S_1+{}^3D_1$ state, for it essentially determines the value of $w^{(1)}(r)/u^{(1)}(r)$ outside the potential well. It is important to realize that the occurrence of the imaginary i in the third condition will result in complex values for B_0/A_0, and the phases $\delta_0{}^{(1)}$ and $\delta_2{}^{(1)}$. The complex nature of the phases may be interpreted as an expression of the "damping" of the S and D states arising from the interconversion caused by their mutual coupling.

The asymptotic form of the scattering wave function, obtained upon insertion of the constants (28) into formula (26), is:

$$\exp[i\mathbf{k}\cdot\mathbf{r}]\chi_1{}^{\pm1}+\frac{e^{ikr}}{r}\left\{\frac{e^{2i\delta_0{}^{(1)}}-1}{2ik}+\frac{1}{4}S_{12}\frac{e^{2i\delta_2{}^{(1)}}-1}{2ik}\right\}\chi_1{}^{\pm1}. \tag{29}$$

The square of the absolute value of the coefficient of e^{ikr}/r represents the scattering cross section per unit solid angle, which, in terms of the real and imaginary parts of the phases,

$$\delta_0{}^{(1)}=\kappa_0{}^{(1)}+i\zeta_0{}^{(1)}, \quad \delta_2{}^{(1)}=\kappa_2{}^{(1)}+i\zeta_2{}^{(1)}, \tag{30}$$

may be written:

$$\begin{aligned}\sigma_{|m|=1}(\vartheta)=\frac{1}{k^2}\{&e^{-2\zeta_0{}^{(1)}}(\sin^2\kappa_0{}^{(1)}+\sinh^2\zeta_0{}^{(1)})+\tfrac{1}{8}(5-3\cos^2\vartheta)e^{-2\zeta_2{}^{(1)}}(\sin^2\kappa_2{}^{(1)}+\sinh^2\zeta_2{}^{(1)})\\&+\tfrac{1}{2}(3\cos^2\vartheta-1)e^{-\zeta_0{}^{(1)}-\zeta_2{}^{(1)}}[\sinh\zeta_0{}^{(1)}\sinh\zeta_2{}^{(1)}+\sinh\zeta_2{}^{(1)}e^{-\zeta_0{}^{(1)}}\sin^2\kappa_0{}^{(1)}\\&+\sinh\zeta_0{}^{(1)}e^{-\zeta_2{}^{(1)}}\sin^2\kappa_2{}^{(1)}+e^{-\zeta_0{}^{(1)}-\zeta_2{}^{(1)}}\sin\kappa_0{}^{(1)}\sin\kappa_2{}^{(1)}\cos(\kappa_0{}^{(1)}-\kappa_2{}^{(1)})]\}.\end{aligned} \tag{31}$$

By integration of this expression over all solid angles, we obtain the total cross section for neutron-proton scattering with magnetic quantum number $m=\pm1$:

$$\sigma_{|m|=1}=\frac{4\pi}{k^2}\{e^{-2\zeta_0{}^{(1)}}(\sin^2\kappa_0{}^{(1)}+\sinh^2\zeta_0{}^{(1)})+\tfrac{1}{2}e^{-2\zeta_2{}^{(1)}}(\sin^2\kappa_2{}^{(1)}+\sinh^2\zeta_2{}^{(1)})\}. \tag{32}$$

The neutron-proton scattering with $m=0$ may be treated in a completely analogous fashion. In place of (28) we must employ the constants

$$A^{(0)}=e^{i\delta_0{}^{(0)}}, \quad \eta^{(0)}=2^{\frac{1}{2}}e^{i(\delta_2{}^{(0)}-\delta_0{}^{(0)})}, \tag{33}$$

in order to obtain the correct asymptotic form of the scattering wave function; namely,

$$\exp[i\mathbf{k}\cdot\mathbf{r}]\chi_1{}^0+\frac{e^{ikr}}{r}\left\{\frac{e^{2i\delta_0{}^{(0)}}-1}{2ik}-\frac{1}{2}S_{12}\frac{e^{2i\delta_2{}^{(0)}}-1}{2ik}\right\}\chi_1{}^0. \tag{34}$$

In deriving the scattering cross section from this asymptotic formula, it is necessary to evaluate the diagonal matrix element of S_{12} with respect to the spins of the two particles. This may be done most easily by noting that the diagonal sum of S_{12} vanishes. Inasmuch as S_{12} has the eigenvalue zero in a singlet state, it follows that the diagonal sum over the triplet states vanishes. Further, it is obvious that the diagonal matrix elements of S_{12} in the states $m=\pm1$ have the value $(3\cos^2\vartheta-1)$, a fact which has been employed in the derivation of the scattering formulae for $m=\pm1$. Therefore, the diagonal matrix element of S_{12} in the $m=0$ state, which is the desired quantity, has the value $-2(3\cos^2\vartheta-1)$.

With the aid of the result, we obtain the following formula for the cross section of the process

in which the particles are scattered through an angle ϑ into unit solid angle:

$$\sigma_{m=0}(\vartheta)=\frac{1}{k^2}\{e^{-2\zeta_0^{(0)}}(\sin^2\kappa_0^{(0)}+\sinh^2\zeta_0^{(0)})+(3\cos^2\vartheta+1)e^{-2\zeta_2^{(0)}}(\sin^2\kappa_2^{(0)}+\sinh^2\zeta_2^{(0)})$$
$$+2(3\cos^2\vartheta-1)e^{-\zeta_0^{(0)}-\zeta_2^{(0)}}[\sinh\zeta_0^{(0)}\sinh\zeta_2^{(0)}+\sinh\zeta_2^{(0)}e^{-\zeta_0^{(0)}}\sin^2\kappa_0^{(0)}$$
$$+\sinh\zeta_0^{(0)}e^{-\zeta_2^{(0)}}\sin^2\kappa_2^{(0)}+e^{-\zeta_0^{(0)}-\zeta_2^{(0)}}\sin\kappa_0^{(0)}\sin\kappa_2^{(0)}\cos(\kappa_0^{(0)}-\kappa_2^{(0)})]\}. \quad (35)$$

The total cross section for scattering in the $m=0$ state is then

$$\sigma_{m=0}=\frac{4\pi}{k^2}\{e^{-2\zeta_0^{(0)}}(\sin^2\kappa_0^{(0)}+\sinh^2\zeta_0^{(0)})+2e^{-2\zeta_0^{(0)}}(\sin^2\kappa_2^{(0)}+\sinh^2\zeta_2^{(0)})\}. \quad (36)$$

The cross section actually observed in the triplet scattering of unpolarized neutron beams is related to the cross sections with definite magnetic quantum number by

$$\sigma_{\text{triplet}}=\tfrac{2}{3}\sigma_{|m|=1}+\tfrac{1}{3}\sigma_{m=0}. \quad (37)$$

Although this cross section would appear to involve eight constants, general conservation theorems provide several connecting relations which serve to reduce to three the number of constants required to describe this type of scattering process. The expression of the stationary state character of a wave function of type (2) is:

$$\left(u^*\frac{du}{dr}-\frac{du^*}{dr}u\right)+\left(w^*\frac{dw}{dr}-\frac{dw^*}{dr}w\right)=0, \quad (38)$$

describing zero flux across the surface of a sphere of radius r. This equation may also be recognized as the generalized Wronskian condition for regular solutions of our system of simultaneous second-order linear differential equations. When applied to the asymptotic forms of the S and D radial functions for the two kinds of magnetic sub-states: $m=0, \pm1$:

$$u^{(m)}(r)\sim e^{i\delta_0^{(m)}}\sin(kr+\delta_0^{(m)}),$$
$$w^{(m)}(r)\sim C^{(m)}e^{i\delta_2^{(m)}}\sin(kr+\delta_2^{(m)}): \quad C^{(1)}=2^{-\frac{1}{2}}, \quad C^{(0)}=-2^{\frac{1}{2}} \quad (39)$$

this Wronskian condition yields:

$$e^{-2\zeta_0^{(m)}}\sinh 2\zeta_0^{(m)}+(C^{(m)})^2e^{-2\zeta_2^{(m)}}\sinh 2\zeta_2^{(m)}=0$$

or

$$(1-e^{-4\zeta_0^{(0)}})+2(1-e^{-4\zeta_2^{(0)}})=0, \quad (1-e^{-4\zeta_0^{(1)}})+\tfrac{1}{2}(1-e^{-4\zeta_2^{(1)}})=0. \quad (40)$$

If there exist two linearly independent regular solutions for a given magnetic sub-state, i.e., u_α, w_α; u_β, w_β, they must be subject to the Wronskian restriction:

$$\left(u_\alpha^*\frac{du_\beta}{dr}-\frac{du_\alpha^*}{dr}u_\beta\right)+\left(w_\alpha^*\frac{dw_\beta}{dr}-\frac{dw_\alpha^*}{dr}w_\beta\right)=0, \quad (41)$$

for an arbitrary linear combination of α and β must satisfy (38). The application of the rotation operator J_x+iJ_y to the $m=0$ wave function produces a regular solution for the $m=1$ magnetic sub-state which differs only in its asymptotic form from that represented in (39). Thus for the $m=1$ state, two linearly independent solutions exist, represented by

$$u_\alpha=u^{(1)}, \quad u_\beta=u^{(0)},$$
$$w_\alpha=w^{(1)}, \quad w_\beta=w^{(0)}.$$

The phases describing the two magnetic sub-

levels are thereby subject to the restriction

$$\delta_0^{(0)*}-\delta_0^{(1)}=\delta_2^{(0)*}-\delta_2^{(1)}$$

or

$$\begin{aligned}\kappa_0^{(0)}-\kappa_2^{(0)}&=\kappa_0^{(1)}-\kappa_2^{(1)},\\ \zeta_0^{(0)}-\zeta_2^{(0)}&=\zeta_2^{(1)}-\zeta_0^{(1)}.\end{aligned}\tag{42}$$

Further, the complex conjugate of a regular solution is again a regular solution, for the fundamental differential equations (6) involve only real coefficients. Hence an equally permissible pair of regular solutions is

$$u_\alpha=u^{(1)},\quad u_\beta=u^{(0)*},$$
$$w_\alpha=w^{(1)},\quad w_\beta=w^{(0)*},$$

which, when inserted in the Wronskian condition (41), introduces the additional equality:

$$e^{2i\delta_0^{(0)}}-e^{2i\delta_2^{(0)}}=e^{2i\delta_0^{(1)}}-e^{2i\delta_2^{(1)}}.\tag{43}$$

These relations, (40), (42) and (43), when suitably combined, yield five independent restrictions; *viz.*,

$$\zeta_0^{(0)}=\zeta_2^{(1)},\quad \zeta_0^{(1)}=\zeta_2^{(0)}$$
$$e^{-2\zeta_0^{(0)}}\cos(\kappa_0^{(0)}-\kappa_2^{(1)})=e^{-2\zeta_0^{(1)}}\cos(\kappa_0^{(1)}-\kappa_2^{(0)}),\tag{44}$$

the first of (42) and either of the Eqs. (40). When full advantage is taken of these relations, the total triplet scattering cross section is reduced to dependence on only three phase constants; *viz.*,

$$\sigma_{\text{triplet}}=(4\pi/k^2)\{e^{-2\zeta_0^{(0)}}(\sin^2\kappa_0^{(0)}+\sin^2\kappa_2^{(1)})+(1-e^{-2\zeta_0^{(0)}})\}.\tag{45}$$

Although the cross section for the scattering of neutrons with zero energy ($E=0$) may be obtained from the previous results by suitable limiting processes, it is more conveniently treated anew. At zero energy only the ${}^3S_1+{}^3D_1$ state is extant. Concerning the form of the wave function of this state within the range of interaction, nothing need be added to what has already been said. Outside the range of interaction, the S and D radial functions obtained by integration of (6) has the form:

$$u(r>r_0)=r+a;\quad w(r>r_0)=b/r^2.\tag{46}$$

The equations of continuity,

$$\left(\frac{r_0}{u}\frac{du}{dr}\right)_{r=r_0}=\frac{r_0}{r_0+a};\qquad \left(\frac{r_0}{w}\frac{dw}{dr}\right)_{r=r_0}=-2,\tag{47}$$

suffice to determine the constants B_0/A_0 and a. With the aid of these quantities, the constants A_0 and b may then be determined from the equations expressing the continuity of the S and D radial wave functions. The scattering is obviously isotropic, with the total cross section $4\pi a^2$.

We shall prove at this point that the S_{12} spin forces do serve to decrease the neutron-proton scattering cross section. For simplicity, we shall consider the case of zero energy. It will be convenient to append the subscript (1) to all quantities associated with triplet states in the continuum; quantities associated with the ground state will remain unmarked. With this notation, the equation expressing the orthogonality of the triplet wave function of zero energy and the ground state wave function reads

$$\int_0^\infty(uu_1+ww_1)dr=0.\tag{48}$$

Introducing the known forms of the S radial functions outside the range of interaction (Eqs. (7) and (46)), the orthogonality relation becomes

$$0=\int_0^{r_0}uu_1dr+\int_0^\infty ww_1dr+(uu_1)_{r=r_0}\times\frac{1}{\alpha}\left[1+\frac{1}{\alpha(r_0+a_1)}\right].\tag{49}$$

Within the range of interaction, the ground state and continuum wave functions differ but little. In addition, the behavior of the two functions at distances greater than r_0 is almost identical in the regions which contribute appreciably to the integral $\int_0^\infty ww_1dr$. It is therefore permissible to replace u_1 and w_1 in Eq. (41) by u and w. In terms of the quantity ϵ, defined by

$$\int_0^{r_0}u^2dr+\int_0^\infty w^2dr=\tfrac{1}{2}\epsilon r_0(u^2)_{r=r_0},\tag{50}$$

the formula obtained from (41) for the total scattering cross section, $4\pi a_1^2$, may be written

$$\frac{4\pi\hbar^2}{M|E_0|}\left(\frac{1}{1+\frac{1}{2}\epsilon\alpha r_0}+\alpha r_0\right)^2.\tag{51}$$

In the absence of the spin forces under discussion, the value of ϵ is close to unity, for the S wave

function u has the form of a sine wave which reaches its maximum amplitude at approximately r_0, and the D wave function w is identically zero. Upon including these forces in the neutron-proton interaction, w assumes finite values while u, as a numerical investigation shows, still preserves the general form of a sine wave. As a consequence, ϵ will become larger than one, resulting in a decrease of the scattering cross section since (43) is a monotonically decreasing function of ϵ. This demonstrates that the spin forces of type S_{12} are capable of at least a partial explanation of the experimental data.

The result thus obtained is supported by numerical calculations of the scattering cross section utilizing the simplified potential we have adopted for analytical convenience. The calculated cross section at zero energy: $\sigma_{\text{triplet}}(E=0)=4.21\times10^{-24}$ cm^2, differs from that obtained by the usual potential well calculation, 4.30×10^{-24} cm^2, by only two percent. This small decrease is, of course, attributable to the quite small magnitude of $\int_0^\infty w^2dr$. The depth of the singlet potential well, and therefore the quantity g, is obtained by requiring that the cross section for scattering of slow neutrons in hydrogen

$$\sigma_0=\tfrac{3}{4}\sigma_{\text{triplet}}(E=0)+\tfrac{1}{4}\sigma_{\text{singlet}}(E=0) \qquad (52)$$

assume[9] the value 20×10^{-24} cm^2. The measure of the relative strength of the spin exchange interaction, g, thus calculated, is $g=0.0715$. It is of some interest to note that had the range been chosen four percent smaller, i.e., $r_0=2.7\times10^{-13}$ cm, the value of g would have been zero. That is, with this choice of range, the data may be represented by an interaction operator composed of an ordinary and a spin-spin interaction term, with no spin-exchange interaction. The difference in singlet and triplet potential energies then arises entirely from the spin dependence embodied in S_{12}. A neutron-proton force of this character bears a suggestive resemblance to that of the symmetrical pseudo-scalar mesotron theory.

Neutron-proton scattering experiments employing the mono-energetic neutrons available from the D–D reaction have been performed in the energy interval 2.5–3.0 Mev. The most accurate experiments in this region, those of Aoki[8] and Zinn, Seely and Cohen,[7] are in fair accord and give $(2.40\pm0.10)\times10^{-24}$ cm^2 at the energy 2.82 Mev, adopted for theoretical calculation. The theoretical cross section is sensitive to the range of forces which, consistent with the fundamental concept of charge independence of the forces, has been chosen as $r_0=2.80\times10^{-13}$ cm, the value derived from the analysis of proton-proton scattering experiments.[10] The ordinary potential well model predicts a total cross section $\sigma(2.82\text{ Mev})=2.56\times10^{-24}$ cm^2. The computations with the spin-spin interaction, employing the methods outlined earlier in this section, result in the following values for the phases:

$$\kappa_0^{(0)}=-0.9454,\quad \kappa_2^{(1)}=0.00812,\quad \zeta_0^{(0)}=-0.01144. \qquad (53)$$

In the actual calculations, no use was made of the connecting relations between the phases, which were reserved for use as checks of the final numbers, with completely satisfactory results. Inserted in the formula (45), these phase constants imply a triplet scattering cross section $\sigma_{\text{triplet}}=2.403\times10^{-24}$ cm^2. Suitably averaged with the singlet cross section, $\sigma_{\text{singlet}}=2.910\times10^{-24}$ cm^2, there ensues the total neutron-proton cross section, $\sigma(2.82\text{ Mev})=2.53\times10^{-24}$ cm^2. Again we have succeeded in obtaining only a two-percent reduction in the triplet cross section.

It is difficult to decide whether a definite discrepancy exists. Although the theoretical value lies but barely higher than the upper limit of the experimental result, the experimental observations have been invariably less than the theoretical prediction appropriate to the range derived from proton scattering. It must be remembered, however, that successive experiments have shown a tendency to yield progressively higher values. If the present experimental magnitude of the cross section be accepted, the range in the triplet state must be reduced to 2.3×10^{-13} cm, thoroughly violating the postulate of charge independence of the forces.

[9] V. W. Cohen, H. H. Goldsmith, J. Schwinger, Phys. Rev. **55**, 106 (1939); H. B. Hanstein, Phys. Rev. **57**, 1045 (1940).

[10] G. Breit, H. M. Thaxton and L. Eisenbud, Phys. Rev. **55**, 1018 (1939).

It is not without interest to examine the non-isotropic angular distribution of the scattering demanded by the S_{12} interaction. The angular distributions in the separate magnetic sub-states are appreciably nonspherically symmetrical:

$$\begin{aligned}\sigma_{|m|=1}(\vartheta) &= (1-0.0263\cos^2\vartheta)\\ &\quad\times(2.381/4\pi)\times10^{-24}\text{ cm}^2,\\ \sigma_{m=0}(\vartheta) &= (1+0.0559\cos^2\vartheta)\\ &\quad\times(2.444/4\pi)\times10^{-24}\text{ cm}^2,\end{aligned}\tag{54}$$

although the triplet angular cross section for unpolarized beams:

$$\begin{aligned}\sigma_{\text{triplet}}(\vartheta) &= (1+0.0017\cos^2\vartheta)\\ &\quad\times(2.402/4\pi)\times10^{-24}\text{ cm}^2\end{aligned}\tag{55}$$

exhibits but negligible deviations from isotropic scattering.

Radiative Capture of Slow Neutrons

The theory of radiative transitions between the discrete and continuum states of the neutron-proton system is of added interest in view of the multiplicity of processes which become possible when the general interaction (3) is employed. The simplest situation realized is that of the radiative capture of slow neutrons in hydrogen, for only continuum S states are involved. In addition to the usual magnetic dipole capture from the singlet state, ${}^1S_0\rightarrow{}^3S_1$, we now have the possibilities of magnetic dipole transitions from the triplet state; i.e., ${}^3S_1\rightarrow{}^3S_1$, ${}^3D_1\rightarrow{}^3D_1$, and electric quadripole transitions from the triplet state; ${}^3S_1\rightarrow{}^3D_1$, ${}^3D_1\rightarrow{}^3S_1$, ${}^3D_1\rightarrow{}^3D_1$. Moreover the conventional treatment of the magnetic dipole capture from the singlet state as modified for the ${}^3S_1$ wave function now constitutes only part of the ground state wave function, thus reducing the capture probability.

The probability per unit time of a magnetic dipole transition from an initial state Ψ_i to a final state Ψ_f, with emission of a light quantum of energy $\hbar\omega$ in the solid angle $d\Omega$ about the direction of the unit vector $\boldsymbol{\kappa}$, is given by the well-known formula:

$$(e^2/\hbar c)(\hbar\omega/Mc^2)^2\omega\times|(\Psi_f,\boldsymbol{\kappa}\times\mathbf{e}\cdot\mathbf{M}\Psi_i)|^2(d\Omega/8\pi).\tag{56}$$

Here $\mathbf{M}$ denotes the operator of the magnetic moment in nuclear magnetons, and $\mathbf{e}$ represents a unit vector in the direction of polarization of the light quantum. To calculate the total transition probability between degenerate states, this expression must be averaged with respect to the magnetic quantum number m of the initial state and summed over all magnetic quantum numbers m' of the final state.

Slow neutron capture from the singlet state occurs between the nondegenerate zero energy state:

$$\Psi_i=[u_0(r)/r]\chi_0^0,\quad u_0(r)\sim r+a_0\tag{57}$$

and the triply degenerate deuteron ground state:

$$\Psi_f=(4\pi)^{-\frac{1}{2}}\{(u/r)+2^{-\frac{1}{2}}S_{12}(w/r)\}\chi_1^{m'}.\tag{2'}$$

To evaluate the required matrix elements we note that, of the three terms contained in the expression (16) for $\mathbf{M}$, only the third contributes to transitions between states of different total spin. Therefore,

$$(\Psi_f,\boldsymbol{\kappa}\times\mathbf{e}\cdot\mathbf{M}\Psi_i)=(\mu_n-\mu_p)(4\pi)^{\frac{1}{2}}\int_0^\infty uu_0dr(\boldsymbol{\kappa}\times\mathbf{e})\cdot(\chi_1^{m'},\tfrac{1}{2}(\boldsymbol{\sigma}_n-\boldsymbol{\sigma}_p)\chi_0^0).\tag{58}$$

The summation over the three final triplet states may be extended over all states, since the diagonal matrix element of $\boldsymbol{\sigma}_n-\boldsymbol{\sigma}_p$ vanishes in the singlet state. Hence

$$\sum_{m'}|\boldsymbol{\kappa}\times\mathbf{e}\cdot(\chi_1^{m'},\tfrac{1}{2}(\boldsymbol{\sigma}_n-\boldsymbol{\sigma}_p)\chi_0^0)|^2=(\chi_0^0,(\boldsymbol{\kappa}\times\mathbf{e}\cdot\tfrac{1}{2}(\boldsymbol{\sigma}_n-\boldsymbol{\sigma}_p))^2\chi_0^0)=(\chi_0^0,(\boldsymbol{\kappa}\times\mathbf{e}\cdot\boldsymbol{\sigma}_n)^2\chi_0^0)=1\tag{59}$$

by the completeness relation and the fact that $\boldsymbol{\kappa}\times\mathbf{e}$ is a unit vector. This is an explicit demonstration that the emitted radiation is isotropic and unpolarized. By summing over the two independent polarization directions, and integrating (56) over all emission directions, we obtain the total capture probability:

$$w_{\text{mag dip}}^{(0\rightarrow1)}=4\pi\frac{e^2}{\hbar c}(\mu_n-\mu_p)^2\left(\frac{|E_0|}{Mc^2}\right)^2\frac{|E_0|}{\hbar}\left(\int_0^\infty u_0udr\right)^2,\tag{60}$$

introducing $|E_0|$, the binding energy of the deuteron, for the energy of the light quantum. The superscript, denoting the spin transition, distinguishes this type of magnetic dipole capture from that involved in capture from the triplet state. The cross section for the process is obtained from the transition probability through division by the incident neutron current density. Inasmuch as the wave function (57) of the initial state is normalized to unit particle density, the current density in the singlet state is numerically equal to the neutron velocity $(2E/M)^{\frac{1}{2}}$, where E denotes the neutron energy. Therefore the total neutron current density equals $4(2E/M)^{\frac{1}{2}}$. The capture cross section thereby obtained may be written

$$\sigma_{\text{mag dip}}^{(0\to 1)}=\pi\frac{e^2}{\hbar c}(\mu_n-\mu_p)^2\left(\frac{|E_0|}{2E}\right)^{\frac{1}{2}}\left(\frac{|E_0|}{Mc^2}\right)^2\alpha\left(\int_0^\infty u_0 u dr\right)^2, \tag{61}$$

where α is defined in (7).

The matrix element of the magnetic moment operator between the initial state:

$$\Psi_i=\left\{\frac{u_1}{r}+2^{-\frac{1}{2}}S_{12}\frac{w_1}{r}\right\}\chi_1^m, \quad u_1(r)\sim r+a_1 \tag{62}$$

and the final state (2′) determines the probability of magnetic dipole capture from the triplet state. In computing this matrix element the operator $\mathbf{M}$ may be replaced by (17), the form utilized in the evaluation of the deuteron moment. It should be noted that the term $(\mu_n+\mu_p)\mathbf{J}$ contained therein gives no contribution to nondiagonal matrix elements. Therefore

$$(\Psi_f, \boldsymbol{\kappa}\times\mathbf{e}\cdot\mathbf{M}\Psi_i)=-\tfrac{3}{2}(4\pi)^{-\frac{1}{2}}(\mu_n+\mu_p-\tfrac{1}{2})\int_0^\infty ww_1 dr\boldsymbol{\kappa}\times\mathbf{e}\cdot(\chi_1^{m'}, \tfrac{1}{2}(\boldsymbol{\sigma}_n+\boldsymbol{\sigma}_p)\chi_1^m). \tag{63}$$

As before, the summation over the three final triplet states may be extended over all states. The justification in this situation proceeds from the diagonal nature of $\frac{1}{2}(\boldsymbol{\sigma}_n+\boldsymbol{\sigma}_p)\equiv\mathbf{S}$. Hence,

$$\sum_{m'}|(\boldsymbol{\kappa}\times\mathbf{e})\cdot(\chi_1^{m'}, \tfrac{1}{2}(\boldsymbol{\sigma}_n+\boldsymbol{\sigma}_p)\chi_1^m)|^2=(\chi_1^m, (\boldsymbol{\kappa}\times\mathbf{e}\cdot\tfrac{1}{2}(\boldsymbol{\sigma}_n+\boldsymbol{\sigma}_p))^2\chi_1^m),$$

which has still to be averaged over the three initial triplet states. We may again use the artifice of extending the summation over all states. The result is a diagonal sum of $(\boldsymbol{\kappa}\times\mathbf{e}\cdot\mathbf{S})^2$; i.e.,

$$\tfrac{1}{3}\sum_{mm'}|(\boldsymbol{\kappa}\times\mathbf{e})\cdot(\chi_1^{m'}, \tfrac{1}{2}(\boldsymbol{\sigma}_n+\boldsymbol{\sigma}_p)\chi_1^m)|^2=\tfrac{1}{3}Sp(\boldsymbol{\kappa}\times\mathbf{e}\cdot\tfrac{1}{2}(\boldsymbol{\sigma}_n+\boldsymbol{\sigma}_p))^2=\tfrac{2}{3}. \tag{64}$$

We obtain the total capture probability by the same discussion presented for singlet state capture:

$$w_{\text{mag dip}}^{(1\to 1)}=6\pi\frac{e^2}{\hbar c}(\mu_n+\mu_p-\tfrac{1}{2})^2\left(\frac{|E_0|}{Mc^2}\right)^2\frac{|E_0|}{\hbar}\left(\int_0^\infty ww_1 dr\right)^2. \tag{65}$$

The total neutron current density corresponding to the triplet wave function (62) is obviously $(4/3)(2E/M)^{\frac{1}{2}}$. Upon performing the required division, we obtain the following formula for the cross section corresponding to magnetic dipole capture from the triplet state:

$$\sigma_{\text{mag dip}}^{(1\to 1)}=\frac{9\pi}{2}\frac{e^2}{\hbar c}(\mu_n+\mu_p-\tfrac{1}{2})^2\left(\frac{|E_0|}{2E}\right)^{\frac{1}{2}}\left(\frac{|E_0|}{Mc^2}\right)^2\alpha\left(\int_0^\infty ww_1 dr\right)^2. \tag{66}$$

The third mechanism effective in the radiative capture of slow neutrons is the electric quadripole capture from the triplet state. The probability of an electric quadripole transition between the initial state (62) and the final state (2′) is represented by

$$(e^2/\hbar c)(\hbar\omega/Mc^2)^4\omega(\hbar/Mc)^{-4}|(\Psi_f, \tfrac{1}{4}\mathbf{e}\cdot\mathbf{r}\boldsymbol{\kappa}\cdot\mathbf{r}\Psi_i)|^2 d\Omega/8\pi. \tag{67}$$

The required matrix element is found, by integrating over angles, to be

$$(\Psi_f, \tfrac{1}{4}\mathbf{e}\cdot\mathbf{r}\kappa\cdot\mathbf{r}\Psi_i)=\frac{(2\pi)^{\frac{1}{2}}}{40}\int_0^\infty r^2(uw_1+wu_1-2^{-\frac{1}{2}}ww_1)dr(\chi_1^{m'}, (\mathbf{e}\cdot\boldsymbol{\sigma}_1\kappa\cdot\boldsymbol{\sigma}_2+\kappa\cdot\boldsymbol{\sigma}_1\mathbf{e}\cdot\boldsymbol{\sigma}_2)\chi_1^m). \tag{68}$$

By proceeding as before, we obtain the total quadripole capture probability:

$$w_{\text{el quad}}^{(1\to1)}=\frac{\pi}{300}\frac{e^2}{\hbar c}\left(\frac{|E_0|}{Mc^2}\right)^2\frac{|E_0|}{\hbar}\alpha^4\left(\int_0^\infty r^2(uw_1+wu_1-2^{-\frac{1}{2}}ww_1)dr\right)^2. \tag{69}$$

The cross section for electric quadripole capture from the triplet state is therefore

$$\sigma_{\text{el quad}}^{(1\to1)}=\frac{\pi}{400}\frac{e^2}{\hbar c}\left(\frac{|E_0|}{2E}\right)^{\frac{1}{2}}\left(\frac{|E_0|}{Mc^2}\right)^2\alpha^5\left(\int_0^\infty r^2(uw_1+wu_1-2^{-\frac{1}{2}}ww_1)dr\right)^2. \tag{70}$$

The theoretical cross section for the magnetic dipole capture of thermal neutrons ($E=kT=0.025$ ev) from the singlet state, predicted by the customary theory, is $\sigma_c=0.312\times10^{-24}$ cm^2. The modification embodied in our formula (61) reduces this value to $\sigma_c=0.302\times10^{-24}$ cm^2, which is approximately the reduction to be expected from the four-percent probability of the $^3D_1$ state. The two additional modes of radiative capture discussed in this section, magnetic dipole and electric quadripole capture from the triplet states, have but a negligible influence on the total capture cross section. Indeed, even if the very existence of these transitions did not depend on the small fraction of $^3D_1$ state adjoined to the $^3S_1$ state, transitions from the triplet state could hardly be expected to compete successfully with a transition from the singlet state, for a neutron-proton system in the singlet state is in approximate resonance at small energies.

The radiative capture of slow neutrons by protons has been extensively investigated.[11] Although the results of the various experiments are not completely harmonious, those of apparently greater accuracy agree in obtaining a cross section equal to $\sigma_c=(0.27\pm0.02)\times10^{-24}$ cm^2. This value supposedly refers to a thermal neutron energy $E=kT$, but in actuality, the principal error in these measurements arises from the necessity of defining an effective energy by averaging over the uncertain energy spectrum of the thermal neutrons. The experiments are therefore insufficiently accurate to make the comparison with the theoretical value (0.30×10^{-24} cm^2) unsatisfactory. It should be stressed that even this measure of accord has been achieved only by employing the value of 20×10^{-24} cm^2 for the neutron-proton scattering cross section. The capture cross section is quite accurately proportional to the scattering cross section, and is effectively independent of the range of the forces. Thus, had the scattering cross section obtained by some investigators[12] ($\sim14\times10^{-24}$ cm^2) been used the capture cross section would be $\sigma_c\sim0.22\times10^{-24}$ cm^2 which is in apparent disagreement with the experimental measurement, particularly since the assumption of thermal equilibrium, used in defining the effective neutron energy, tends to underestimate the experimental capture cross section.

Photo-Disintegration of the Deuteron

Transitions from the ground state of the deuteron to the dissociated continuum states, induced by γ-ray absorption, may proceed by essentially four types of radiative processes: electric dipole, magnetic dipole and electric quadripole transitions to triplet states, and magnetic dipole transitions to singlet states. We shall confine our attention to low energy γ-rays, and therefore we shall neglect the magnetic dipole and electric quadripole transitions to the triplet state. Further, we shall adopt the

[11] E. Amaldi and E. Fermi, Phys. Rev. **50**, 899 (1936); C. H. Westcott, Proc. Camb. Phil. Soc. **33**, 122 (1937); O. R. Frisch, H. von Halban, Jr. and J. Koch, Kgl. Danske Vid. Sels. Math.-fys. Medd. **15**, 10 (1938); A. H. Spees, W. F. Colby and S. Goudsmit, Phys. Rev. **53**, 326 (1938).

[12] L. Simons, Kgl. Danske Vid. Sels. Math.-fys. Medd. **17**, 7 (1940); E. Amaldi, D. Bocciarelli, G. C. Trabacchi, Ricerca Scient. **11**, 121 (1940).

usual approximation which disregards the effect of nuclear forces on the ^3P states arising from electric dipole absorption.

Photoelectric absorption corresponds to a transition from the initial state described by the wave function (2), Ψ_i, to the P part of the plane wave $\exp[i\mathbf{k}\cdot\mathbf{r}]\chi_1^{m'}$, i.e.,

$$\Psi_f = 3i\left(\frac{\mathbf{k}\cdot\mathbf{r}}{kr}\right)\frac{g_1(kr)}{kr}\chi_1^{m'}, \quad \left(\frac{\hbar^2k^2}{M} = \hbar\omega - |E_0|\right). \tag{71}$$

The cross section for the absorption of a light quantum of energy $\hbar\omega$ described by the unit vectors $\mathbf{e}$, $\boldsymbol{\kappa}$, with the emission of the disintegration products into the solid angle $d\Omega$ about the propagation vector $\mathbf{k}$, is represented by:

$$\frac{e^2}{\hbar c}\frac{Mk}{\hbar^2}\hbar\omega\tfrac{1}{3}\sum_{m,m'}|(\Psi_f, \tfrac{1}{2}\mathbf{e}\cdot\mathbf{r}\Psi_i)|^2\frac{d\Omega}{4\pi}. \tag{72}$$

The required matrix element, simplified by performing the angle integrations, is composed of the terms describing the transitions $^3S_1\rightarrow{}^3P$, $^3D_1\rightarrow{}^3P$:

$$(\Psi_f, \tfrac{1}{2}\mathbf{e}\cdot\mathbf{r}\Psi_i) = -i\frac{\pi^{\frac{1}{2}}}{k}\left(\chi_1^{m'}, \left\{\frac{\mathbf{e}\cdot\mathbf{k}}{k}\int_0^\infty rg_1udr + \frac{2^{-\frac{1}{2}}}{5}\left(\frac{3}{2}\boldsymbol{\sigma}_1\cdot\frac{\mathbf{k}}{k}\boldsymbol{\sigma}_2\cdot\mathbf{e} + \frac{3}{2}\boldsymbol{\sigma}_1\cdot\mathbf{e}\boldsymbol{\sigma}_2\cdot\frac{\mathbf{k}}{k} - \frac{\mathbf{e}\cdot\mathbf{k}}{k}\right)\int_0^\infty rg_1wdr\right\}\chi_1^m\right). \tag{73}$$

The technique of averaging over the magnetic sub-states, described in the previous section, permits a simple derivation of the result:

$$\tfrac{1}{3}\sum_{m,m'}|(\Psi_f, \tfrac{1}{2}\mathbf{e}\cdot\mathbf{r}\Psi_i)|^2 = \frac{\pi}{k^2}\left\{\cos^2\Theta\left(\int_0^\infty rg_1udr\right)^2 + \frac{1}{25}(3+\cos^2\Theta)\left(\int_0^\infty rg_1wdr\right)^2\right\}. \tag{74}$$

Here $\cos\Theta = \mathbf{e}\cdot\mathbf{k}/k$, with Θ thus representing the angle at which the emitted particles emerge with respect to the polarization vector of the light quantum. The experimental situation pertains to an unpolarized beam of γ-rays, which necessitates the replacement of $\cos^2\Theta$ by its average over all directions of $\mathbf{e}$ perpendicular to $\boldsymbol{\kappa}$; *viz.*, $\frac{1}{2}\sin^2\vartheta$, where ϑ denotes the angle of emergence of the disintegration products with respect to the direction $\boldsymbol{\kappa}$ of the γ-ray. The cross section for electric dipole absorption, with emission into the solid angle $d\Omega$ is thus:

$$\frac{\pi}{2}\frac{e^2}{\hbar c}\frac{M\omega}{\hbar k}\left\{\sin^2\vartheta\left(\int_0^\infty rg_1udr\right)^2 + \frac{1}{25}(6+\sin^2\vartheta)\left(\int_0^\infty rg_1wdr\right)^2\right\}\frac{d\Omega}{4\pi}. \tag{75}$$

It is noteworthy that the spin-spin forces demand a spherically symmetric term in addition to the usual $\sin^2\vartheta$ photoelectric angular distribution. The total photoelectric cross section is then

$$\sigma_{\text{el dip}} = \frac{\pi}{3}\frac{e^2}{\hbar c}\frac{M\omega}{\hbar k}\left\{\left(\int_0^\infty rg_1udr\right)^2 + \frac{2}{5}\left(\int_0^\infty rg_1wdr\right)^2\right\}. \tag{76}$$

The permissible transitions induced by magnetic dipole absorption to the singlet state are: $^3S_1\rightarrow{}^1S_0$, $^3D_1\rightarrow{}^1D_2$. The latter transition would be of little interest were it not that it interferes with the transition to the $^1S_0$ state and therefore modifies the angular distribution of the particles. The cross section for magnetic dipole absorption is obtained from (72) by replacing the component of the electric moment in the direction of the electric polarization vector, i.e., $(e/2)\mathbf{e}\cdot\mathbf{r}$ by its magnetic analog, *viz.*, $(e\hbar/2Mc)\boldsymbol{\kappa}\times\mathbf{e}\cdot\mathbf{M}$. Therefore,

$$\tfrac{1}{4}(e^2/\hbar c)(\hbar\omega/Mc^2)k\tfrac{1}{3}\sum_{m'}|(\Psi_f, \boldsymbol{\kappa}\times\mathbf{e}\cdot\mathbf{M}\Psi_i)|^2(d\Omega/4\pi) \tag{77}$$

describes the cross section for a magnetic dipole transition to the nondegenerate final state,

$$\Psi_f=\left\{e^{-i\delta_0}\frac{u_0(r)}{kr}-\frac{5}{2}\left(3\left(\frac{\mathbf{k}\cdot\mathbf{r}}{kr}\right)^2-1\right)\frac{g_2(kr)}{kr}\right\}\chi_0{}^0,\quad u_0(r)\sim\sin(kr+\delta_0). \tag{78}$$

Here we have written only the perturbed $^1S_0$ continuum state[13] and the ^1D portion of the plane wave $\exp[i\mathbf{k}\cdot\mathbf{r}]\chi_0{}^0$. Upon performing the summation over the magnetic quantum number m of the initial state, and averaging the result with respect to the polarization vector of the light quantum, one obtains the formulae:

$$\frac{\pi}{3}\frac{e^2}{hc}(\mu_n-\mu_p)^2\frac{h\omega}{Mc^2}\frac{1}{k}\left\{\left(\int_0^\infty uu_0dr\right)^2-2^{-\frac{1}{2}}\cos\delta_0\left(\int_0^\infty uu_0dr\right)\left(\int_0^\infty g_2wdr\right)(3\cos^2\vartheta-1)\right.$$
$$\left.+\frac{1}{4}(5-3\cos^2\vartheta)\left(\int_0^\infty g_2wdr\right)^2\right\}\frac{d\Omega}{4\pi}, \tag{79}$$

$$\sigma_{\text{mag dip}}=\frac{\pi}{3}\frac{e^2}{hc}(\mu_n-\mu_p)^2\frac{h\omega}{Mc^2}\frac{1}{k}\left\{\left(\int_0^\infty u_0udr\right)^2+\left(\int_0^\infty g_2wdr\right)^2\right\}, \tag{80}$$

which represent, respectively, the differential and total cross sections for the photomagnetic transition to the singlet state.

Numerical calculations have been performed for $\hbar\omega=2.62$ Mev, the strong γ-ray line of Th C″. The kinetic energy of the disintegration products is therefore 0.45 Mev. At this small energy the functions g_1 and g_2 are minute within the region in which w is appreciably different from zero, and thus no significant contribution is to be expected from the transitions initiating in the $^3D_1$ state. Indeed, the principal modification is to reduce the cross sections for these two processes proportionately to the reduction in the integral $\int_0^\infty u^2dr$, the S state probability. The total cross section for the photoelectric process is found to be $\sigma_{\text{el dip}}=11.99\times10^{-28}$ cm^2, which is to be compared with 12.31×10^{-28} cm^2, computed from a simple rectangular well. The angular distribution represented in (75) differs but slightly from a $\sin^2\vartheta$ distribution: $\sin^2\vartheta+0.0007$. However, we shall show in the sequel that consideration of the interaction in P states, combined with large γ-ray energies, produces an appreciable relative intensity in the forward direction. The total photomagnetic cross section is $\sigma_{\text{mag dip}}=3.28\times10^{-28}$ cm^2, while the angular distribution: $1-0.0035\cos^2\vartheta$ is slightly altered from spherical symmetry by the interference with the ^1D state. The latter effect increases rapidly with energy and at the higher energies considered in the subsequent paper produces a significant reduction in the forward intensity of the photomagnetic particles.

The quantities to be compared with experiment are the total cross section: $\sigma_{\text{photo}}=15.27\times10^{-28}$ cm^2, and the net angular distribution: $(\sin^2\vartheta+0.182)$. The experiments of von Halban[14] reveal a most disturbing contradiction with this theory. The measured total cross section is only $(10\pm0.8)\times10^{-28}$ cm^2, while the intensity of the photo-neutrons ejected in the forward direction is at most 5 percent of that at right angles, in contrast with the theoretical expectation of 15 percent. Experiments of Chadwick, Feather and Bretscher[15] have provided confirmatory evidence by showing that a similar situation exists for the angular distribution of the photo-protons. These discrepancies could be removed if the photomagnetic cross section were much smaller than current theories predict. One point which should be mentioned is the weak 3.2-Mev γ-ray line which according to Ellis,[16] accompanies the main 2.6-Mev line of Th C″. This fact, however,

[13] The phase factor $e^{-i\delta_0}$ is introduced to make the asymptotic form of Ψ_f correspond to a plane wave and a *converging* spherical wave. Cf. N. F. Mott and H. S. W. Massey, *The Theory of Atomic Collisions* (Oxford University Press, 1933), p. 258.

[14] H. von Halban, Jr., Comptes rendus **206**, 1170 (1938).
[15] J. Chadwick, N. Feather and E. Bretscher, Proc. Roy. Soc. **A163**, 366 (1937).
[16] C. D. Ellis, Proc. Phys. Soc. **50**, 213 (1938).

provides but little solace, for to explain the angular distribution the 3.2-Mev line would have to be the principal component of the spectrum. This is a rather serious situation since the photo-disintegration process is simply the inverse of the magnetic capture process, which is in good accord with experiment. The only evident explanation is that there exists a further contribution to the magnetic moment operator arising from mesotron exchange currents. However, it is not clear why the small energy difference between the two continuum states involved in capture and photo-disintegration (450 kev) should have such a marked effect.

The general conclusion to be drawn from the preceding sections is that a satisfactory phenomenological theory of the neutron-proton system can be developed, with the exception of the magnetic photo-disintegration process, where for the first time we meet a phenomenon whose explanation apparently demands a detailed application of a field theory.

This investigation was begun by one of us (J. S.) at the University of Wisconsin while the recipient of a Tyndall Traveling Fellowship from Columbia University (1937–1938). He wishes to thank Professors Breit and Wigner for the benefit of stimulating discussions. We are also indebted to Professor J. R. Oppenheimer for his interest in this work.

MARCH 1, 1941 PHYSICAL REVIEW VOLUME 59

X-Ray Diffraction Maxima at Other Than Bragg Angles

PAUL KIRKPATRICK
Stanford University, California

(Received December 2, 1940)

Photographic observations of molybdenum $K\alpha$ lines internally reflected from (111) planes of diamond show that the angle of deviation is not constant with angle of incidence but varies in qualitative agreement with Zachariasen's theory of diffuse scattering and with observations of Raman and Nilakantan. Observations of the variation of line intensity and width with angle of incidence do not agree well with the theory in the cases observed. Spectrometer observations of reflections from calcite with slightly ground and with untreated cleavage surfaces upon which monochromatic radiation was incident at angles differing from the Bragg angle show detectable reflection over an 11° range of angles of incidence in the former case but only 2° in the latter. The large difference between these ranges indicates that disordered crystal particles are the principal source of reflected intensity at other than Bragg angles with the predominant crystal planes in the former case. The presumption is strong that this source has operated as a partial or complete explanation of some of the reflections hitherto reported as anomalous.

THE fact that x-rays may diffract from crystals in directions not precisely assignable to Bragg planes has been repeatedly discovered during the past thirty years. A frequent experience has been the observation of unexpected spots or radial streaks on Laue-spot photographs located close to, and presumably causally associated with, the ordinary and more readily explicable ones.[1]

The effects are usually such as to suggest that the reflecting planes, or some of them, possess in addition to the usual reflecting or diffracting characteristics the ability to reflect incident radiation in directions such that the angles of incidence and reflection are not precisely equal or that the latter angle is not limited to a single well-defined value. Such characteristics might result, it has been or may be suggested, from wavy "planes" having reflecting areas not sharing the general inclination, from mosaic blocks slightly askew, or from transient disorder accompanying thermal vibration. The latter suggestion, advanced in general terms of Faxén,[2]

[1] Many references are given by I. E. Knaggs, K. Lonsdale, A. Muller, A. R. Ubbelohde, Nature **145**, 820 (1940).

[2] H. Faxén, Zeits. f. Physik **17**, 226 (1923).

receives strong support from the recent detailed theory of such an effect put forward by Zachariasen.[3] It is too early as yet to say how completely this theory covers the matter, few of the necessary experiments having been performed. The present paper offers data relating to this question.

Sir C. V. Raman and collaborators[4] in recent discussions of unexpected maxima in Laue patterns present a less explicit theoretical treatment developing the view that the anomalous spots represent reflection of x-rays with change of frequency. They also offer a semi-empirical formula defining the directions of the abnormally reflected rays, with supporting numerical data from their own Laue-spot observations. There is described below an attempt to check and improve on certain measurements in these papers.

Diffraction by Diamond

The ordinary Laue-spot technique is not adapted to the precise measurement of angles and in this work narrow slits, replacing the customary round holes, limited the divergence of the incident beam in the plane of incidence to 0.0010 radian, while the crystal-to-film distance was increased to 13 cm. A diamond crystal of gem quality, prepared in the manner known to lapidaries as "rose cut," was mounted for internal reflection at room temperature by (111) planes. The orientation of the crystal about an axis normal to the plane of reflection and lying in the plane of the slits was subject to control and measurement. Molybdenum radiation, filtered through zirconium to emphasize the $K\alpha$ lines, was allowed to illuminate the stationary crystal in step-by-step exposures timed to obtain photographic recording of the alpha-lines for angles of incidence varying over a range of 1°41′, approximately centered on the Bragg angle.

Developed films showed, in general, two lines; a normally reflected general radiation line with wave-length and position dependent upon the crystal orientation, and the unresolved $K\alpha$ doublet at or near a position given by its characteristic deviation of twice the Bragg angle. This is the "anomalous" line or spot of past references.

A rigorous application of Bragg's law to an ideal crystal accounts for the first line only. The second line, long since observed in this laboratory with other crystals by both photographic and ionization methods, has been locally ascribed to crystal imperfection, i.e., blocks or surface disorder. No doubt this view has been held elsewhere, for insofar as the disordered conditions exist a line is inevitable. One suspects that the explanation is incomplete on finding, as did Raman and Nilakantan, that diamond, a crystal often possessing a high degree of structural perfection, shows the second line (spot) over a 20 percent variation of the angle of incidence. Investigation of the constancy of the angle of deviation offers the possibility of a crucial test.

From microphotometer records of seven films the angles of deviation of the centers of gravity of all lines from the direct ray were determined to about 0.5′. Figure 1 shows the resulting variation of the $K\alpha$ deviation with departure of the incidence angle (deduced from the position of the general radiation line) from the Bragg angle of the $K\alpha$ lines. In a general way this result agrees with and tends to confirm the diamond observations of Raman and Nilakantan whose results are also shown in the Fig. 1. These investigators summarized their observations by an empirical formula which is shown as a graph in the figure. However, in the view of the writer neither the present results nor any evidences offered in the papers of Raman and Nilakantan directly support the claim of these authors that this type of reflection is accompanied by a change of frequency.

In the theory of Zachariasen, lattice vibrations cause a type of diffuse scattering which for any wave-length and plane set has a well-marked intensity maximum near the direction of Laue-Bragg reflection; a maximum which has its greatest value when the crystal orientation is such that the ordinary reflection takes place but which exists with other orientations. The direction of the Zachariasen maximum is not constant with crystal orientation but shifts slightly in the manner which for small crystals is shown by the curve Z of Fig. 1. This curve is quite close to the

[3] W. H. Zachariasen, Phys. Rev. **57**, 597 (1940).
[4] C. V. Raman and P. Nilakantan, Proc. Ind. Acad. Sci. **11**, 379 (1940); **12**, 141 (1940); Nature, **145**, 667 (1940); **145**, 860 (1940). C. V. Raman and N. S. N. Nath, Proc. Ind. Acad. Sc. **12**, 83 (1940).

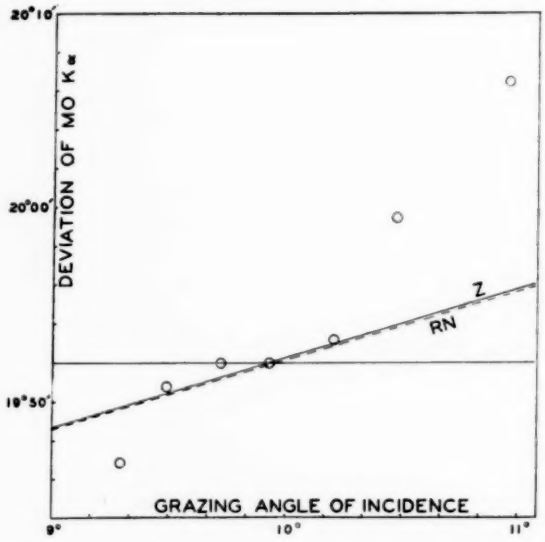

FIG. 1. Deviation of Mo $K\alpha$ as function of grazing angle of incidence upon (111) planes of diamond. The horizontal line shows deviations to be expected in the case of Bragg reflection from disordered crystal blocks. The line Z results from an application of Zachariasen's theory. In close agreement is the line RN from a semi-empirical equation of Raman and Nilakantan. Present observations are shown by circles, confirming, though only qualitatively, the asserted variability of the deviation.

empirical curve of Raman and Nilakantan and predicts shifts of direction in general agreement with, but less than, those of present observations. Siegel and Zachariasen have shown from their own experiments that the width and intensity of this line (as scattered by rocksalt) vary in fair agreement with the latter author's theory; the data above add a similar qualified confirmation as to angle of scattering.

In these results the intensity of the line in question diminished as the inclination of the crystal to the incident beam receded in either direction from the position of ordinary reflection of Mo $K\alpha$. Since exposure conditions were not carefully controlled, it is useless to compare directly the densities of the line on separate films. Rather the density of the line with which we are now concerned was ascertained for each film in terms of the density of the neighboring Laue-Bragg line. The latter probably bore an almost constant relation to the incident intensity in all cases since the angle of incidence was varied over a range of no more than fourteen percent. If this change is neglected the relative intensity variation with angle of incidence of the auxiliary line may be plotted as in curve A, Fig. 2, in which the area under the microphotometer trace has been taken as the measure of line intensity. The curve is therefore an approximate representation of the variation of total scattered line intensity with angle of incidence. The maximum shown is too steep for good agreement with Zachariasen's theory, which would require the curve to descend from its central peak in two approximately hyperbolic curves. If instead of plotting line areas we plot the heights of the microphotometer curve maxima, the graph B which is obtained does not differ significantly from A. It follows that the observed lines do not show a pronounced variation of width with angle of incidence, though there is some indication that width increases as the angle of incidence departs from the Bragg value, which would be in agreement with Zachariasen.

DIFFRACTION BY CALCITE

Strong emission lines may be observed with a Bragg spectrometer even though the inclination of the crystal to the incident radiation be very different from the Bragg angle. The $K\alpha$ doublet from a molybdenum target reflects most strongly from cleft calcite at an angle of 6°43′ but it is definitely observable over a range which, in the case shown in Fig. 3, extends at least from three to fourteen degrees. The spectrometer crystal in this case (curve A) was one which had been lightly ground with a fine abrasive to increase its reflecting power. The method of observation was to incline the crystal at a selected angle and go over the line by moving the ion chamber step by step across its usual position for reception of this wave-length. The height of the maximum of the curve so obtained, after deduction of the background, was taken as a measure of the relative intensity of the reflection. Figure 3 shows the variation of this reflected intensity with crystal angle. The conditions are such that observation of the Zachariasen diffuse radiation (or "anomalous" reflection of other investigators) might be expected but the radiation observed requires no special explanation, being, predominantly at least, ordinary reflection from disordered particles on the surface of the crystal.

The evidence for this is curve *B*, which was obtained in the same manner as curve *A* except that an untreated cleavage calcite surface was the reflector. The range of values of the angle of incidence within which reflection is detectable is eleven degrees for the ground surface and two degrees for the untreated surface. The scales of the two curves are such that their maximum ordinates are equal but *B* falls away very much more rapidly as the angle of incidence recedes either way from the value allowing reflection from the fundamental lattice.

Disordered surface crystalline particles contribute strongly to *transmission* reflection also, so this factor should be considered and eliminated before pronouncing an unexpected Laue spot "anomalous." The *existence* of an unusual spot does not prove anomaly (in the sense of a spot not allowed by Laue diffraction) though its precise position, width or variation of intensity with temperature may establish the case. Though calcite is homologous in structure with sodium nitrate (a crystal thought by Raman and Nilakantan to produce modified reflection), the data upon which Fig. 3 is based did not show variations of width or angular position which might identify the reflections with Zachariasen's diffuse scattering, though the precision of angular observations should have been sufficient for the test. With regard to calcite, then, no extraordinary reflection was found but instead an explicable intensity maximum of a sort which may have been taken in the past for the result of an anomalous or unexplained process. Further precise observations with these and other crystals have been started.

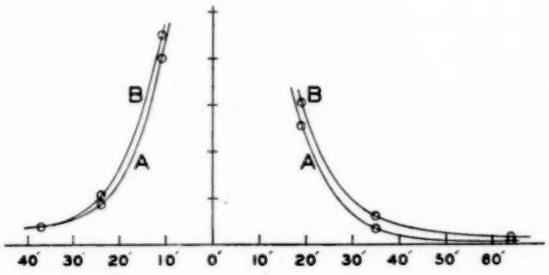

FIG. 2. Relative intensities of reflected Mo $K\alpha$ as function of grazing angle of incidence with (111) planes of diamond. (Zero of abscissa scale designates the Bragg angle.) Ordinates of curves *A* are proportional to areas under microphotometer traces of photographic records of reflected lines. Ordinates of curves *B* are proportional to peak heights of the same traces. Angle of incidence increases to right.

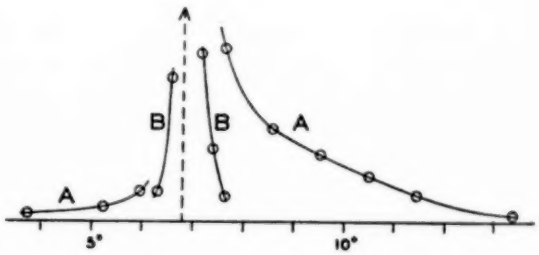

FIG. 3. Relative intensity of reflected Mo $K\alpha$ from calcite as function of grazing angle of incidence with abraded (*A*) and untreated (*B*) cleavage faces. The scales are such that the maxima of *A* and *B* at the Bragg angle (indicated by the broken line) reach the same height. The relatively wide base of curve *A* shows the important part which disarranged crystal particles may play in the production of diffraction maxima at other than Bragg angles of incidence.

Note on the Theory of the Modified Reflection of X-Rays by Crystals

G. E. M. JAUNCEY
Wayman Crow Hall of Physics, Washington University, St. Louis, Missouri

(Received January 6, 1941)

The existence of diffuse spots in x-ray crystal photographs which do not belong to the Laue pattern is now well established. Preston suggests that these modified reflections are caused by the breaking up of the crystal into small groups of atoms by thermal agitation. Bragg has derived a formula for the intensity of x-rays scattered by a group of eight atoms arranged at the corners of a cube of edge a. In this note the Bragg formula is further examined for the shift in the position of the diffraction maximum as the group is turned away from the position for the Laue-Bragg diffraction maximum. The theory shows that the approximate formula for the shift is the same as that derived on entirely different assumptions by Zachariasen and by Raman and Nath.

THE existence of diffuse spots and streaks in x-ray photographs which do not belong to the Laue pattern has been established by various experimenters.[1–5] Theories of these streaks and spots have been advanced by Preston,[1] Zachariasen,[6] and Raman and Nath.[7] Zachariasen[6] and, independently, Raman and Nath[7] have arrived at the theoretical relation

$$\tan \phi_{mB} = \frac{2 \sin \theta_B \cos j}{1 - 2 \sin \theta_B \sin j}, \tag{1}$$

where θ_B is the ordinary Bragg glancing angle of incidence for reflection of x-rays of wave-length λ from a set of planes whose grating space is d, j is the experimental glancing angle of incidence of x-rays on the same set of planes, and ϕ_{mB} is the angle of scattering to the most intense part of the modified Bragg reflection associated with the same set of planes. If j differs only slightly from θ_B (the crystal having been turned slightly from the ordinary Bragg position) so that $j-\theta_B$ is small, Zachariasen[3,6] has shown that (1) reduces to

$$\phi_{mB} - 2\theta_B = 2(j-\theta_B) \sin^2 \theta_B. \tag{2}$$

Raman and Nath[7] have also suggested that the alternative theoretical relation

$$j + r = 2\theta_B \tag{3}$$

holds for certain crystals. In (3), r is the glancing angle of reflection from the set of crystal planes to which θ_B is referred. For these crystals (3) holds for values of j considerably removed from θ_B.

In this note we shall confine ourselves to a discussion of Preston's theoretical ideas, according to which the crystal is broken up into small groups of atoms by thermal agitation. Preston[1] suggests that the group may consist of an atom and its twelve neighbors. These groups tend to scatter x-rays somewhat independently of each other. This independent scattering must be far from complete, otherwise a crystal would scatter x-rays in a fashion similar to the scattering by a molecular gas such as carbon tetrachloride and the intensities of the diffraction maxima would not be comparable with those experimentally found for the Laue-Bragg maxima. However, it may be that for a given set of crystal planes the groups of atoms cooperate in their scattering for $j=\theta_B$ but that, as the set of planes is turned from $j=\theta_B$ to $j=j$, this cooperation ceases and the independent scattering by the small groups of atoms becomes relatively more important. It might be expected that such independent scattering would produce observable intensities for small but not large values of $(j-\theta_B)$.

Bragg[8] has recently subjected Preston's suggestion to quantitative theoretical study. Bragg has calculated the intensity of x-rays scattered by a group of eight point-atoms (diffracting

[1] G. D. Preston, Proc. Roy. Soc. **A172**, 116 (1939).
[2] C. V. Raman and P. Nilakantan, Proc. Ind. Acad. Sci. **11A**, 379 (1940).
[3] S. S. Siegel and W. H. Zachariasen, Phys. Rev. **57**, 795 (1940).
[4] K. Lonsdale, I. E. Knaggs and H. Smith, Nature **146**, 332 (1940).
[5] G. E. M. Jauncey and O. J. Baltzer, Phys. Rev. **58**, 1116 (1940).
[6] W. H. Zachariasen, Phys. Rev. **57**, 597 (1940).
[7] C. V. Raman and N. S. G. Nath, Proc. Ind. Acad. Sci. **12A**, 83 (1940).
[8] W. H. Bragg, Nature **146**, 509 (1940).

centers) arranged at the corners of a cube of edge a. Let the edges of the cube be parallel to the axes of x, y and z and let the primary beam of x-rays be in the plane of xy and make an angle i with the axis of x (hence the glancing angle of incidence on an xz face of the cube is i). The direction cosines of the incident beam are $\cos i$, $-\sin i$, 0. Let the direction cosines of the diffracted or scattered beam be q_1, q_2, q_3. Bragg finds that the amplitude of the diffracted ray is proportional to

$$\cos A \cos B \cos C, \tag{4}$$

where

$$A = \pi a(\cos i - q_1)/\lambda, \tag{5}$$

$$B = -\pi a(\sin i + q_2)/\lambda, \tag{6}$$

and

$$C = -\pi a q_3/\lambda. \tag{7}$$

However, (4) may be put in a more interesting and instructive form by multiplying numerator and denominator by $\sin A \sin B \sin C$. Then, on squaring the result, we find that the intensity of the scattered beam is given by

$$I = \text{const} \times \frac{\sin^2 NA}{\sin^2 A} \cdot \frac{\sin^2 NB}{\sin^2 B} \cdot \frac{\sin^2 NC}{\sin^2 C}, \tag{8}$$

where $N=2$. It can be shown that (8) holds for a simple cubic lattice of principal grating space a with N atoms on an edge of the lattice cube, where N is any integer greater than unity. Equation (8) is the well-known formula for the intensity of x-rays diffracted by a large mosaic block of a crystal such as sylvine with, say, $N=5000$ atoms on a cube edge. The principal maxima occur when A, B, C, respectively, equal $h\pi$, $k\pi$, $l\pi$, where h, k, l are integers, one of which must be different from zero. Let a principal maximum occur when $i=i_B$ and

$$q_1, q_2, q_3 = q_{1B}, q_{2B}, q_{3B},$$

respectively. Then from (5), (6), (7)

$$q_{1B} = \cos i_B - \lambda h/a, \tag{9}$$

$$q_{2B} = -\sin i_B - \lambda k/a, \tag{10}$$

$$q_{3B} = -\lambda l/a. \tag{11}$$

Squaring and adding, we obtain

$$\lambda(h^2+k^2+l^2) = 2a(h \cos i_B - k \sin i_B). \tag{12}$$

Consider the plane whose normal has direction cosines proportional to hkl. We shall call this plane the hkl plane. When N is a large number such as 5000, the plane will represent a plane of atoms or a set of such planes, but when N is a small number such as 2, no plane of atoms will in general be discernible. The glancing angle of incidence θ_B on the hkl plane is given by

$$\sin \theta_B = (h \cos i_B - k \sin i_B)/(h^2+k^2+l^2)^{\frac{1}{2}}. \tag{13}$$

Hence (12) may be written in the form

$$\lambda(h^2+k^2+l^2)^{\frac{1}{2}} = 2a \sin \theta_B. \tag{14}$$

Thus the directions of the principal diffraction maxima are given by the same formula for a simple cubic lattice with $N=2$ as for such a lattice with $N=5000$. The maxima in the latter case are, of course, very much sharper than in the former. In either case we shall refer to the maxima as Laue-Bragg maxima. These maxima occur when $i=i_B$ and the scattering angle $\phi=\phi_B=2\theta_B$.

Let the cube (or the crystal of which the cubic group is a part) be turned about the axis of z through an angle $i-i_B=\delta i$, where δi is small but not infinitesimal. With δi fixed the intensity of the scattered beam varies with ϕ, reaching a maximum at $\phi=\phi_{mB}$. We shall call this maximum the modified Bragg diffraction maximum. The position of this maximum is found by putting $\partial I/\partial\phi=0$ and solving for ϕ. For brevity and simplicity we shall restrict ourselves to the modified Bragg reflections which occur in the equatorial plane, which is the xy plane. In this case $q_1=\cos(\phi-i)$, $q_2=\sin(\phi-i)$ and $q_3=0$. Equation (8) now becomes

$$I = \text{const} \times \frac{\sin^2 NA}{\sin^2 A} \cdot \frac{\sin^2 NB}{\sin^2 B}, \tag{15}$$

where

$$A = (\pi a/\lambda)\{\cos i - \cos(\phi - i)\}, \tag{16}$$

$$B = -(\pi a/\lambda)\{\sin i + \sin(\phi - i)\}. \tag{17}$$

Hence at a modified Bragg maximum

$$(N \cos NB - \sin NB \cot B) \sin NA \cos(\phi - i) = (N \cos NA - \sin NA \cot A) \times \sin NB \sin(\phi - i). \tag{18}$$

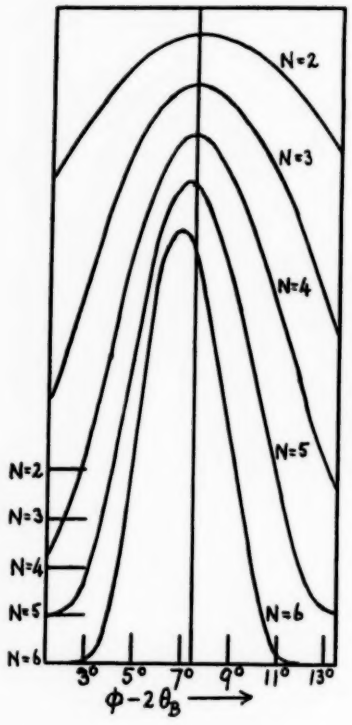

FIG. 1. Graphs of intensity of x-rays *versus* scattering angle for $N=2$, 3, 4, 5, 6. The maxima are adjusted to be of the same height. The zero ordinate for each curve is shown on the left of the diagram.

We have assumed that $i-i_B=\delta i$ is small. Consequently, we may also assume that $\phi_{mB}-\phi_B=\delta\phi$ is small. From (16)

$$\begin{aligned}\delta A &= (\pi a/\lambda)\{-\sin i_B\delta i+\sin(\phi_B-i_B)\delta\phi \\ &\qquad -\sin(\phi_B-i_B)\delta i\} \\ &= -(\pi a/\lambda)\{2\sin\tfrac{1}{2}\phi_B\cos(\tfrac{1}{2}\phi_B-i_B)\delta i \\ &\qquad -\sin(\phi_B-i_B)\delta\phi\}\end{aligned} \tag{19}$$

and similarly from (17)

$$\begin{aligned}\delta B = -(\pi a/\lambda)\{&2\sin\tfrac{1}{2}\phi_B\sin(\tfrac{1}{2}\phi_B-i_B)\delta i \\ &+\cos(\phi_B-i_B)\delta\phi\}.\end{aligned} \tag{20}$$

Since $A=h\pi+\delta A$ and $B=k\pi+\delta B$ and since δA and δB are small, $\sin A=(-1)^h\delta A\{1-(\delta A)^2/6\}$, $\cos A=(-1)^h\{1-(\delta A)^2/2\}$, $\sin NA=(-1)^{Nh}N\delta A\{1-(N\delta A)^2/6\}$, $\cos NA=(-1)^{Nh}\{1-(N\delta A)^2/2\}$, and corresponding relations for B. Consequently (18) may be replaced by the approximate relation

$$\delta A\sin(\phi_B-i_B)=\delta B\cos(\phi_B-i_B). \tag{21}$$

In virtue of (19) and (20), this becomes

$$\delta\phi=2\sin^2\tfrac{1}{2}\phi_B\delta i. \tag{22}$$

Since we are dealing with a modified $hk0$ reflection (see Jauncey and Baltzer[5] for notation), $i-i_B=j-\theta_B$ and (22) may be written in the form

$$\phi_{mB}-2\theta_B=2(j-\theta_B)\sin^2\theta_B. \tag{23}$$

which is the same as the Zachariasen-Raman-Nath relation (2).

It is astonishing that the Preston-Bragg assumption of scattering by small groups of atoms should lead to the same approximate relation as the very different assumptions of Zachariasen[6] and of Raman and Nath.[7] In the derivation of (22) it is assumed that δi, $\delta\phi$, δA, $N\delta A$, δB and $N\delta B$ are small. Just how small must these quantities be in order that (22) may be a good approximation? For the equatorial Bragg and modified Bragg spots, rocksalt may be treated as a simple cubic crystal with $a=2.814$A. The 310 Bragg reflection of Cu $K\alpha_1$ x-rays from rocksalt occurs at $\theta_B=59°\,40'$ and $i_B=41°\,20'$. (i_B is the glancing angle of incidence on a 100 cleavage face, not that on the 310 planes.) The intensity I as given by (15) has been plotted against ϕ for $i-i_B=5°$. The graphs for $N=2$, 3, 4, 5, 6 are shown in Fig. 1. The graphs are not symmetrical about their respective maxima and are somewhat difficult to plot. As nearly as can be judged from the graphs the maxima occur at $\phi_{mB}-2\theta_B=7°\,27'$, the value given by (22) or (23), for $N=2$, 3, 4. This position is shown by the vertical line near the center of Fig. 1. The graphs for $N=5$ and 6 show maxima at angles $(\phi_{mB}-2\theta_B)$ distinctly less than $7°\,27'$ and the approximation becomes poor.

Letters to the Editor

PROMPT publication of brief reports of important discoveries in physics may be secured by addressing them to this department. Closing dates for this department are, for the first issue of the month, the eighteenth of the preceding month, for the second issue, the third of the month. Because of the late closing dates for the section no proof can be shown to authors. The Board of Editors does not hold itself responsible for the opinions expressed by the correspondents.

Communications should not in general exceed 600 words in length.

The Reflection and Diffraction of Molecular Beams at Lithium Fluoride Cleavage Surfaces

WILLIAM H. BESSEY*
Research Laboratory of Molecular Physics, Carnegie Institute of Technology, Pittsburgh, Pennsylvania
February 4, 1941

IN their study of the reflection and diffraction of molecular beams at crystal surfaces, Frisch and Stern[1] found certain anomalies which they suggested might be due to diffraction from a secondary structure such as was postulated by Zwicky.[2] It seemed desirable to investigate the matter further, as there were no conclusive proofs of the existence of such a structure. For this purpose many reflectivity curves of the following type were made. A beam of helium atoms or hydrogen molecules fell on a freshly cleaved lithium fluoride crystal at a glancing angle of 18 degrees and was reflected into a fixed slit which led to a hot wire manometer. The crystal was rotated about the axis in its face perpendicular to the plane containing the normal and the incident beam, and the intensity was plotted as a function of the angle.

It was found that the intensity patterns were not the simple triangles expected from theory, but contained varying numbers of maxima separated by angles of a degree or less. Typical examples are shown in Fig. 1. The same results were found with both hydrogen and helium. If they had been diffraction effects, the angular distances between consecutive maxima would have been different for the two gases. This is due to the fact that with the crystal, as with all gratings, the deviations of a diffracted beam depend upon the wave-lengths, and, for the small angles used here, are proportional to them. The ratio of the de Broglie wave-lengths of hydrogen and helium, and, therefore, the ratio of the distances between corresponding orders of diffraction, is $\sqrt{2}$ to 1. In every case these angular distances were exactly the same for both hydrogen and helium; a typical example is shown in Fig. 2. Here the angular separation for helium is one degree. That for hydrogen is certainly the same to within two or three minutes; it cannot possibly be $\sqrt{2}$ degrees or 1° 25′. Therefore, the effect cannot be explained as a diffraction effect. Thus there was found in the present work no evidence for the existence of a Zwicky structure. These results are not in agreement with those of Johnson[3] who found indications of diffraction from a secondary lattice when he was studying a beam of atomic hydrogen and detecting it by chemical means.

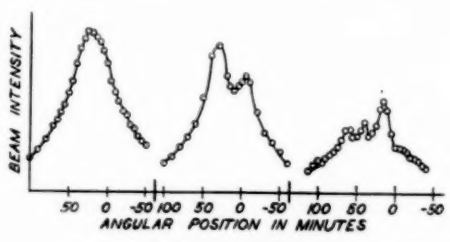

FIG. 1. Typical reflectivity curves.

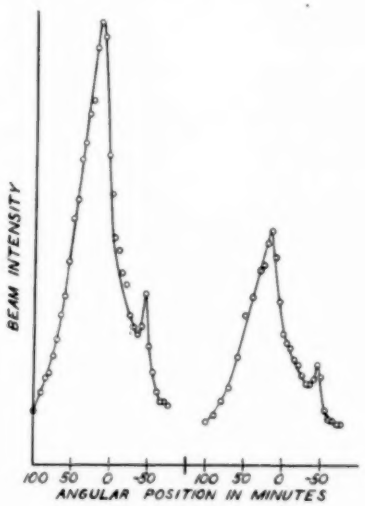

FIG. 2. Comparison of the reflectivity of hydrogen and helium.

A simple explanation of the shape of the curves is that the crystals, although considered single by ordinary criteria, are not ideal, but are made up of many crystallites of sizes up to a millimeter in diameter, tipped at small angles to each other. This would seem to verify the work of Renninger,[4] who found in his x-ray studies of the reflectivity of artificially grown rocksalt crystals that they were made up of microcrystals of the same size as those found in the molecular beam work, but with angles between them much smaller. This discrepancy might be due to the difference in the materials studied. The two effects are almost certainly related, but nothing more definite can be said until further investigations are made.

The author wishes to express his thanks to Professor O. Stern, who suggested the problem, and whose constant advice made it possible to carry it out. This work was aided by a grant from the Buhl Foundation.

* Now at North Carolina State College.
[1] R. Frisch and O. Stern, Zeits. f. Physik **84**, 430 (1933).
[2] F. Zwicky, Proc. Nat. Acad. Sci. **15**, 816 (1929) and elsewhere.
[3] T. H. Johnson, Phys. Rev. **37**, 87, 847 (1931).
[4] M. Renninger, Zeits. f. Krist. **89**, 344 (1934).

Direct Measurement of the Mass of the Mesotron

L. LEPRINCE-RINGUET, S. GORODETZKY, E. NAGEOTTE, AND R. RICHARD-FOY
Laboratoire de l'Ecole Polytechnique, Paris, and Laboratoire de l'Electro-aimant, Bellevue, France
February 8, 1941

WITHOUT doubt the most direct method of measuring the mass of a cosmic-ray mesotron is that of observing in a Wilson cloud chamber the elastic collision between the mesotron and an electron of the gas.

This method brings in only the fundamental laws of electricity (action of a current on an electrical particle in motion) and of classical mechanics (conservation of energy and momentum), while the other usable methods depend on hypotheses or on formulae which have in general been subjected to experimental investigation only in a range considerably removed from the one in which they are used.

The diagram of a collision for the case which can be utilized for a measurement of the mass of the incident particle is shown in Fig. 1. PQ is the trajectory of the incident particle, ABC is that of the struck electron which is deflected a distance f from PQ. If one designates by ρ_1 and ρ_3 the radii of curvature of the mesotron and the electron, one should obtain the ratio $\mu_0=M_0/m_0$ of the rest masses of the two particles as a function of ρ_1, ρ_3 and f by writing the laws of elastic collision at the point A. In the diagram the trajectories are assumed to be in a plane perpendicular to the direction of the magnetic field.

Unfortunately the probability of obtaining a favorable example of this phenomenon is very small. In view of the large energy of cosmic-ray particles a strong magnetic field should be used in order to obtain ρ_1 with precision, but in that case the displacement f would be very small on account of the nature of the incident ray, and this makes a precise measurement difficult. If one uses a weak magnetic field, the distance f becomes greater and can be more accurately measured, but then the curvature of the incident ray is generally too small to permit of a good evaluation. It does not appear that the photographs so far obtained of collisions in the gas[1] have permitted precise measurements.

We have had the good fortune of obtaining in the course of our cosmic-ray studies with a Wilson cloud chamber of 55 cm diameter, operating in a weak field of 2650 gauss supplied by the Bellevue magnet, a picture (Fig. 2) of a collision in which all the quantities are measurable with precision.[2] The picture was obtained in March 1939, but it has not been possible, on account of the war, to send it in for publication until September, 1940.

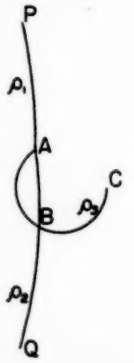

FIG. 1.

The formula for the collision can be written in the following simple form for the present case in which $\rho_3 \ll \rho_1$ and on the logical assumption that the particles have the same electric charge

$$\mu_0=\frac{M_0}{m_0}=\frac{\rho_1}{\rho_0(r_4-\rho_0)}\left[(r_3+r_4-\rho_0-f)(r_3-r_4+\rho_0-f)\right]^{\frac{1}{2}}$$

in which:

M_0 is the rest mass of the incident particle
m_0 is the rest mass of the electron
ρ_0 is the length m_0C^2/ecH (which can be called the radius of curvature corresponding to the rest mass of the electron)
r_4 is the length $r_4^2+\rho_0^2$
$r_3=\rho_3/\cos\theta$, θ being the angle (supposed small) which the secondary makes with the plane normal to the magnetic field.

The following are the measurements from our picture:

$115<\rho_1<120$ cm
$1.05<\rho_3<1.10$ cm
$0<f<0.03$ cm
$\cos\theta=0.97$.

The particle is negative and its mass as calculated from the above values is $M_0=240m_0$. The value obtained by Neddermeyer and Anderson[3] for a positive particle from the measurement of its curvature and range has given a result which is close to ours.

In studying the influence of possible errors (errors in the values of H, f, ρ_1, ρ_3, $\cos\theta$ and those due to the photographic conditions) one finds that the value of the mass of the mesotron should be accurate to somewhat less than ± 10 percent. On this basis we take

$$M_0=(240\pm 20)m_0.$$

From a stereoscopic examination of the picture there seems to be no possibility of error in regard to the secondary nature of the ejected electron. It should also be mentioned that if the incident particle had been an electron the deflection would have been 4 mm while it was actually not more than $\frac{1}{3}$ mm; also, if the mass of the incident particle were that of a proton, the radius of curvature ρ_3 would not have been more than one-tenth of that actually observed.

Another interesting point can be seen by the examination of the track after the collision. The mesotron traverses a box containing two G-M coincidence counters and appears after this traversal with a decrease in its energy. The kinetic energy of the mesotron changes from a value of 29×10^6 ev above the counters to a value of 9×10^6 ev below the counters. This corresponds to a loss of energy $\Delta w=20\times 10^6$ ev in traversing a thickness of 4.5 mm of metal of sp. gr. 8. This energy loss is in good accord with the curves of ionization as a function of $H\rho$.[4] For a mass $=250$ and $\log H\rho=5.31$, we find for the expected mean ionization loss a value of 160 ion pairs per cm of air traversed, which corresponds to 19×10^6 ev. This is in

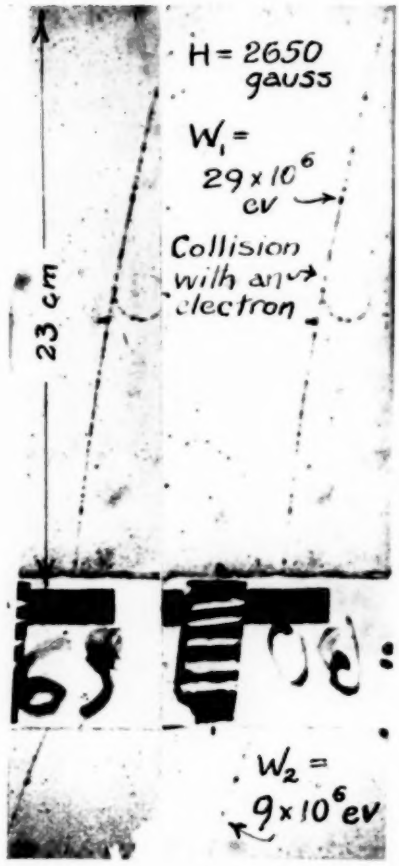

FIG. 2. Stereoscopic cloud-chamber photograph of a cosmic-ray mesotron of mass $M_0=(240\pm20)\ m_0$. The measurement of the mass was obtained from the elastic collisions with an electron of the gas in the chamber.

good accord with the value 20×10^6 ev obtained directly from our picture.

Finally, after the traversal of the box of counters, the track shows a heavier ionization; it appears more like a continuous line instead of the discrete droplets which one sees above the absorber.

[1] J. G. Wilson, Proc. Roy. Soc. London **A166**, 482 (1938); P. M. S. Blackett, *La Radiation Cosmique* (Hermann, 1935), plate X; L. Leprince-Ringuet and J. Crussard, J. de phys. et rad. **8**, 207 (1937).
[2] L. Leprince-Ringuet, S. Gorodetsky, E. Nageotte and R. Richard-Foy, Comptes rendus (Oct. 14, 1940).
[3] S. H. Neddermeyer and C. D. Anderson, Phys. Rev. **54**, 88 (1938).
[4] R. Brode, Rev. Mod. Phys. **11**, 223 (1939).

Pair Production in the Field of an Electron

KENICHI SHINOHARA AND MITIO HATOYAMA
Institute of Physical and Chemical Research, Hongo, Tokyo
January 17, 1941

F. PERRIN[1] predicted and studied from a theoretical point of view the possibility of pair production by a photon in the field of an electron. M. da Silva[2] found a triplet of two negative and one positive electrons starting from a point in a thin lead foil in a cloud chamber placed near an active deposit from Th, which he attributed to pair production by the gamma-rays from ThC″ in the field of an electron.

FIG. 1. A photograph of pair production in the field of an electron. Three tracks, two negative and one positive, start from a point (indicated by an arrow) in the gas filling the chamber. Another small black point is seen which resembles a track of a heavy particle, but stereoscopic examination reveals this to be a dust at the bottom of the chamber.

We obtained during the study of gamma-rays from fluorine bombarded with protons a photograph shown in Fig. 1.

Three electron tracks, two negative and one positive, start from a point in the gas filling the cloud chamber. The energies of these three electrons are: positron 2.38 Mev; electron 2.38 Mev; electron 0.17 Mev. These values give 4.93 Mev as the total kinetic energy of the three electrons, which in turn gives the value 5.95 Mev for the energy of the incoming photon, assuming that this is really another case of pair production by a photon in the field of an electron. To this value must be added a probable error of ±2 percent this value agrees within the limits of experimental error with our[3] value of 6.1 ± 0.1 Mev for the energy of gamma-rays from $F+p$ and also with the values given by Lauritsen and others.[4]

Further search for photographs of such triplets is in progress, the result of which will soon be published in a Japanese journal.

[1] F. Perrin, Comptes rendus **197**, 1100 (1933).
[2] A. Marques da Silva, Ann. de physique **11**, 504 (1939).
[3] K. Shinohara and M. Hatoyama, to be published soon.
[4] L. A. Delsasso, W. A. Fowler and C. C. Lauritsen, Phys. Rev. **51**, 527 (1937); C. C. Lauritsen, W. A. Fowler and T. Lauritsen, Phys. Rev. **56**, 858 (1939).

Soft Component and Decay of Mesotrons at 3000 Meters

NIKITIN FEDORENKO
Physico Technical Institute, Leningrad, U.S.S.R.
February 10, 1941 (By cable)

WE found the ratio of soft and hard component independent of zenith angle. We thus conclude both components to be in mutual equilibrium. This ratio increases from sea level to 3000 meters 1.33 times. Our results lead to the conclusion that electrons take only one-half of the decay energy of mesotrons. The remainder is probably given to neutrinos. Mean lifetime of mesotrons follows 2 5 microseconds.

On the Spin of the Mesotron

J. R. OPPENHEIMER
Physics Department, University of California, Berkeley, California
February 14, 1941

IN two papers in this issue of *The Physical Review* Christy and Kusaka[1] have given minimum estimates for the probability of radiative collisions by mesotrons, and have shown that these involve, for a mesotron of spin one and mass of the order of two hundred electron masses, a frequency of burst production greater by more than an order of magnitude than that actually found. In the case of mesotrons of zero spin the agreement with observation is good; in the case of mesotrons of spin $\frac{1}{2}$ and unit magnetic moment the calculated values exceed the experimental by a factor of about 1.6, a factor which probably lies within the uncertainties of the calculation, in particular the rather large uncertainty introduced by the unknown mass m of the mesotron. Nevertheless the many experimental indications of the beta-instability of mesotrons, and in particular the result of Nelson's analysis[2] of the data of Neher and Stever, that about one-half of the energy of mesotron decay is shower producing, would seem fully to have confirmed Yukawa's suggestion that mesotrons can disintegrate into electrons and neutrinos; and this would in our opinion make a half-integral value of the mesotron spin improbable. These arguments would then establish that the mesotron was described by a scalar or pseudoscalar field. It may be remarked in this connection that the neutron proton forces derived[3] from a charged pseudoscalar field by "classical" or perturbation-theoretic approximation agree in sign and spin dependence, though not of course in their singular dependence upon distance, with the sign and magnitude of the singlet triplet difference and the quadripole moment of the deuteron system, whereas the corresponding theory for charged mesotrons of unit spin gives a quadripole moment of wrong sign. The results of CK can thus not be regarded as adding a further difficulty to this in itself highly unsatisfactory theory of nuclear forces.

The calculations of CK give minimum estimates of burst production for the following reasons:

(1) They have in each case been made with that value of the magnetic moment which gives the smallest radiative probabilities compatible with the spin considered.

(2) They do not include nuclear collisions, and any electromagnetic or nuclear secondaries such collisions might produce.

(3) They include only those processes whose probability can legitimately be computed by perturbation theory; in them any contribution from processes that do not satisfy this condition has been discarded.

The first two points are fully discussed in the papers of CK, and of Corben and Schwinger.[4] It is only the last we wish to review here, since on this depends the cogency of the conclusions reached.

The radiative collisions of a mesotron of mass m and energy ξmc^2, $\xi \gg 1$, with the Coulomb field of a nucleus of charge Z and radius $\hbar Z^{\frac{1}{3}}/mc$, may with good approximation, insofar as they are extranuclear, be treated as the Compton scattering by the mesotron of the virtual quanta in the contracted field of the nucleus. In this coordinate system, where the mesotron is at rest, the maximum field acting on the mesotron, when it is nearest to the nucleus, is of the order $eZ^{\frac{1}{3}}\xi(mc/\hbar)^2$. The ratio of the interaction energy of this field with the mesotron charge and current is $Z^{\frac{1}{3}}\alpha^{\frac{1}{3}}(\alpha = e^2/\hbar c)$; and the probability of processes involving the absorption of n virtual quanta is small of the order $(\alpha Z^{\frac{1}{3}})^{n-1}$ compared to that of the absorption of one virtual quantum. This circumstance makes it possible to treat the effect of the various virtual quanta additively, and in particular to eliminate the possibility that the presence of a small intensity of high frequency quanta can sensibly alter the reaction of the mesotron to radiation of lower frequency.

For the further consideration of what happens when a quantum of frequency ν is absorbed by a mesotron, it is convenient to introduce a coordinate system in which mesotron and quantum have equal and opposite momenta, in which all momenta are of the order $P = (mh\nu)^{\frac{1}{2}}$, and all scattering processes are essentially isotropic. For the validity of the perturbation-theoretic treatment of the Compton effect, it is now further necessary that the coupling energy between light quanta of momentum P and mesotrons of momentum P be small compared to the energy of light quantum or mesotron, a condition which is satisfied if and only if $P < mc/\alpha^{\frac{1}{2}}$. This condition is not only necessary for the formal derivation of the scattering formula, but is also the condition that processes involving the simultaneous emission of several light quanta or several mesotron pairs be unlikely compared to the calculated process of simple scattering. In fact the relative probability that q quanta and p pairs be emitted is of the order $S_{q,p}(\alpha P^2/m^2c^2)^{q+2p}$, where the $S_{q,p}$ are numbers of order unity but presumably less than one, of which only the first, $S_{1,0} = (5/72)^{\frac{1}{2}}$, has been computed. For virtual quantum frequencies higher than $mc^2/h\alpha$, one may then expect the emission of large numbers of quanta and mesotron pairs: of these the former but not the latter will be burst-producing. For frequencies under this limit, multiple processes are unlikely, and there is no reason to expect competition[5] from them to reduce the probability of single scattering, or to doubt the applicability of perturbation theory.

What CK have done is to leave out altogether all scattering processes of virtual quanta of frequency above $mc^2/h\alpha$, and to show that their results on burst production, especially for the smaller burst sizes, are not at all critically dependent on the exact frequency of this "cut-off." It is true that the calculations of CK necessarily involve the application of the quantum theory of the electromagnetic field to space time regions smaller than any for which this theory has heretofore been directly verified. But apart from this it would seem that no valid argument could be found against the cogency of their conclusions.

[1] R. F. Christy and S. Kusaka, Phys. Rev. **59**, 405, 414 (1941) quoted as CK.
[2] E. Nelson, Phys. Rev. **58**, 771 (1940).
[3] W. Rarita and J. Schwinger, Phys. Rev. **59**, 436 (1941). This result is obtained by using a pure pseudovector coupling, and introducing suitable square well potentials for the radial dependence of the forces.
[4] H. C. Corben and J. Schwinger, Phys. Rev. **58**, 953 (1940).
[5] See for instance L. Landau, J. Phys. USSR **2**, 483 (1940). I am indebted to Professor Pauli for calling to my attention the relevance of Landau's argument to the calculations of CK.

Simultaneous Emission of Particles and Pair Production

SERGIO DE BENEDETTI*
Laboratoire Curie, Paris, France
February 9, 1941

THE agreement between the theory and the experimental results on pair production by radioactive substances has not always been satisfactory. Authors working with cloud chambers[1-4] observe a number of positrons which is much larger than the theoretical predictions, but such an excess was not detected by several authors using counters;[5,6] furthermore some investigators have recorded pair emission by β-rays,[2-4,7] that others have not been able to confirm.[5,6,8] In connection with this problem, simultaneous emission of charged particles has been studied by means of coincidence counters.[9]

The radioactive sources, obtained from the active deposit of thorium were placed between two counters (having windows covered by aluminum foils 10μ thick), so that coincidences were produced by at least two simultaneous rays. Special care was taken to eliminate the effects of electron reflection and of chance coincidences.

By means of absorption measurements and by separating the different bodies of the active deposit from each other, it has been possible to show that the coincidences were chiefly due to the following phenomena: (i) emission of α-particles from ThC′ following the β-disintegration of ThC with a period of the order of 10^{-7} sec.;[10] (ii) emission of electrons of atomic internal conversion from ThB in coincidence with the β-ray of disintegration; (iii) simultaneous emissions from ThC″ probably connected with pair emission.

The absorption of the simultaneous rays from ThC″ (separated by recoil from the active deposit) was consistent with the hypothesis that they were originated by internal production of pairs by the γ-rays of 2.6 Mev; an attempt to study the distribution in angular opening between the simultaneous rays seemed to show a faint asymmetry in agreement with the theory of internal pair emission.[11] The number of pairs emitted per disintegration was evaluated by taking into account the geometrical conditions and the fact that from pair production originate three simultaneous rays (e^+, e^-, and β-ray of disintegration). The number of pairs observed was about 50 times greater than the theoretical prediction; the order of magnitude of this result agrees with the determination from cloud-chamber experiments and shows that it is not the counter technique itself that is responsible for the discrepancy between the results previously obtained by these two methods.

Comparing the number of coincidences observed from the active deposit as a whole (after elimination by absorption of the coincidences due to α-rays and to the soft electrons of atomic internal conversion) with the number of coincidences from ThC″ alone, it was found that pair production from ThC″ was equal to pair production from the whole active deposit. This seems to prove that there is no internal pair production by β-rays, because in this case we should have observed pair production from ThC, which emits β-rays of energetic distribution similar to that of ThC″.

I take this occasion to thank all the persons who, with their friendly reception and their constant help, made possible and pleasant my work at the Laboratoire Curie. In particular I wish to express my profound gratitude to Madame Joliot-Curie for her interest in this work and for her valuable advice. I am indebted to the Caisse Nationale des Recherches of the free French Government for a fellowship.

* Now at the Bartol Research Foundation of the Franklin Institute Swarthmore, Pennsylvania.
[1] J. Chadwick, P. M. S. Blackett and G. P. S. Occhialini, Proc. Roy. Soc. **144**, 235 (1934).
[2] D. Skobeltzyn and E. Stepanowa, J. de phys. et rad. **6**, 1 (1935).
[3] A. Marques da Silva, Ann. de physique **11**, 504 (1939).
[4] G. J. Sizoo and F. Berendregt, Physica **6**, 1085 (1939).
[5] A. I. Alichanow, A. I. Alichanian and M. S. Kosodaef, J. de phys. et rad. **7**, 163 (1936).
[6] S. De Benedetti, J. de phys. et rad. **7**, 205 (1936).
[7] M. Monadjémi, Comptes rendus **204**, 1560 (1937).
[8] H. R. Crane and J. Halpern, Phys. Rev. **55**, 837 (1939).
[9] This letter is only a qualitative exposition of some results of a research made during last year. A more complete account will be given if I receive the notes containing the numerical data that remained in France. An article, for which I have already corrected the proofs, will perhaps appear in the *Journal de Physique et le Radium*.
[10] J. V. Dunworth, Nature **144**, 152 (1939).
[11] M. E. Rose and G. E. Uhlenbeck, Phys. Rev. **48**, 211 (1935).

Proceedings of the American Physical Society

Minutes of the Philadelphia, Pennsylvania, Meeting
December 26–28, 1940

THE 42nd Annual Meeting (the 239th regular meeting) of the American Physical Society was held at Philadelphia, Pennsylvania, on Thursday, Friday and Saturday, December 26, 27 and 28, 1940, in affiliation with Section B—Physics—of the American Association for the Advancement of Science. The regular sessions of the Society were held in the Towne School of Engineering of the University of Pennsylvania.

On Friday afternoon, December 27, at two-thirty o'clock the Society held a joint session with Section B of the American Association for the Advancement of Science and with the American Association of Physics Teachers in the auditorium at the Drexel Institute of Technology. The program consisted of three addresses: "Ions in gases" by Professor John Zeleny of Yale University, President of the Physical Society; "Higher energies" by Professor Ernest O. Lawrence of the University of California, retiring Vice President of Section B; and "Applications of nuclear physics" by Professor Robley D. Evans of the Massachusetts Institute of Technology. Professor A. L. Hughes of Washington University and Vice President of Section B presided.

On Friday morning, December 27, the Society held a joint session with Section E—Geology—of the American Association for the Advancement of Science. The program consisted of four invited papers as follows: "A hydro-physical approach to the quantitative morphology of drainage basins" by Dr. Robert E. Horton, Voorheesville, New York; "Problems of orogeny" by Professor Chester R. Longwell, Yale University; "Physical frontiers in seismology" by Professor L. Don Leet, Harvard University; and "The radio-elements in the water and sediments of the ocean" by Dr. William D. Urry, Geophysical Laboratory, Washington, D. C. Dr. Hugh D. Miser of the U. S. Geological Survey and Chairman of Section E presided.

On Friday evening, December 27, the Society held a joint dinner with the American Association of Physics Teachers at the Benjamin Franklin Hotel. The attendance was two hundred and twenty-two. Professor John Zeleny acted as toastmaster. A special feature of the dinner was the presentation of the Duddell Medal by The Physical Society, London, to Professor Ernest O. Lawrence in recognition of his services in the invention and development of the cyclotron. The presentation, which was to have been made by the late Lord Lothian, was made by Mr. Neville Butler, Counsellor and Chargé d'Affaires of the British Embassy. Before the presentation, Dr. R. H. Fowler, who is a member of The Physical Society, spoke on the importance of the cyclotron in the development of modern physics. Dr. Lawrence spoke briefly in accepting the medal. The other speakers were Dr. Richard M. Sutton, President of the American Association of Physics Teachers, and the President-Elect of the Physical Society, Dr. George B. Pegram.

Annual Business Meeting. The regular Annual Business Meeting of the American Physical Society was held on Friday afternoon, December 27, 1940, at two o'clock, President Zeleny presiding.

Dr. William H. Crew reported for the tellers that the following had been elected as officers for the year 1941:

President, George B. Pegram; *Vice President*, G. W. Stewart; *Secretary*, Karl K. Darrow; *Treasurer*, George B. Pegram; *Managing Editor*, John T. Tate; *Members of the Council*, Joseph C. Boyce and Arthur E. Ruark; *Members of the Board of Editors*, A. C. G. Mitchell, I. I. Rabi and George E. Uhlenbeck.

The tellers reported a vote of 262 to 11 in favor of the amendments to the Constitution, which had been approved by the Council and submitted to the Fellows for balloting in accordance with the provisions of the Constitution, Article X.

Amendments to the by-laws, which had been recommended by the Council for presentation to the Society, were submitted to the Fellows and adopted by a unanimous vote.

The Secretary reported that during the year 269 persons had accepted election to membership. He reported the deaths of 12 members, that 35 had resigned and 57 had been dropped. The membership as of December 24, 1940 was as follows: Fellows: 821; Members: 2802; Honorary Members: 5; Total membership: 3628.

The Treasurer presented a summary of the financial conditions of the Society. The Treasurer's financial report will be audited, printed and distributed to the members.

The Managing Editor made a brief report on the general status of the publications of the Society and stated that a detailed and audited financial report for 1940 would be printed and distributed to the members.

On motion of Dr. A. L. Hughes the Society passed a resolution thanking the Local Committee, particularly Mr. Henry B. Allen, Professor Thomas D. Cope and Professor G. P. Harnwell, for their services in making arrangements for the meeting.

The meeting adjourned at two-twenty-five P.M.

Meeting of the Council. At the meeting of the Council held on Thursday afternoon, December 26, 1940, the deaths of two fellows were reported (William B. Cartmel and T. Russell Wilkins). Seven members were transferred from membership to fellowship and five candidates were elected to fellowship. One hundred and nine candidates were elected members. *Transferred from membership to fellowship:* Donald W. Kerst, Harold J. Kersten, Harry A. Kirkpatrick, Lyle W. Phillips, Norman F. Ramsey, Jr., Robert K. Waring, Martin D. Whitaker. *Elected to fellowship:* J. C. M. Brentano, Peter J. W. Debye, Wilfried Heller, Stanislaw Mrozowski, and Wolfgang Pauli *Elected to membership:* Felix Adler, Charles O. Ahonen, L. Thomas Aldrich, Henry D. Arnett, Julius Ashkin, Frederick A. Babcock, Roger S. Bender, J. E. Binns, Joseph H. Blickman, John H. Bollman, Richard H. Bolt, Joseph S. Brock, Sidney H. Browne, Robert A. Buerschaper, T. Finley Burke, Thomas D. Carr, Howard A. Christensen, Fred Chromey, E. Lynn Cleveland, Bernard K. Croninger, Sidney M. Dancoff, Kenneth E. Davis, Max Delbrück, J. E. Dinger, Richard W. Dodson, W. Crawford Dunlap, Jr., Alfred A. Ebert, Jr., Lloyd G. Elliott, Victor R. Ells, Herbert F. Engelmann, Lewis I. Estep, Dwight T. Ewing, Robert E. Faires, Francis L. Friedman, Henry H. George, John R. Graham, Jr., Kenneth I. Greisen, Eugene Greuling, Harold H. Grossman, Edith Haggstrom, Maurice B. Hall, David Halliday, Clarence Hammer, Henry Harrison, T. N. Hatfield, Robert H. Hay, Mary S. Hewlett, John M. Hinkle, James M. Hush, Elmer S. Imes, Gene Irish, Arnold A. Jensen, Arthur S. Jensen, Toyozo Kambara, Erwin W. Kammer, J. Warren Keuffel, Joseph M. Kime, Gilbert W. King, Joseph J. Kleimack, Howard R. Kratz, William J. Kroeger, David Lawler, D. C. MacDonald, Charles E. Mandeville, Jordan J. Markham, Albert B. Martin, John H. Martin, Fred M. Mayes, Paul W. McDaniel, Richard P. Metcalf, Tomokuni Mituisi, Kiyotosi Miyazaki, Norman H. Moore, L. Tarver Morris, Byron F. Murphey, Thomas A. Murrell, Basanti D. Nag, Charles F. Otis, William E. Parkins, Clarence M. Parshall, Karl A. Parsons, Simon Pasternack, Gerald M. Petty, Carl B. Post, Jan A. Rajchman, B. P. Ramsay, René G. Rhodes, A. F. Robertson, Glenn M. Roe, Clifford M. Ryerson, Matthew L. Sands, Wayne W. Scanlon, Charles W. Sheppard, J. Oliver Shock, Ralph Simon, Richard L. Snyder, Jr., Lyman Spitzer, Jr., Robert L. Sproull, Guy A. Stone, Richard G. Stoudenheimer, Irvin H. Swift, John W. Trischka, Hirosi Ueda, Francis M. Walters, 3rd, Gerhard L. Weissler, Sherrerd B. Welles, Father Anthony J. Westland, David C. Whitmarsh, Jr., Dexter E. Woodford, and William M. Woodward.

The regular scientific program of the Society consisted of sixty contributed papers of which five, numbers 10, 17, 30, 41 and 44, were read by title. The abstracts of the contributed papers are given in the following pages. An Author Index will be found at the end.

HAROLD W. WEBB, *Acting Secretary*
Columbia University, New York, New York

Abstracts of Contributed Papers

1. Quantum Likelihood. E. C. Westerfield and W. B. Pietenpol, *University of Colorado.*—A statistical formula is developed for the likelihood that an arbitrarily chosen quantity q is a fundamental unit for a given set of data. An experimental datum frequently involves several quanta. When, as in the oil-drop experiment, the number of quanta involved in a single measurement is small and the experimental error is small compared with the value of the individual quantum, the number of quanta in each datum may be easily determined by inspection or by simple arithmetic procedures. However, when the probable error is of appreciable magnitude compared with the value of the quantum, the quantum nature of the phenomenon may be completely masked by the experimental error. Without a previous knowledge concerning the value or even the existence of a possible quantum, any set of data falls potentially into this borderline case. The formula developed for the quantum likelihood weights the data in accordance with their probable errors and hence is applicable only to data for which the probable errors are known or can be estimated. The mathematical quantity involved is a function of two variables and is tabulated graphically in order to apply the theory to a given set of data.

2. The Electron, a Quantum Unit in Nuclear Disintegrations. W. B. Pietenpol, *University of Colorado.*—The previously developed method of analysis for the likelihood that an arbitrary quantity is a fundamental unit is applied to a set of nuclear disintegrations. The data considered are those of the important reactions produced by deuterons and protons with the yielding of charged particles. Use is made of the experimental results summarized by Livingston and Bethe in their article on Nuclear Physics.[1] The 24 listed reactions with the corresponding energy evolutions and probable errors are considered. The results of the analysis are indicated by curves of quantum likelihoods for different energy values. The optimum values indicate that the mass energy of the electron is a possible unit in such nuclear processes.

[1] M. S. Livingston and H. A. Bethe, Rev. Mod. Phys. **9**, 245 (1937), Table LXXII.

3. Proton Distribution in the O. P. Process. Everett C. Smith and Ernest Pollard, *Yale University.*—A recent study by Volkoff[1] of the theoretically expected proton distribution in the O. P. process indicates that a maximum in the yield should occur for proton energies slightly greater than the incident deuteron energies. It is found in studies of the elements of medium atomic weight that a large yield at about this value is always found. This yield can be ascribed to the O. P. process or to carbon contamination of the target. We have shown that very clean surfaces of chromium and nickel do not have appreciable N^{13} radioactivity after deuteron bombardment but give high yields of protons of about 3 to 4 Mev. These are therefore due to the true O. P. process. While group structure is apparent, an examination of the yields shows agreement with Volkoff's theory for chromium in that a maximum occurs at 4.1 Mev of half-width 2.1 Mev (predicted values 4.0 and 2.25, respectively), but apparently no agreement for nickel as the maximum is certainly below 2.5 Mev while the predicted value is 4.1 Mev.

[1] G. M. Volkoff, Phys. Rev. **57**, 866 (1940).

4. Energy Levels of Mg^{26} and Si^{30} formed by Deuteron Bombardment. Ernest Pollard and Richard F. Humphreys, *Yale University.*—In order to answer the question as to whether a final nucleus exhibits the same set of levels if formed in different manners, it is necessary to produce the same nucleus by bombardment of differing target elements. Among the better studied nuclei are Mg^{26} and Si^{30}, produced by alpha-particle bombardment of Na^{23} and Al^{27}, respectively, with emission of a proton. Studies of these protons indicate excited states for Mg^{26} at 2.3 and 4.0 Mev and for Si^{30} at 2.3, 3.6, and 4.9 Mev. The group structure of protons from $Mg^{25}(dp)Mg^{26}$ and $Si^{29}(dp)Si^{30}$ has been observed by coincidence counting. In the case of $Mg^{25}(dp)Mg^{26}$ three definite groups are obtained giving excited states at 1.85 and 3.00 Mev. The yield from silicon is rather less, but the work up to the present shows that the very long range protons occur in several groups, tentatively assigned to excited states at 0.9, 1.9, 2.8, and 3.6 Mev. It can thus be seen that the energy levels found depend on the type of reaction, which suggests a greater density of levels than found in any one transmutation and strong selection rules depending on the manner of formation of the final nucleus.

5. Possibility of Ternary Fission. R. D. Present, *Purdue University.*—Disintegration of the uranium nucleus into three fragments is dynamically possible with the excitation energies available from neutron capture. Such a ternary fission would be highly exothermic; the maximum energy release, occurring for a division into three equal parts, exceeds that for binary fission by nearly 20 Mev. The dynamical course of the fission follows a path over a potential energy surface in the configuration space whose dimensions represent the amplitudes of nth harmonic deformations of the liquid drop. A large positive amplitude deformation of the fourth-harmonic type creates a pair of tropical furrows, which deepen as the drop elongates, forming three collinear droplets connected by liquid necks. The relative sizes of the central and outer droplets depend on the amplitudes and phases of the second and fourth-harmonic deformations. Probable asymmetry causes a droplet to detach itself, leaving a distorted fragment which divides spontaneously. The energy surface shows no obstructions to passage of the configuration point from the saddle region into the region where ternary fission is indicated. The activation energy is the same as for binary fission, but the deviation from the path of steepest descent renders ternary fission less likely than binary fission for low neutron energies.

6. The Internal Temperature-Density Distribution in the Sun.—H. A. BETHE, *Cornell University*, G. BLANCH AND A. N. LOWAN, Mathematical Tables Project, Work Projects Administration, *New York City*, AND R. E. MARSHAK, *University of Rochester*.—An accurate determination has been made of the internal temperature-density distribution of the sun using the point-convective model. Account is taken of the variation of the guillotine factor throughout the star in contrast to all previous calculations on this model. The hydrogen content is adjusted so that the radiative envelope fits onto the convective core where all the energy-production is assumed to take place. The integration is started from the surface of the sun and it turns out that a hydrogen content of 35 percent by weight gives a good fitting of envelope to core, whereas hydrogen contents of 40 percent or 30 percent give evident lack of fitting in opposite senses. The central temperature is 25.7×10^{6}°C and the central density 110 g/cm^3; values considerably higher than those usually taken for the sun. The carbon cycle now leads to an energy production about 100 times too large. Since 98 percent of the luminosity is contributed by the convective core, the assumptions underlying the point-convective model are self-consistent. The variation of the molecular weight caused by progressive ionization has not been considered. If this correction should fail to lower the central temperature sufficiently and if the carbon-nitrogen concentration is still taken as one percent by weight, the discrepancy has to be explained by the presence of an appreciable amount of helium.

7. Statistical Theory of the Spacing of Nuclear Levels. H. MARGENAU, *Yale University*.—The density of energy levels of a nucleus around a given excitation energy E is determined, aside from factors varying slowly with E, by e^S, where S is the entropy as a function of E and A the number of nuclear particles. In current theories S is calculated with the use of Sommerfeld's asymptotic formulas familiar from the theory of metals, the alleged justification being the high degree of degeneracy (in the Fermi-Dirac sense) of a nucleus for values of E around 10 Mev. As a matter of fact these formulas also involve the assumption, valid in the theory of metals, that the number of energy states of an individual particle be large. For a nucleus (potential well model) of atomic number about 100 there are less than ten such energy states. While this circumstance makes the ordinary theory very inaccurate, it opens the possibility of computing S numerically without much difficulty since the summations encountered have only about ten terms. Such calculations, made on the basis of the model of free particles within a spherical hole, and carried out mainly for atomic numbers around 116 (end of a closed shell), show that the "asymptotic" formula for e^S may be in error by a factor of several hundred in either direction. For $A=116$ it gives too large a density of levels. The effect of shell structure is very pronounced; for instance, for $A=100$ (near middle of a shell) the asymptotic formula errs in the opposite direction.

8. Preliminary Results on Two New Ion Sources. I. A. GETTING,* *Harvard University*.—The gasomagnetron of Vigdorchick[1] and the high frequency ring discharge have been investigated as ion-sources for high voltage tubes. As the name indicates, the gasomagnetron is simply a magnetron filled at low pressure with hydrogen. Its greatest assets are: high ion current (over 2 ma); low power consumption (15 watts excluding cathode heating); and very low gas flow. With a pumping speed of 50 liters per second at the acceleration tube, an increase of only 10^{-5} mm was noted. The gasomagnetron suffers from the short life of the cathode and especially from the low percentage of atomic ions. The high frequency ring discharge possesses some very attractive properties. The discharge tube was built of glass in the shape of a doughnut.[2] It was excited with a coil of ten turns at the center tuned to a 12.8-megacycle 100-watt oscillator. The discharge formed essentially a shorted secondary of one turn of a transformer. The discharge is a positive column of an arc wrapped around itself without a cathode fall. The spectrum showed as many as 17 Balmer lines with little trace of band structure. Currents up to 130 microamperes have been obtained from the source tube. Unfavorable features were the high gas flow and limited ion currents. The discharge runs well at 0.1 mm, but can be maintained at 0.03 mm. The unique feature is that there is no cathode to burn out.

* Society of Fellows.
[1] I. Vigdorchick, J. Phys. Acad. Sci., U.S.S.R. **1**, 151 (1939).
[2] Suggested by C. G. Smith.

9. The Mechanism of Proportional Counter Action. M. E. ROSE AND S. A. KORFF, *Bartol Research Foundation of the Franklin Institute*.—In order to clarify the interpretation of porportional counter measurements, we have investigated the operation of counters below the Geiger threshold. A theory of the amplification factor of proportional counters has been made in which the primary assumption is the neglect of fluctuations in energy loss and specific ionization of the secondary electrons. It was found that the energy variation of the ionization mean free path is an essential element which the theory must include. The amplification factor then varies essentially exponentially with counter voltage and depends on one empirical constant, the threshold voltage for proportional amplification. The theory predicts a dependence of amplification on counter geometry, pressure and constitution of gas mixture. The voltage dependence of the size of the pulse produced by alpha-particles has been measured. The amplification has been determined by measuring the range of the particles in the counter and using the known average energy loss per ion-pair. Using various experimental arrangements good agreement with the theory is found. The application of these results to the interpretation of other experiments, for example the exclusion of gamma-ray counts in the observation of neutrons with BF_3 counters, is discussed.

10. Soil Studies with Radioactive Phosphorus: the Phosphate Fixation of Soils.* STANLEY S. BALLARD AND L. A. DEAN, *University of Hawaii Agricultural Experiment Station*.—Methods described elsewhere[1] have been applied to a study of phosphate fixation by soils. To determine this property, measurements were made of the uptake by test

plants—tomatoes, Sudan grass, and radishes—of radio-phosphorus added to soils. These values were then compared with the uptake by plants grown in water and sand cultures, to give a measure of the absolute fixation of the soils. The relative amounts taken up by the thirteen soils varied greatly for the three test plants. Thus, the significance of phosphate fixation depends upon the plant as well as the soil in which it is grown. It was found that for tomatoes this biological measure of fixation obtained with radio-phosphorus agreed with the chemical measure—the recovery of nonradioactive phosphorus in equilibrium with a soil-water system. A full discussion of these results is being submitted for publication. The gift by the Radiation Laboratory of the University of California of the radioactive phosphorus is gratefully acknowledged.

* To be read by title.
[1] S. S. Ballard and L. A. Dean, J. App. Phys. **11**, 366–370 (1940).

11. The Use of Radioactive Materials in Measuring the Thickness of Enamel Coatings. E. P. MILLER AND A. V. COHEE, *Purdue University.*—Thickness measuring devices as used in the synthetic enamel industry are limited in their application by their method of operation. Those working on an electrical or magnetic principle are limited to use on coatings on magnetic or conducting surfaces and all of them require that the coating be completely dry before their operation is satisfactory. In certain types of work with synthetic enamels these are serious limitations. A method of measuring film thickness which overcomes these difficulties would be desirable. Radioactive means have been used with success to answer this need. By mechanically mixing uranyl acetate with the paint pigment in a concentration of 18 grams of acetate to 100 cc of pigment, a series of test samples were sprayed on shim stock and their thickness, when dry, accurately measured with micrometer gauges. The activity per unit area of these samples was then measured with a Geiger-Mueller counter and a scale-of-four circuit. By plotting the counts against the thickness a calibration curve for this radioactive concentration was obtained. This curve is linear up to a coating thickness of 0.0035 inch, the largest value used. With this curve the thickness of unknown coatings can be measured before they are baked or dried to the same accuracy as one can use a micrometer gauge.

12. Solving a Type of Nonlinear Simultaneous Equations with a Mechanical Harmonic Synthesizer. S. LEROY BROWN AND LISLE L. WHEELER, *The University of Texas.*—Consider a pair of nonlinear simultaneous equations that are homogeneous in x and y:

$$a_1x^n+a_2x^{n-1}y+a_3x^{n-2}y^2+\cdots+a_{n+1}y^n=A, \quad (1)$$
$$b_1x^n+b_2x^{n-1}y+b_3x^{n-2}y^2+\cdots+b_{n+1}y^n=B, \quad (2)$$

and substitute $x/y=\cos\theta$. This gives

$$y^n[a_1\cos^n\theta+a_2\cos^{n-1}\theta+\cdots+a_{n+1}]=A, \quad (3)$$
$$y^n[b_1\cos^n\theta+b_2\cos^{n-1}\theta+\cdots+b_{n+1}]=B, \quad (4)$$

or
$$B[a_1\cos^n\theta+a_2\cos^{n-1}\theta+\cdots+a_{n+1}]= A[b_1\cos^n\theta+b_2\cos^{n-1}\theta+\cdots+b_{n+1}]. \quad (5)$$

The powers of $\cos\theta$ may be expressed in cosines of multiple angles [$\cos^2\theta=\frac{1}{2}(1+\cos 2\theta)$, $\cos^3\theta=\frac{1}{4}(3\cos\theta+\cos 3\theta)$, etc.]. The amplitudes of the fundamental and its harmonics in Eq. (5) may be set on a mechanical synthesizer and the value (or values) of θ determined for which this equation is satisfied if there is a ratio (real value of x to real value of y) between -1 and $+1$ for which it is satisfied. Then substitute $y/x=\cos\phi$ in Eqs. (1) and (2) and this gives (instead of Eq. (5))

$$B[a_1+a_2\cos\phi+a_3\cos^2\phi+\cdots+a_{n+1}\cos^n\phi]= A[b_1+b_2\cos\phi+b_3\cos^2\phi+\cdots+b_{n+1}\cos^n\phi]. \quad (6)$$

After Eq. (6) is expressed in terms of cosines of multiple angles, the amplitudes may be set on the synthesizer and solved for angle ϕ. Thus the ratios y/x (between -1 and $+1$) that satisfy Eq. (6) are determined. Consequently, these solutions of Eqs. (5) and (6) give all the ratios (real value of x to real value of y) that satisfy the two simultaneous equations. Substitution of a value of θ_1, as determined by the machine, in Eqs. (3) or (4) determines y_1 and x_1 ($x_1=y_1\cos\theta_1$) that satisfy Eqs. (1) and (2). This method is essentially a machine solution of a polynomial which is obtained from this type of equations, or equations that may be transformed to this type.

13. High Rotational Speed with Small Rotors. L. E. MACHATTIE, *University of Virginia. (Introduced by J. W. Beams.)*—The axial magnetic suspension in vacuum offers small frictional drag to the rotation of the suspended body.[1] With it an attempt has been made to spin small steel rods and balls to as high speeds as possible. An "inductance control" has been substituted for the original light beam photo-cell arrangement for vertical stabilization. Damping of horizontal motion of the rotor is necessary in order to overcome precession in the case of vertically suspended rods and circular motion of increasing amplitude in the case of a spinning ball. Rotors were spun by means of a 112-kilocycle rotating magnetic field. It was found that when a spinning rod reaches a speed approximately equal to the frequency of its first mode of free flexural vibration, it bends double because of the effect of centrifugal force in making the straight shape unstable. A $\frac{3}{16}''$ diameter drill rod $\frac{7}{8}''$ long and tapered at each end reached 36,000 r.p.s. before bending double. A $\frac{3}{32}''$ diameter steel ball such as is used in ball bearings withstood a speed of 110,000 r.p.s. without bursting. On a similar ball two rough-ground faces were made to test the feasibility of use as a rotating mirror. It was spun to over 100,000 r.p.s.

[1] Holmes, Rev. Sci. Inst. **8**, 444 (1937); Nature **140**, 30 (1937); Smith, Rev. Sci. Inst. (in press).

14. A New Analytical Ultracentrifuge. ARTHUR L. STAUFFACHER, J. W. BEAMS AND L. B. SNODDY, *University of Virginia.*—The well-known theory shows that, if the concentration of the material in two regions of a convection-free centrifuge cell at different distances from the axis of rotation can be measured, the molecular weight of the material can be determined. A convection-free centrifuge rotor has been developed in which the material is centri-

fuged in a large number of similar small sector-shaped cells near the periphery of the rotor. The material is injected into the cells through the hollow shaft when the rotor is at full speed. After the centrifuging is completed, the material in each cell is separated into two parts along a surface perpendicular to the radius by a displacement method. From analytical measurements of the concentration in one or both of these parts after the centrifuge is stopped, and that of the original material, the molecular weight is determined. Either the rate of sedimentation or the equilibrium methods for determining molecular weights may be used with this machine. Measurements have been made in the case of proteins and of ordinary inorganic electrolytes.

15. A Lattice Type Acoustic Filter. II. HAROLD K. SCHILLING, *Union College, Lincoln, Nebraska.*—Lattice type acoustic filters were described recently[1] which are built up of parallel grooved slats. They produce sound elimination bands whose positions in the frequency range are determined mainly by the depth of the grooves. This circumstance restricts their suitability to the filtration of high frequencies. They may be adapted to use with low frequencies by covering the slats with plates which are perforated by rows of small holes or by long narrow slits. When the plates are in position, the perforations are parallel with and immediately above the grooves. The perforations are also narrower than the grooves. Hence the plates partially close or cover the grooves. In this manner the filter side branches become Helmholtz resonators, the grooves being the resonator cavities and the perforations the resonator "necks" or channels. These resonators have lower resonance frequencies than do the simple grooves themselves. For such filters, therefore, one obtains attenuation bands at considerably lower frequencies, the cut-offs for any one being determined mainly by the volume of a groove, by the cross-sectional area of a perforation, and by the thickness of a cover plate, i.e., the length of a resonator "neck."

Experimental models of these filters have been constructed whose cut-off frequencies are as low as 700. Their behavior may be understood in terms of theory discussed earlier.[1]

[1] Harold K. Schilling, Bull. Am. Phys. Soc. **15**, Chicago Meeting, 1940, abstract 28.

16. Motion of the Earth's Fluid Core. D. R. INGLIS, *Johns Hopkins University.*—It may be considered probable that the core of the earth has a very low viscosity, such as is typical of molten metals. The earth has a considerable angular acceleration characterized mainly by the 27,000-year precession of its axis about a 24° cone. If the transfer of angular momentum down into the core is not sufficient to cause rigid rotation, the rotation of the interior of the core must lag behind the earth's rotation. The core is so large that its flow is expected to be turbulent, unless there is practically rigid rotation or marked stratification of the core. The turbulent drag has been estimated roughly, on the basis of a semi-empirical relation of von Karman, and it is found that the speed of relative rotation expected on these assumptions is about one percent of the earth's angular speed, in order of magnitude. The axis of relative rotation precesses around the earth daily, so that a particle in the core circulates in a rather small region. The forces of magnetic induction are expected to be less important than those due to turbulence. A direct effect of such a relative rotation on the diurnal variation of the earth's magnetism would be prevented by the shielding of metallic layers outside of the core.

17. Temperature Correction Methods in Calorimetry.* ALLEN KING AND HORACE GROVER, *Rensselaer Polytechnic Institute.*—Temperature correction methods in calorimetry are divided into three categories; namely, those in which a function of the temperature difference between the source of heat and the calorimeter fluid is unspecified but the heating period is limited, those in which this function has a specified analytical form and those in which graphical schemes are employed. A self-consistent method for correcting a temperature rise of the first type is developed and published methods of other investigators are compared with it. Rigorously none of these methods should be used in specific heat, bomb calorimetric, and similar experiments. For such experiments in which the heating period is unlimited, the function mentioned above may be specified in the Rowland manner. Rowland's fundamental assumptions are reexamined and a correct method based on them is deduced. Comparison of this method with those of Regnault-Pfaundler, Rowland-Hoare, and Dickinson by application to a set of data reveals significant discrepancies. A simple approximation of the new method is proposed and a graphical scheme based on this is suggested. Other graphical methods are critically reviewed.

* To be read by title.

18. 27-Day Recurrence Tendency in North American Precipitation. J. W. MAUCHLY, *Ursinus College.*—Most of the numerous attempts to correlate weather phenomena with solar activity have utilized some measure of solar variation as, for instance, the relative sunspot numbers. It is possible, however, to infer the influence of solar variations on terrestrial phenomena if one can discover in the latter approximate 27-day recurrences without strict periodicity. Daily totals of the precipitation reported on the Washington Daily Weather Maps (1927–40) have been converted to a "daily precipitation index," P, in which seasonal and other long period variations are absent. Fourier coefficients have been calculated for the first four harmonics for each 27-day interval in the series. An analysis of variance indicates that, although there is no evidence for persistent periodicity, the coefficients for adjacent 27-day intervals are more alike than would be expected from random data. The usual characteristics of time-series have been considered in connection with these tests. An upper limit for the "probability of chance" is hard to give, but may be taken as 10^{-3} in the opinion of the author. Evidence for solar influence on weather is further strengthened by other work not yet completed.

19. Gamma-Radiation from Airplane Instruments. ROBERT B. TAFT, *103 Rutledge Avenue, Charleston, S. C.*—A recent newspaper article caused much interest among air pilots by stating that the gamma-radiation from the luminous paint used on the instrument dials of a modern air liner would give the pilots a near-lethal dose of radiation in a few years. The author conducted tests in the cockpit of a Douglas DC3 and a Lockheed Electra and while there was a surprisingly large amount of radiation, the total dose was far under that generally accepted as perfectly safe for radium workers. Apparatus and measurements will be briefly demonstrated by colored lantern slides.

20. Correlation between Cosmic-Ray Intensities and Meteorological Conditions over Washington for 1939. NIEL F. BEARDSLEY, *University of Chicago.*—A series of correlation studies has been made between the meteorological conditions over Washington and the cosmic-ray intensities observed at Cheltenham. The air was divided into four layers, three of 4000 meters each and a fourth layer consisting of all the air above 12,000 meters. By multiple correlations between these layers and the surface cosmic-ray intensities, pressures and temperatures, it was found that the variance of the cosmic-ray intensity depends about 15 percent on the total air pressure, 40 percent on the distribution of the air mass and only 10 percent on world-wide magnetic changes. This leaves 30 percent of the variance unaccounted for. In a second computation, the heights of given densities of air at which the mesotrons may be considered as being formed[1] were correlated with the surface cosmic-ray intensities. This gives a method of determining the mean path before disintegration of those mesotrons with sufficient energy to penetrate to the surface from their place of formation. These results are quite in accord with other determinations of the mean path before disintegration.

[1] P. M. S. Blackett, Phys. Rev. **54**, 973 (1938).

21. Fluctuational Effects in Cosmic-Ray Ionization. V. A. LONG* AND R. M. WHALEY,** *University of Colorado.*—Continuous observations of the cosmic-ray ionization have been made at Boulder (alt. 5400 ft., lat. 40°N, long. 105°W). Professor Broxon's[1] high pressure chamber, equipped with five-inch lead shield, radioactive compensation, and an Askania-Werke photographic recorder, was employed in a temperature-controlled room in the basement of a thick-walled stone building. Data for the period June 1, 1938, to Nov. 30, 1939, have been analyzed partially for the various fluctuational effects by the least-squares method. After making the usual barometric corrections, the out-door temperature, magnetic, and humidity coefficients were determined. Both short and long time temperature effects were observed in general agreement with those of Hess[2] and others. A positive magnetic effect is indicated for magnetically undisturbed periods. About 25,000 bursts (some smaller than usually detected) have been observed and classified. Agreement with the usual frequency-magnitude relation is in evidence, and there is indication of diurnal and seasonal periodicities of the very small bursts.

* Now at Ottawa University, Ottawa, Kansas.
** Now with G. M. Laboratories, Chicago.
[1] J. W. Broxon, Phys. Rev. **37**, 1320 (1931).
[2] V. F. Hess, Phys. Rev. **57**, 781 (1940).

22. Cosmic-Ray Recurrences. JAMES W. BROXON, *University of Colorado.*—Eighteen-month cosmic-ray measurements by Long and Whaley at Boulder, corrected for bursts and barometric fluctuations, are being analyzed by Chree's[1] method as adapted by Gill[2] and Monk and Compton.[3] Following Monk and Compton, zero-days were selected from the first fifteen months for *subsequent* pulses to $n=135$, and from the last fifteen months for *previous* pulses to $n=-135$. "Positive-pulse" curves have been completed. These display some slight indication of pulses at intervals of about 27 days. It is expected that "negative-pulse" curves will be obtained before the meeting. These and the "difference" curves may bring out more clearly whether or not the data display pulses at definite intervals. Perhaps differences between curves obtained by the same procedure may depend upon locations of observation stations. While the Boulder data show clearly the influence of out-door temperature, Monk and Compton's data were obtained at Teoloyucan, Mexico, where (according to Gill[2]) both temperature range and temperature dependence are small. *Note added in proof.*—The difference curves confirm Monk and Compton.

[1] C. Chree, Phil. Trans. **A212**, 76 (1913).
[2] P. S. Gill, Phys. Rev. **55**, 429 (1939).
[3] A. T. Monk and A. H. Compton, Rev. Mod. Phys. **11**, 173 (1939).

23. Cosmic Rays and the Nature of the Field in Magnetized Iron. W. F. G. SWANN AND WAYNE L. LEES, *Bartol Research Foundation of the Franklin Institute.*—Some time ago one of us showed that in the case of a classical model of a piece of magnetized iron in which the magnetic entities were small in size, while the true average field which would determine the deflection of a cosmic ray in passing through the iron is the magnetic induction B, this average is made up in part of a number of very rare events, with the result that the practically measured average is liable to be $B-2\pi I$, where I is the intensity of magnetization. In view of the subtlety of certain points in the mathematical reasoning, it has been thought advisable to perform an experiment upon a model composed of randomly distributed iron spheres polarized by the magnetic field of a solenoid. By a suitably designed long thin coil, it has been possible to investigate in the space between the spheres the average field which in a practical case would be responsible for deflecting a cosmic ray, and the experimental conclusions have verified the mathematical expectations within the limits of accuracy of the experiments.

24. A Large Wilson Cloud Chamber for Cosmic-Ray Studies. T. H. JOHNSON, J. G. BARRY AND R. P. SHUTT, *Bartol Research Foundation of the Franklin Institute.*—The paper describes the construction of a large cloud chamber in operation at the Bartol Laboratory. The chamber is of the vertical, rubber diaphragm type and is operated by compressed air. It is 23″ in diameter and 6″ deep and its

metal parts are simple rings and disks cut from rolled steel plates. The stops for the diaphragm are grill plates fabricated by winding alternate corrugated and flat steel strips into a flat spiral subsequently dipped in tin. With argon and a mixture of propyl alcohol and water vapors the expansion ratio for good tracks is 1.070. A magnetic field of 12.0 gauss per ampere is produced by simulated Helmholtz coils, series resistance 0.5 ohm. The chamber is illuminated by a capillary mercury arc mounted at the focus of a cylindrical parabolic reflector. The arc tube is maintained at a steady temperature of 240°C and when excited a current of about 55 amperes runs through a 4-mm quartz capillary sleeve 24" long inserted into the sealed off Pyrex tube. A 5-kw 2200-volt transformer supplies the power for a small integral number of half-cycles. Expansions are controlled by a set of coincidence counters.

25. The Relative Stopping Powers of Carbon and Lead for Slow Mesons. MARTIN A. POMERANTZ AND THOMAS H. JOHNSON, *The Bartol Research Foundation of the Franklin Institute.*—An experimental determination of the relative stopping powers of carbon and lead for slow mesons has been made with an anticoincidence arrangement of G-M counters. For mesons having an average energy of approximately 4×10^7 ev, the experiments revealed that 28.5 g/cm² of carbon is equivalent in stopping power to 24 ± 5 g/cm² of lead. This gives a value for the ratio of the stopping powers of equal masses of carbon and lead, $S_C/S_{Pb}=0.84\pm0.18$, to be compared with the theoretical value of $S_C/S_{Pb}=1.82$ calculated with the ionization theory. However, it is not necessary to invoke a hitherto unknown absorption process to account for this discrepancy, since it may be explained as arising from the scattering and transition effects. The data corrected for these effects show that 28.5 g/cm² of carbon is equivalent in stopping power to 45 ± 7 g/cm² of lead, and $S_C/S_{Pb}=1.6\pm0.3$, in agreement with the theoretical value within the experimental uncertainty. These experiments indicate that in a dense absorber any additional absorption process is unimportant compared with ionization for mesons having energies of about 4×10^7 ev, or higher.

26. On the Scattering of Mesons of Spin $\hbar/2$ by Atomic Nuclei. R. E. MARSHAK AND V. F. WEISSKOPF, *University of Rochester.*—The nonelectric scattering of charged mesons by protons and neutrons is calculated as a first-order effect in the heavy electron pair theory of nuclear forces. The mesons were assumed to be identical with electrons in every respect (spin $\hbar/2$, Dirac "hole" theory, etc.) except that their rest mass was taken equal to the cosmic-ray meson mass μ. It had previously been shown[1] that the meson pair theory gives qualitatively both the correct spin dependence of nuclear forces and the positive quadrupole moment of the deuteron. An upper limit for the scattering cross section has been found: it is less than 5×10^{-20} cm² for mesons of energy $E=\mu c^2$ and less than 2.6×10^{-29} for $E=3\mu c^2$. These values are about 1000 times smaller than the corresponding results obtained on the basis of meson theories of nuclear forces which ascribe to the meson a spin $\hbar$. In contrast to the latter theories the values obtained in the present paper are in agreement with the upper limits of the scattering cross section found experimentally by Wilson[2] and others. For meson energies large compared to the rest energy of the proton or neutron, the scattering cross section increases linearly with the energy; it first attains the value 10^{-26} for meson energies of the order of 10^{11} ev.

[1] R. E. Marshak, Phys. Rev. **57**, 1101 (1940).
[2] J. G. Wilson, Proc. Roy. Soc. **174**, 73 (1940).

27. Slow Protons and Mesotrons at 4300 Meters. WILSON M. POWELL, *Kenyon College.*—In 602 expansions at random of a large Wilson cloud chamber containing five horizontal lead plates each one cm thick 162 tracks appeared which passed through two lead plates or more without producing accompanying particles. 13 of these tracks can be identified as slow mesotrons and 8 can be identified as slow protons. Mesotrons show heavy ionization on one side only of a lead plate or pass through at least two plates and stop in the third showing no heavy ionization. Protons show recognizably heavy ionization on two sides of a lead plate. The energy ranges over which slow mesotrons and slow protons can be recognized by this method will be discussed. This work was done in the Denver University M.I.T. Laboratory on Mt. Evans in Colorado.

28. The Transition Effect for Large Showers of Cosmic Rays. C. G. MONTGOMERY AND D. D. MONTGOMERY, *Yale University.*—The increase in the number of rays in a large shower from the air upon passing through a thin layer of material was measured. The spherical ionization chamber, 40 cm in diameter and filled with nitrogen to 200 lb. pressure, had walls of magnesium only one centimeter thick and so produced a negligible effect. Over the chamber were placed layers of magnesium, iron, and lead and the bursts of ionization in the chamber were recorded photographically. The amounts of ionization corresponded to showers of about 75 rays through the chamber. The increase in shower size depends upon the ratio E/E_c, where E is the energy of a ray of the original shower and E_c the critical radiation energy, which varies inversely as the atomic number. For thicknesses of material corresponding to two radiation unit lengths, it can be estimated from the cascade theory that the number of rays will be increased by the factors 4.4; 1.8; 1.0 for Pb; Fe; and Mg, if we choose $E=2\times10^8$ ev. The observed factors were approximately 1.1; 1.1; 1.0. We must therefore conclude that either (a) the rays in the original shower are not electrons or (b) the variation of E_c with atomic number is incorrectly given by the theory. We believe the second alternative to be correct.

29. The Frequency-Extension Curves for the Soft and Penetrating Components of Extensive Cosmic-Ray Showers. NORMAN HILBERRY, *University of Chicago and New York University,* AND VICTOR H. REGENER, *University of Chicago.*—The frequency *vs.* extension curves for the soft and penetrating components of extensive cosmic-ray showers have been determined at the Mt. Evans high altitude laboratory. One set of three G-M tubes was used

as a "core selector"; the tubes were placed parallel to each other in a horizontal plane with an inter tube separation of 14 cm; the set was permanently shielded with 5 cm of lead and was connected in threefold coincidence. A second set of two G-M tubes was connected in twofold vertical coincidence as the exploring unit. The "extension" of the shower was measured between the center of the core selector and the vertical axis of the exploring pair. The twofold and threefold coincidences were combined and recorded by a mixing circuit. The data obtained are given in the table.

Extension in meters		.28	.64	4.0	12.0
Counts per hour	unshielded	10.7±1.0	11.1±1.0	9.4 ±.9	5.1±.6
	shielded	2.1± .4	1.9± .3	.67±.21	.3±.17

The expected curve for the soft component has been computed using the low energy cut-off value fixed by the 5-cm lead shield over the core selector. The agreement with the present data is satisfactory. A discussion of the penetrating component data will be given.

30. The Diffraction of X-Rays by Liquid Oxygen.*† P. C. Sharrah and N. S. Gingrich, *University of Missouri.*—The x-ray diffraction patterns of liquid oxygen at 90°K and at 62°K have been obtained and analyzed for the atomic distribution. Crystal reflected Mo$K\alpha$ radiation was incident upon a circular thin glass capillary of 7.8 mm diameter filled with liquid oxygen. The camera was evacuated and an exposure of about 30 hours was sufficient to give a pattern of suitable density. The lower temperature, 62°K, was reached by reducing the pressure. At atmospheric pressure, the oxygen was 96 percent pure, and at the reduced pressure it was of approximately the same purity. The intensity patterns showed a strong main peak and two broad peaks more like plateaus. The main peak is at $\sin\theta/\lambda=0.160$ for 90°K and at 0.165 for 62°K. The first plateau has its center roughly at 0.33 and the second plateau has its center roughly at 0.50. At 90°K, these plateaus are not prominent. The distribution curve for the 90°K case shows very nearly one discrete nearest neighbor at about 1.3A, a weak concentration at about 2.2A, a peak at 3.3A and at 4.2A. At 62°K, there is nearly one nearest neighbor at 1.3A, and further concentrations at 2.2A, 3.2A, 4.0A, 5.0A, 5.9A and 6.8A.

* This work was supported in part by a grant from the Elizabeth Thompson Science Fund.
† To be read by title.

31. X-Ray Determination of the Particle Size of Electro-Deposited Coatings. C. H. Ehrhardt, *Universal Oil Products Corp.*, and E. P. Miller, *Purdue University.*—The equation developed by Kochendorfer[1] for the x-ray particle size determination for flat samples, reduces to the Scherrer equation for lines which are exactly in focus. It is therefore easily possible to determine the particle size of very thin flat deposits where the number of observable diffraction lines is small. The particle size in nickel coatings plated on brass stampings under commercial conditions has been determined in this way. Using a special camera with a radius of 7.615 cm built to fulfill the theoretical requirements of the method, a number of diffraction patterns of nickel plate have been obtained with copper $K\alpha$ radiation. The particle size of the material was shown to be in the range of 10^{-6} cm. Using a section of the sample which was approximately cylindrical and copper $K\alpha$ radiation reflected from a crystal monochromator, the Scherrer equation could be applied. The particle size determined in this way agreed well with the former evaluation. By using the diffraction lines of the base brass material, the natural breadth of the Scherrer equation could be independently checked. The precautions which are necessary for the successful application of the x-ray method are pointed out.

[1] Kochendorfer, Zeits. f. Krist. **97**, 469–475 (1937).

32. The Atomic Arrangement of Sylvanite. G. Tunell, *Geophysical Laboratory.* (*Introduced by L. H. Adams.*)—The crystal structure of sylvanite has been determined by röntgenographic analysis of measured faceted crystals from Cripple Creek, Colorado, from Săcărâmbu (Nagy-Ág), Transilvania (Siebenbürgen), and from the Buena Mine, Jamestown district, Colorado. The dimensions of the unit cell, all determined by purely röntgenographic measurements, are $a_0=8.94$A, $b_0=4.48$A, $c_0=14.59$A, all ±0.02A, and $\beta=145°26'\pm20'$. The unit cell contains 2 "molecules" of $AuAgTe_4$, and a small proportion of the silver atoms required by this ideal formula is replaced by gold atoms. The space-group is $P2/c-C_{2h}^4$. The gold atoms are situated in (a) 000, $00\frac{1}{2}$, the silver atoms in (e) $0y\frac{1}{4}$, $0\bar{y}\frac{3}{4}$, with $y=0.43$; and the two sets of tellurium atoms in (g) xyz, $\bar{x}\bar{y}\bar{z}$, $\bar{x},y,\frac{1}{2}-z$; $x,\bar{y},\frac{1}{2}+z$; with $x_1=0.30$, $y_1=0.03$, $z_1=0.00$, and $x_2=0.28$, $y_2=0.42$, $z_2=0.24$. Each gold atom and each silver atom is surrounded octahedrally by six tellurium atoms and each tellurium atom is surrounded octahedrally by three tellurium atoms, two gold atoms and one silver atom, or by three tellurium atoms, two silver atoms and one gold atom.

33. The *L* Emission Band of Sodium. Willoughby M. Cady and D. H. Tomboulian, *Cornell University.*—The intensity distribution in the emission band of sodium at about 405A has been determined photometrically. The band is caused by transitions from conduction levels to the *L* levels. The metal was distilled in vacuum upon a copper target which was operated at −45°C. The sodium surface remained spotless and solid during bombardment. The band "width" appears to be about 3.05 volts, in agreement with the value of O'Bryan and Skinner.[1] A comparative study of the *L* band of sodium with the *L* bands of magnesium and aluminum[2] shows, in each case, a low frequency "tail" of which the intensity amounts to some 9 percent of the intensity of the entire band. For each of these elements the ordinary continuous x-ray spectrum was observed. For sodium the peak intensity (as corrected for underlying continuum) is 1.7 times as great as that of the continuum; for magnesium and aluminum the corresponding factors are 7 and 11.

[1] O'Bryan and Skinner, Phys. Rev. **45**, 370 (1934).
[2] Tomboulian and Cady, Phys. Rev. **57**, 1055 (1940).

34. The Auger Effect in the Relative Intensities of X-Ray Lines. JOHN N. COOPER,* *Cornell University.*—The Auger effect should play an important role in determining the relative intensities of x-ray lines, since any atom which leaves an excited state by an Auger (radiationless) transition cannot contribute to the intensities of lines arising from that state. Consequently, as the probabilities of Auger transitions from a given state increase, the relative intensities of lines arising from that state should decrease. It is known (from theoretical considerations,[1] from data on the relative intensities of the $L\alpha$ satellites, and from data on the widths of L-series lines[2]) that the probabilities of the Auger transitions $L_{\mathrm{I}} \rightarrow L_{\mathrm{III}} M_{\mathrm{IV,V}}$ increase rapidly with atomic number in the range $73 \leq Z \leq 81$. As a result the intensities of the L_{I} lines relative to the intensities of the L_{II} and L_{III} lines should decrease with atomic number in this range. To verify this prediction, the relative intensities of selected L_{I}, L_{II}, and L_{III} lines were measured with a two-crystal spectrometer. The data obtained are in complete accord with expectations and show strikingly the dependence of the relative intensities of x-ray lines on the probabilities of Auger transitions.

* Now at the University of Southern California.
[1] Coster and Kronig, Physica **2**, 14 (1935).
[2] J. N. Cooper, Phys. Rev. **57**, 1055A (1940).

35. A Timer for Spark Breakdown Studies. E. C. EASTON, *Newark College of Engineering,* AND J. D. COBINE, *Harvard Graduate School of Engineering.*—To aid in the study of the time lag of spark breakdown, a device has been constructed to apply and measure the length of rectangular voltage waves from one to 5000 microseconds in duration. Oscillograms of switching transients and test-gap voltages indicate that many previous investigators have been deceived by assuming a rectangular wave of applied voltage, and that others may have introduced errors by assuming the gap voltage to be influenced by reflections. It has been found possible to apply an essentially rectangular voltage by (1) maintaining the spark which closes the applying switch before the contacts meet mechanically, and (2) by making the test-gap circuit aperiodic. The length of the applied wave is determined by a vacuum tube circuit designed to pass a constant current output as long as the bias to the first tube exceeds a predetermined value. The output current is passed through a ballistic galvanometer whose reading is a measure of the time during which the gap voltage remains above the datum level. A thyratron circuit has been arranged to supply the timer with rectangular waves for the purpose of calibration. Cathode ray oscillograms showing errors of 5 percent to 10 percent indicate that the accuracy of the apparatus is quite sufficient for most breakdown studies.

36. Scattering of Low Velocity Ion Beams. JOHN A. ELDRIDGE, *University of Iowa.*—Rouse has investigated the scattering of potassium ions in passing through certain gases. There were many complicating effects in his experiment: electrons produced by ionization and by emission from electrodes, multiple collisions of ions, effects of slits, etc. These effects have been studied; in the case of scattering by mercury vapor, corrections for these secondary processes can be made without difficulty and the primary scattering determined as a function of angle and voltage. There is a great deal of small-angle scattering; the scattering falls to a minimum at about 110° and increases for larger angles. (This is true either for the center of mass system or for the laboratory system of coordinates.) The large angle scattering varies inversely as the velocity of the ions. Scattering in krypton and xenon has also been studied; here the corrections are larger and definite results have not yet been obtained for these gases.

37. Photoelectric and Electric Properties of Thin Bismuth Films of Measured Thickness. A. H. WEBER AND L. J. EISELE, S.J., *Saint Louis University.*—The photoelectric threshold shift with thickness in thin bismuth films deposited on glass has been further investigated, following a previous report,[1] with some important modifications in apparatus and method including measurement of the film thicknesses[2] and extension of the temperature range in which the DuBridge analysis[3] is applied. The present experiments are in good agreement with the previous preliminary work[1] but show some differences. For example, the threshold shows little change with film thickness below some 100 atomic layers of thickness. In the region of 100 atomic layers thickness there appears a sudden increase in threshold wave-length followed by a more gradual shift in threshold wave-length toward the red with increasing film thickness. The limiting value of the threshold wave-length appears to be about 2785A. Work in progress on the electrical conductivity and the photoconductivity of the bismuth films, measured simultaneously with the photoelectric emission, will be discussed as far as the accumulated data permit.

[1] A. H. Weber, Phys. Rev. **53**, 895 (1938).
[2] A. H. Weber, Phys. Rev. **57**, 1042 (1940).
[3] L. A. DuBridge, Phys. Rev. **39**, 108 (1932).

38. Images Projected from Etched Surfaces of Quartz Crystals. HARRY H. HUBBELL, JR., *Wesleyan University.*—The study reported by W. G. Cady[1] of the patterns formed by a beam of parallel light passing through the surface of a quartz crystal cut normal to the optic axis and etched in hydrofluoric acid has been continued. Following the procedure of Gramont,[2] the beam is focused on a ground glass or photographic film in the focal plane of a lens placed immediately above the etched surface. The three-pointed star patterns formed are quite sensitive to the time of etching and to the previous grinding and cleaning of the surface. A doubling of the patterns often appears, as though a second, fainter, three-pointed star were superposed on the first with its points rotated about 30° counterclockwise. The patterns usually become less diffuse as the microscopic trihedral pyramids formed on the surface become larger with longer etching, but their form becomes more complex. The points of the star make an angle of about 10° with the electric axes of the crystal. A technique of preparation of the surface and of etching is being developed which it is hoped will permit the routine determination of the electric axes of a z cut slab of quartz within about a degree.

[1] W. G. Cady, Proc. I.R.E. **28**, 144 (1940).
[2] A. de Gramont, *Recherches sur le Quartz Piézoélectrique* (Paris, 1935), Chap. 3.

39. Deviations from Ohm's Law at High Current Densities. LEVERETT DAVIS, JR.,* *California Institute of Technology.*—One would expect that a theoretical expression for the deviations from Ohm's law at high current densities could be obtained by considering the higher approximations of a theory whose first approximation gives Ohm's law. A possible method of treatment can be based on the assumption that a relaxation time, $\tau(\mathbf{k})$, can be defined. In this case Boltzmann's equation for the distribution function, $f(\mathbf{k})$, is

$$\mathcal{E}\epsilon\tau(\partial f/\partial k_1)-\hbar[f-f_0]=0,$$

where $\mathcal{E}$, the electric field, is assumed to be in the x direction, $-\epsilon$ is the charge of the electron, $\mathbf{k}$ is the wave vector, and f_0 is the equilibrium distribution function which we will assume to be the Fermi function. If we expand f in a power series in $\mathcal{E}^n$, we find that

$$f=\sum_{n=0}^{\infty}\mathcal{E}^n\left[\frac{\epsilon}{\hbar}\tau\frac{\partial}{\partial k_1}\right]^n f_0.$$

It follows that the current density is

$$J=-\frac{\epsilon}{4\pi^3\hbar}\Sigma\left(\frac{-\epsilon}{\hbar}\right)^n\mathcal{E}^n\int\frac{\partial f_0}{\partial k_1}\tau\left[\frac{\partial}{\partial k_1}\tau\right]^{n-1}\frac{\partial E}{\partial k_1}dV,$$

where $E(\mathbf{k})$ is the energy and dV is an element of volume in $\mathbf{k}$ space. If τ is assumed to be a constant and the energy that of the free electron case, only the linear term of this series is not zero. Consequently, Ohm's law is exact in this case. Other assumptions as to the dependence of E and τ on $\mathbf{k}$ will, in general, give deviations from Ohm's law. In some cases difficulties concerning the convergence of the series may arise.

* Now at the Rockefeller Institute for Medical Research.

40. Dispersion and Absorption in Dielectrics. ROBERT H. COLE, *Harvard University,* AND KENNETH S. COLE, *Columbia University.*—It will be shown that experimental results on a considerable number of liquid and solid dielectrics are represented by the empirical formula

$$\epsilon^*-\epsilon_\infty=(\epsilon_0-\epsilon_\infty)/[1+(i\omega\tau)^{1-\alpha}]. \qquad (1)$$

In this formula ϵ^* is the complex dielectric constant, ϵ_0 and ϵ_∞ are the "static" and "infinite frequency" dielectric constants, respectively, ω is the angular velocity, and τ is a generalized relaxation time. The parameter α can assume values between 0 and 1, the former value giving the result of Debye for polar dielectrics. The expression (1) requires that the locus of the dielectric constant in the complex plane be a circular arc with end points on the axis of reals, and center below this axis. The equivalent three-element electrical circuit requires a complex impedance with the property that the phase angle is a constant independent of the frequency. The significance of the empirical result (1), which is not satisfactorily described by any of the present dispersion theories, will be briefly discussed.

41. Coulomb Wave Functions in Repulsive Fields.* H. M. THAXTON, L. E. BAILEY AND H. E. WEBB, *The Agricultural and Technical College of North Carolina.*—Coulomb wave-functions Φ_L, Φ_L^*, Ψ_L, Ψ_L^*, Θ_L for the differential equation $d^2F/d\rho^2+[1+2\eta/\rho-L(L+1)/\rho^2]F=0$ have been calculated for the region $1.0\leqq\ln\eta^{-1}\leqq2.0$ and $0.01\leqq\rho\leqq0.10$ at small constant intervals in η and ρ. The values of L used were $L=0, 1, 2, 3$. In this region the series expansions[1] are practicable. These expansions have been used and checked by numerical integration of the differential equation. Many checks have also been made by $\Psi_L\Phi_L^*-\Psi_L^*\Phi_L-\rho^{2L+1}P_L\Phi_L^2=2L+1$. The coefficients A_j, a_j were computed directly, then checked by calculating $B_j=A_j/n_j$ and $b_j=a_j/n_j$. In this region coefficients A_{12} give an accuracy of 0.01 in Φ^* for $L=0$ with higher accuracy for $L=1, 2, 3$ for largest ρ and η. Similarly, a_{15} gives an accuracy of 0.01 in Ψ^* for largest ρ and η. For the region $1\leqq\eta\leqq100$ and $0.1\leqq\rho\leqq1$ the series method converges slowly. Calculations for this region are proceeding by another method.[2]

* To be read by title.
[1] F. L. Yost, G. Breit and J. A. Wheeler, Phys. Rev. **49**, 174 (1936).
[2] J. A. Wheeler, Phys. Rev. **52**, 1123 (1937).

42. Vibration-Rotation Energies of the Planar XY_3 Molecular Model. SAMUEL SILVER AND WAVE H. SHAFFER, *Ohio State University.*—The vibration-rotation energies of the planar XY_3 molecule have been obtained to the second order of approximation. The appropriate Hamiltonian was derived by the method of Wilson and Howard[1] so as to include cubic and quartic anharmonic terms in the potential energy, the dependence of the moments of inertia upon the vibrational states, the centrifugal expansion effects, and the Coriolis interactions between the internal angular momenta arising from the degenerate modes and the total angular momentum. The energy expressions were obtained by a method involving a contact transformation which was developed for this type of problem by Shaffer, Nielsen, and Thomas.[2] The energies are given in the form:

$$E=hc(G_{\text{vib}}+F_{\text{rot}})\pm\frac{\zeta h}{4\pi^2c_0c}(l_2+l_4)K, \qquad (1)$$

where

$$G_{\text{vib}}=G_0+\sum_{i=1}^{4}\left(V_i+\frac{d_i}{2}\right)\nu_i+\sum_{i=1}^{4}\left(V_i+\frac{d_i}{2}\right)^2G_{ii}$$
$$+\sum_{i<k}\left(V_i+\frac{d_i}{2}\right)\left(V_k+\frac{d_k}{2}\right)G_{ik}+(l_2^2-1)g_{22}$$
$$+l_2l_4g_{24}+(l_4^2-1)g_{44},$$
$$F_{\text{rot}}=J(J+1)B_v-K^2C_v-J^2(J+1)^2D_J$$
$$-K^4D_K-J(J+1)K^2D_{JK}$$

with

$$B_v=\dot{B}_e-\alpha_0-\sum_{i=1}^{4}\left(V_i+\frac{d_i}{2}\right)\alpha_i,$$
$$C_v=C_e-\beta_0-\sum_{i=1}^{4}\left(V_i+\frac{d_i}{2}\right)\beta_i,$$

and the third term in (1) representing the Coriolis interactions arising from the doubly degenerate modes ν_2 and ν_4. The parameters G_0, G_{ii}, g_{22}, $\cdots$, D_{JK} have been obtained explicitly as functions of the molecular constants occurring in the Hamiltonian.

[1] E. B. Wilson and J. B. Howard, J. Chem. Phys. **4**, 260 (1936).
[2] W. H. Shaffer, H. H. Nielsen and L. H. Thomas, Phys. Rev. **56**, 895, 1051 (1939).

43. Self-Consistent Field Calculations for Nickel. ROBERT B. GRAY AND MILLARD F. MANNING, *University of Pittsburgh.*—As a preliminary to energy band calculations, self-consistent field calculations for the d^8s^2 configuration have been carried out. The initial estimates were made by the method described by Manning and Millman[1] using previous results for Fe, Cu^+, and Zn. The 3d wave functions proved to be highly sensitive to changes in the assumed initial field. A satisfactory estimate of a new value of Z for the 3d electrons was found by adding to the initial Z one-third of the difference between final field and initial field. The final values of Z are consistent within 0.010 electronic unit.

[1] M. F. Manning and J. Millman, Phys. Rev. **49**, 849 (1936).

44. On the Universal Constants h, c, and e. ALFRED LANDÉ, *Ohio State University.*—The value of e in terms of h and c can be understood on the basis of defining the velocity ratio v/c in two reciprocal ways. First by means of the energy ϵ and the momentum p occurring in Einstein's equation $\epsilon^2-(pc)^2=\epsilon_0^2$, second by means of the time t and the path r traveled during t, occurring in the "signal equation" $t^2-(r/c)^2=t^2$. Just as ϵ_0 is the production energy so t_0 is the critical wave period of a production process. The close analogy between production, annihilation, and scattering leads to identifying t_0 with the time interval of a light signal traveling across the universal scattering cross section σ of Thomson. That is, the light path $a=ct$ is determined either by the equation $a^2=\sigma$ (a=path along the side of a quadratic area σ), or by the equation $a^2=2\sigma$ (a=path along the diagonal of σ). The latter definition of the production period, together with a quantization in the space of Einstein's and the signal equation, leads directly to the value 137.1273.. of Sommerfeld's constant. We do not have a convincing classical theory of the factor 2 in $a^2=2\sigma$, however.

45. The Deflection of Light Rays by a General Anisotropy. PHILIPP FRANK, *Harvard University.*—The refractive index of a medium may be $\mu=\mu_0(\mathbf{r})+\mu_1(\mathbf{r},\mathbf{s})$, the vector $\mathbf{r}$ denoting the coordinates of a point and the unit vector $\mathbf{s}$ the direction of the light ray, while μ_1 may be any function of $\mathbf{s}$. The deflection of a ray pencil $\mathbf{s}=\mathbf{s}(\mathbf{r})$ by the anisotropy μ_1 is defined by the "curvature vector $\mathbf{k}$ of the deflected rays relative to the rays in the isotropic medium μ_0." We find $\mathbf{k}=\mathbf{s}\times\text{rot}\,\mathbf{A}(\mathbf{r},\mathbf{s})$, $\mathbf{s}$ being $\mathbf{s}(\mathbf{r})$ and $\mathbf{A}=\mu_1\mathbf{s}+\text{grad}_s\,\mu_1-\mathbf{s}(\mathbf{s}\,\text{grad}_s\,\mu_1)$, grad_s implying differentiation with respect to the components of $\mathbf{s}$. The simplest case, notwithstanding the anisotropy of crystals, is $\mu_1=\mathbf{sg}(\mathbf{r})$, $\mathbf{g}$ being an arbitrary function of $\mathbf{r}$. This case covers, for example, the deflection of light rays by the motion of the medium. We have only to put $\mathbf{g}=-(1/c^2)\mu_0^2\mathbf{w}(\mathbf{r})$. Here μ_0 is the refractive index and $\mathbf{w}$ the velocity distribution in the medium. A second example is the deflection of electron rays in an electromagnetic field. We have to put $\mathbf{g}=(\epsilon/c)\mathbf{a}(\mathbf{r})$. Here $\mathbf{a}$ is the vector potential of the field.

46. Carbon Isotope Effect in Acetylenes. FORREST F. CLEVELAND AND M. J. MURRAY, *Illinois Institute of Technology.*—Glockler and Renfrew[1] have reported carbon isotope shifts in the triple-bond frequency in the Raman spectra of liquid acetylene and dimethylacetylene. Herzberg[2] has reported a similar isotope effect for $H-C\equiv N$. Since the triple-bond line is very intense, it seemed that it might be possible to observe such shifts for other substituted acetylenes. Assuming a linear, four-mass system and using the force constants listed by Crawford,[3] the isotope shifts for $CH_3-C^{13}\equiv C^{12}-CH_3$, $CH_3C^{13}\equiv C^{12}H$ and $CH_3C^{12}\equiv C^{13}H$ were calculated from the valence force equations to be -33, -50 and -26 cm^{-1}, respectively. Examination of spectrograms of 5-decyne, 3-octyne and 1-phenyl-1-butyn-3-one[4] disclosed the presence of weak lines which would correspond to isotope shifts of -38, -36 and -37, respectively. A long exposure of carefully purified 1-heptyne gave a weak line which would correspond to isotope shifts of -52 and -21 cm^{-1} for the two possible isotopic molecules. Semiquantitative measurement of the relative intensities of the two lines in 1-phenyl-1-butyn-3-one indicated that the intensity of the weak line was one-hundredth to one-fiftieth times that of the strong line.

[1] G. Glockler and M. M. Renfrew, J. Chem. Phys. **6**, 340 and 408 (1938).
[2] G. Herzberg, J. Chem. Phys. **8**, 847 (1940).
[3] B. L. Crawford, Jr., J. Chem. Phys. **8**, 526 (1940).
[4] This compound was synthesized by Mr. R. E. Dineen.

47. Infra-Red Transmission of the Human Body. C. HAWLEY CARTWRIGHT,* JOHN DANIEL† AND ALEX PETRAUSKAS, *Massachusetts Institute of Technology.*—The percentage reflection and transmission of a human cheek were measured as a function of wave-length in the visible and infra-red spectra. Absolute values were obtained to 12,000A by using a special photo-cell and an integrating sphere for collecting all the light. The reflection of the cheek reaches a maximum of about 50 percent in the visible red and gradually decreases for longer wave-lengths. The cheek (10 mm thick) is opaque below 6050A and increases its transmission linearly to about 2 percent of that entering the skin at 7000A. Between 7000A and the water absorption band at 10,000A, the transmission is rather uniform. Beyond 10,000A the transmission rises, reaches a maximum value of about 3 percent at 11,000A and decreases to zero beyond 13,500A, because of the water absorption. Using as a control a bearable discomfort on the outside of the cheek, measurements of the temperature rise inside the mouth were made using various sources of radiation. The best of these was a tungsten lamp with a water filter. An increase in temperature of 3°F was obtained inside the cheek without external discomfort.

* Corning Glass Works.
† U. S. Bureau of Public Health.

48. The Ultraviolet Absorption Spectra of Different Regions of *Trichophyton mentagrophytes* Spores.—PETER A. COLE, *National Institute of Health.* (*Introduced by F. S. Brackett.*)—The ultraviolet absorption spectrum of various portions of spores of *Trichophyton mentagrophytes* has been determined in the wave-length range 3021A to 2265A using a Zeiss ultraviolet microscope. A photographic method of photometry was employed using a focal plane rotating step-

sectored disk. Absorption maxima of different intensity and wave-length (2800A to 2500A) are observed for different regions within the same spore. Absorption curves and corresponding ultraviolet photomicrographs will be shown for several cells.

49. Afterglows in Nitrogen Rare Gas Mixtures. JOSEPH KAPLAN AND S. M. RUBENS, *University of California at Los Angeles.*—The spectra of nitrogen-helium, nitrogen-neon and nitrogen-argon mixtures have been studied in the auroral afterglow. Similar differences are observed between these and the Lewis-Rayleigh afterglows in rare-gas nitrogen mixtures as are observed when the auroral afterglow in pure nitrogen is compared with the Lewis-Rayleigh glow. The most interesting characteristic of the nitrogen-helium afterglow is the large intensity of forbidden radiations of nitrogen. No helium lines are obtained in either discharge or afterglow. Both the absolute and the relative intensities of the forbidden radiations are high. The argon-nitrogen afterglow closely resembles the afterglow in pure nitrogen at the same total pressure. The Goldstein-Kaplan bands are stronger in argon. The enhancement of the relative intensity of the forbidden radiations late in the afterglow is also observed. The neon-nitrogen afterglow is intermediate between the argon and helium afterglows. There appears to be a connection between the intensity of the first-negative bands in the narrow portion of the tube and the intensity of the forbidden nitrogen line 3467 in the neighboring portion of the tube where the afterglow is observed. This may lead to an understanding of excitation processes in the aurora.

50. On the Molecular-Field Theory of Volume Magnetostriction. R. SMOLUCHOWSKI, *Princeton University.*—In a saturated ferromagnetic substance all elementary magnets are aligned under the influence of the molecular-field proportional to the magnetization. Quantum mechanics relates this field to the exchange forces between electrons of the atoms. Since these forces depend upon interatomic distance we would expect the molecular field to be volume dependent. Interpretation of corresponding magnetostriction data has been given by Becker and Kornetzki who assumed a volume independent saturation magnetization at absolute zero. Since this assumption is questionable a different procedure was adopted: We treat the Brillouin functions in the formalism of the molecular-field theory as known, assuming $j=\frac{1}{2}$ or $j=1$ corresponding to uncoupled or coupled (in pairs) electrons. Using the experimental data on the magnetostriction of iron this method allows us to obtain values for (a) the molecular-field "constant" N; (b) its dependence on the relative change of volume $(1/N)\,(\partial N/\partial\omega)$; and (c) the dependence on volume of the saturation magnetization at 0°K $(1/I_0)\,(\partial I_0/\partial\omega)$. The value of N agrees well with that obtained from magnetocaloric measurements. The dependence of saturation magnetization agrees with the value expected from the change of density. The check of the value of $(1/N)\,(\partial N/\partial\omega)$ is made considering the "magnetic" specific heat caused by the change of the magnetization energy. Thermodynamical considerations lead to an additional term proportional to this magnitude. A comparison with the experimental data provides a good check of the obtained value. All quantitative checks of our theory, including the probable change of Curie point under pressure, are more satisfactory assuming electrons coupled in pairs $(j=1)$ than uncoupled $(j=\frac{1}{2})$.

51. Magnetic Properties of Antimony-Tin Monocrystals. S. H. BROWNE AND C. T. LANE, *Yale University.*—According to the Bloch theory, in metals the energy states of electrons are pictured as falling into zones (Brillouin zones). In particular, Mott and Jones[1] have shown that for bismuth-like structures the first and second Brillouin zones overlap slightly. The magnetic susceptibility of the crystal parallel to the trigonal axis ($\chi_{\parallel}$) is caused by these overlapping electrons while the susceptibility perpendicular to this axis ($\chi_{\perp}$) is due to the vacant spaces (positive holes) in the first zone. We have investigated this theory by measuring $\chi_{\parallel}$ and $\chi_{\perp}$ for monocrystals of antimony-tin, up to eight percent tin. In this range a solid solution is formed, leaving the antimony crystal structure unchanged, but because of the difference in valence each tin atom removes one electron from the crystal. In accordance with expectation $\chi_{\parallel}$ decreases sharply, and eventually (at approximately 1.11 atomic percent tin) changes from diamagnetic to paramagnetic. $\chi_{\perp}$ remains diamagnetic, but decreases slightly (by approximately 15 percent at the inversion point). From the inversion point of $\chi_{\parallel}$ it is estimated that there are approximately 10^{-2} overlapping electrons per atom in the second zone in antimony.

[1] N. F. Mott and H. Jones, *The Theory of the Properties of Metals and Alloys* (Oxford, 1936).

52. Magnetic Susceptibility of Metallic Lithium. C. STARR AND A. R. KAUFMANN, *Massachusetts Institute of Technology.*—The magnetic susceptibility of metallic lithium has been studied as a function of temperature between 300°K and 13.9°K. The experimentally determined volume susceptibility (per cc) is given by the equation $\chi\times10^6=1.90+7.8/T$. The lithium specimen contained more than 99 percent Li, with a remainder of Na, K, N_2 and about 0.01 percent Fe. The major part of the temperature dependent term may be caused by the effect of the dissolved iron impurity. A small amount of iron in solid solution generally behaves as a paramagnetic substance and contributes a Curie law term to the susceptibility. Theoretical study[1] indicates that the paramagnetic susceptibility of pure lithium would be expected to increase with decreasing temperature, but the magnitude of this effect is not known.

[1] J. B. Sampson and F. Seitz, Phys. Rev. **58**, 633 (1940).

53. Hall e.m.f. and Intensity of Magnetization. EMERSON M. PUGH, *Carnegie Institute of Technology.*—The experimental fact that the Hall e.m.f. in the majority of ferromagnetic materials is directly proportional to the intensity of magnetization in the material can be explained by assuming that the Hall electric field $\mathbf{E}_H$ at any point

in the material is given by $\mathbf{E}_H = R\mathbf{i}\times\mathbf{I}f(I)$ for any function of the intensity of magnetization at that point. This is true since the magnetic domains in the material are always saturated and any $f(I)$ must be a constant throughout the material. Therefore the contribution of any domain to the whole e.m.f. is proportional to its contribution to the macroscopic intensity of magnetization of material. The justification for this assumption will be reviewed. These conclusions probably apply to all of the transverse effects.

54. A Taylor Dislocation Near a Cylindrical Boundary. J. S. KOEHLER,* *University of Pennsylvania.*—It has been suggested by Taylor and others that the low plastic yield strengths of solids are caused by line dislocations. The exact mechanism by which dislocations are created is not known, but there is evidence that they are formed at crystalline surfaces. A solution of the elastic equations for a continuous isotropic solid has been found for the case of a line dislocation near a cylindrical boundary. The elastic energy associated with the dislocation is computed as a function of the distance from the surface. From this result the forces acting on the dislocation near a plane boundary in the absence of an external stress is found and tends to attract the dislocation to the surface.

* Rackham Postdoctoral Fellow of the University of Michigan.

55. Dislocations and the Theory of Creep. FREDERICK SEITZ, *University of Pennsylvania.*—It is pointed out that two different qualitative pictures can be used to discuss creep in single crystals on the basis of the theory of dislocations. One of these is based on the notion that the rate of creep is determined primarily by the relatively slow motion of dislocations present in the solid; the other is based on the notion that dislocations move almost instantaneously and that creep is tied up primarily with the rate of generation of dislocations. The equations associated with each of these pictures are, respectively,

$$\frac{dS}{dt}=\lambda v N, \qquad \frac{dS}{dt}=\lambda L\frac{dN}{dt}.$$

Here dS/dt is the rate of strain, N is the number of dislocation lines per unit area, λ is the slip distance associated with the passage of one dislocation, v is the average velocity of the dislocations, and L is the average distance moved by a dislocation. Examination of the meager available creep data for a quantitative comparison of the merits of these equations indicates that neither furnishes a completely satisfactory correlation of all experimental material. The first meets difficulty because the required velocity v must be unreasonably low for reasonable values of N; the second meets difficulty at low temperatures and stresses because the assumed values of dN/dt are unreasonably high.

56. Damping of Mechanical Vibrations in Copper Crystals. THOMAS A. READ,* *Westinghouse Research Laboratories.*—In a recent paper[1] on the internal friction of zinc crystals it was suggested that the damping of longitudinal vibrations in zinc single-crystal rods results from the production of dislocations by the oscillating stress and their motion under the influence of that stress. Data will be shown which indicate that the internal friction of copper crystals at small strain amplitudes must be ascribed only to the motion of dislocations already present in the crystals. This evidence may be summarized as follows: (1) the decrement of a copper crystal is not changed by the oscillations, (2) the application of a static compressive stress of 100 lb. per sq. in. increases the decrement of a copper crystal, and (3) the internal friction of copper single crystals is only slightly temperature dependent.

* Westinghouse Research Fellow.
[1] T. Read, Phys. Rev. **58**, 371 (1940).

57. Order-Disorder Questions and Certain Spinels. F. C. BLAKE, *Ohio State University.*—It has been previously shown that one of the spinels (lithium ferrite) can be explained as having both long range and short range order of magnitude 100 percent by the method of lattice enlargement from a cube of edge 4.14 angstroms to one of edge 33.2 angstroms. For certain other spinels this method did not work, apparently. However, for one of this latter group, a *smaller* rather than a *larger* lattice gives a unique solution, the space group changing from cubic to tetragonal with the axial ratio equal to $\sqrt{2}$. It is not claimed that a hundred percent short range—and long range—ordered solution can always be found as a substitute for any so-called disordered solution, though less violence is done to our theories of valence by ordered rather than disordered solutions.

58. Phase Transition in Liquid Helium. L. I. SCHIFF, *University of Pennsylvania.*—A method for treating the quantum-mechanical many-body problem at temperatures so low that degeneracy plays a dominant role[1] has been applied to the phase transition in liquid helium. It is shown that the correction to London's free-particle model due to two-body encounters does not affect the transition temperature, or the continuity of either the energy or the specific heat at the transition temperature. Explicit calculations on the basis of the elastic sphere model, considering only S collisions, show that the specific heat is lowered in the neighborhood of the transition temperature. These results suggest the possibility that the observed phase transition in liquid helium is characteristic of a condensed system, and cannot be obtained from gas approximation methods such as the present.

[1] L. I. Schiff, Science **92**, 482 (1940).

59. Description of the Liquid Helium Equipment at Yale University. C. T. LANE, *Yale University.*—A plant for producing liquid helium in quantity has recently been completed, and is in satisfactory operation. The design of the liquefier is based on the work of Kapitza,[1] making use of an expansion engine working adiabatically to bridge the temperature interval between 65° and 10°K. Consequently, the only refrigerant used is liquid air; greatly reducing the cost of the equipment and eliminating the dangers of work with hydrogen. The helium distribution and purifying systems are very simple and compact; the whole plant may

be placed in a room about 18 feet square. For reasons of efficiency the stage from 10°K to liquefaction is accomplished by means of Joule-Thomson expansion between the limits 13 to 1.5 atmospheres. The subsidiary machinery (compressor, vacuum pumps etc.) is composed entirely of commercial equipment. Approximately 1¼ hours are required to reach the liquefaction point, and thereafter liquid helium is made at the rate of about 1½ liters per hour. About 10 liters of liquid air are necessary to cool the liquefier to the helium point, and roughly 2 liters per hour thereafter. Photographs of the plant will be shown and an estimate of the cost given.

[1] P. Kapitza, Proc. Roy. Soc. **A147**, 189 (1934)

60. Raman Spectrum of 6-Dodecyn-5-one.* FORREST F. CLEVELAND AND M. J. MURRAY, *Illinois Institute of Technology.*—The Raman spectrum of 6-dodecyn-5-one, $CH_3(CH_2)_4C{\equiv}CCO(CH_2)_3CH_3$, has been obtained. The spectrum is interesting because the triple-bond frequency at 2212 cm^{-1} is single, rather than double or multiple as is the case for most disubstituted acetylenes, and is lower than usual for such molecules. For example, 6-dodecyne, which differs from the above molecule only by the presence of two hydrogen atoms in place of the oxygen atom, has in this region the frequencies 2231(7), 2248(2) and 2294(4). If the multiplicity of lines in this case is caused by resonance interaction, the single line observed for 6-dodecyn-5-one can be understood by supposing that the drop in the triple-bond frequency occasioned by the introduction of the oxygen atom causes it to be no longer in sufficiently exact coincidence with the overtone or combination frequency to permit resonance interaction. Consistent with this hypothesis is the fact that only a single line was observed by the authors for phenyliodoacetylene. The frequency in this case was 2183 which is also considerably less than the usual value for disubstituted acetylenes. Another possibility is that the introduction of the oxygen atom may have changed the value of the fundamental or fundamentals whose overtone or combination frequencies interacted with the triple-bond frequency in the 2200 region. The frequency characteristic of the C=O group is also lower than usual for a ketone as is to be expected for conjugation with a triple-bond.

* To be called for after Paper No. 49.

ABSTRACTS OF INVITED PAPERS

A. A Hydro-Physical Approach to the Quantitative Morphology of Drainage Basins. ROBERT E. HORTON, *Voorheesville, New York.*—The purpose of this paper is to show how fundamental principles of physics, hydraulics and hydrology may be applied quantitatively to the study of drainage basins and their stream systems. As the basis for this study, numerical factors are needed which characterize the physical features of a drainage basin and its stream net quantitatively. Particular stress is laid on two closely related factors, drainage density and infiltration-capacity, as indicative of degree and rate of basin and channel development. Except in regions of karst topography, stream basin development by aqueous erosion is conditioned almost wholly by surface runoff, exclusive of ground-water flow. The independent physical variables controlling surface runoff are: rain intensity, rain duration and intensity distribution, infiltration-capacity, surface roughness, surface slope, length of overland flow and type of overland flow. These factors, in conjunction with the hydraulic laws of sheet flow (Manning's formula for turbulent, Poiseuille's formula for laminar, flow), together with the law of continuity, afford a basis for a complete rational treatment of surface runoff phenomena. Hence the purely hydraulic and hydrologic phases of the subject may be considered as completely solved. The second phase of the subject—determination of the rate of sheet erosion corresponding to a given surface runoff regimen—is almost as completely unsolved. Assuming merely that, for a given drainage basin, sheet erosion is a function of hydrologic conditions, conclusions can be drawn which are helpful in understanding the physiographic characteristics of drainage basins and their drainage nets.

B. Problems of Orogeny. CHESTER R. LONGWELL, *Yale University.*—*Orogeny* is defined as large-scale crustal deformation characterized by folding, thrusting, and other evidences of compression. The chief objectives in the study of orogenic structures are: (1) To determine the geometric pattern of features that record deformation in the several orogenic zones. The first step to this end is accurate mapping of mountain belts; but even if this part of the task were fully accomplished, the third dimension would still present large uncertainties—the depth to which deformation extends, and the nature of deformation at all depths below the zone of observation. Some attempts to calculate depth of deformation from surficial evidence have reached questionable conclusions. (2) To establish the nature of stresses responsible for the several kinds of deformation in orogenic zones. The stresses are to be inferred from the field facts, with the assistance of laboratory experiments, particularly experiments using scale models. (3) To date the orogenic events as closely as possible. The development of any one zone can be understood only after the correct order of events in that zone is determined. Exact dating of all orogenic movements would go far toward settling the controversy as to whether diastrophism is "periodic" and "world-wide" in character. (4) To detect the ultimate forces responsible for diastrophism. This subject is still in the speculative stage, and can be approached only by the method of multiple working hypotheses. A comprehensive study of orogeny must consider its relation to the other kinds of crustal deformation—major warping, or *epeirogeny*, and regional block-faulting, sometimes designated *tafrogeny*.

C. Physical Frontiers in Seismology.—L. Don Leet, *Harvard University.*—Seismology has reached a critical stage where serious discrepancies between observations and current theories have been established. Investigation of these is awaiting the interest and abilities of mathematical and experimental physicists. It is believed that solutions will lead to results of geological importance in connection with data on the structure of the earth's crust, mantle, and core. Over a year ago, the writer reported observations of a new wave form, tentatively called the "coupled wave," which is not explained by the classical theory of elasticity. It was first found in the vicinity of dynamite blasts and in some cases dominated the motion. Subsequent search by Collins on earthquake records at the Harvard Seismograph Station revealed it at certain distances as the wave which had previously been called the shear wave of classical theory. This led further to the discovery that the so-called shear wave is actually compressional in character over certain distance ranges, a coupled wave over others, and shows the characteristics of a true shear wave over only a relatively narrow range. Birch, at Harvard, has made one of the first fundamental attacks on these widening physical frontiers in seismology by investigating the effect of pressure upon elastic parameters of isotropic solids, according to Murnaghan's theory of finite strain. He suggests "that a more rigorous solution of the equations of motion derived from the theory of finite strain might prove of value in interpreting the oscillatory character of seismic records, as well as the direction of the ground motion associated with various wave types."

D. The Radio-Elements in the Water and Sediments of the Ocean. William D. Urry, *Geophysical Laboratory, Washington, D. C.*—The radioactive relations existing in the ocean and its sediments are complex in comparison with the simple relations for the igneous and sedimentary rocks that form the continents. This is because neither in the ocean nor in the upper layers of the ocean bottom are elements such as uranium, ionium and radium in radioactive equilibrium. In discussing the distribution of the radio-elements the dimension of time is therefore of prime importance. The sediments underlying the deeper portions of the ocean provide suitable material, correlated with this dimension, for studying the growth and decay of these elements. Glacial and other stratifications in some of these sediments greatly complicate the radioactive relations. These studies indicate the possibility of establishing the rate of deposition of the ocean sediments.

Author Index to Abstracts of the Philadelphia Meeting

Bailey, L. E.—see Thaxton, H. M.
Ballard, Stanley S. and L. A. Dean—No. 10
Barry, J. G.—see Johnson, T. H.
Beams, J. W.—see Stauffacher, Arthur L.
Beardsley, Niel F.—No. 20
Bethe, H. A., G. Blanch, A. N. Lowan and R. E. Marshak—No. 6
Blake, F. C.—No. 57
Blanch, G.—see Bethe, H. A.
Brown, S. Leroy and Lisle L. Wheeler—No. 12
Browne, S. H. and C. T. Lane—No. 51
Broxon, James W.—No. 22

Cady, Willoughby M. and D. H. Tomboulian—No. 33
Cartwright, C. Hawley, John Daniel and Alex Petrauskas—No. 47
Cleveland, Forrest F. and M. J. Murray—Nos. 46, 60
Cobine, J. D.—see Easton, E. C.
Cohee, A. V.—see Miller, E. P.
Cole, Kenneth S.—see Cole, Robert H.
Cole, Peter A.—No. 48
Cole, Robert H. and Kenneth S. Cole—No. 40
Cooper, John N.—No. 34

Daniel, John—see Cartwright, C. Hawley
Davis, Leverett, Jr.—No. 39
Dean, L. A.—see Ballard, Stanley S.

Easton, E. C. and J. D. Cobine—No. 35
Ehrhardt, C. H. and E. P. Miller—No. 31
Eisele, L. J.—see Weber, A. H.
Eldridge, John A.—No. 36

Frank, Philipp—No. 45

Getting, I. A.—No. 8
Gingrich, N. S.—see Sharrah, P. C.
Gray, Robert B. and Millard F. Manning—No. 43
Grover, Horace—see King, Allen

Hilberry, Norman and Victor H. Regener—No. 29
Horton, Robert E.—No. A (Friday A.M.)
Hubbell, Harry H., Jr.—No. 38
Humphreys, Richard F.—see Pollard, Ernest

Inglis, D. R.—No. 16

Johnson, Thomas H.—see Pomerantz, Martin A.
——, **J. G. Barry and R. P. Shutt**—No. 24

Kaplan, Joseph and S. M. Rubens—No. 49
Kaufmann, A. R.—see Starr, C.
King, Allen and Horace Grover—No. 17
Koehler, J. S.—No. 54
Korff, S. A.—see Rose, M. E.

Landé, Alfred—No. 44
Lane, C. T.—No. 59
—— see Browne, S. H.
Lees, Wayne L.—see Swann, W. F. G.
Leet, L. Don—No. C (Friday A.M.)
Long, V. A. and R. M. Whaley—No. 21
Longwell, Chester R.—No. B (Friday A.M.)
Lowan, A. N.—see Bethe, H. A.

MacHattie, L. E.—No. 13
Manning, Millard F.—see Gray, Robert B.
Margenau, H.—No. 7
Marshak, R. E.—see Bethe, H. A.
—— **and V. F. Weisskopf**—No. 26
Mauchly, J. W.—No. 18
Miller, E. P.—see Ehrhardt, C. H.
—— **and A. V. Cohee**—No. 11
Montgomery, C. G. and D. D. Montgomery—No. 28
Montgomery, D. D.—see Montgomery, C. G.
Murray, M. J.—see Cleveland, Forrest F.

Petrauskas, Alex—see Cartwright, C. Hawley
Pietenpol, W. B.—No. 2
—— see Westerfield, E. C.
Pollard, Ernest—see Smith, Everett C.
—— **and Richard F. Humphreys**—No. 4
Pomerantz, Martin A. and Thomas H. Johnson—No. 25
Powell, Wilson M.—No. 27
Present, R. D.—No. 5
Pugh, Emerson M.—No. 53

Read, Thomas A.—No. 56
Regener, Victor H.—see Hilberry, Norman
Rose, M. E. and S. A. Korff—No. 9
Rubens, S. M.—see Kaplan, Joseph

Schiff, L. I.—No. 58
Schilling, Harold K.—No. 15
Seitz, Frederick—No. 55
Shaffer, Wave H.—see Silver, Samuel
Sharrah, P. C. and N. S. Gingrich—No. 30
Shutt, R. P.—see Johnson, T. H.
Silver, Samuel and Wave H. Shaffer—No. 42
Smith, Everett C. and Ernest Pollard—No. 3
Smoluchowski, R.—No. 50
Snoddy, L. B.—see Stauffacher, Arthur L.
Starr, C. and A. R. Kaufmann—No. 52
Stauffacher, Arthur L., J. W. Beams and L. B. Snoddy—No. 14
Swann, W. F. G. and Wayne L. Lees—No. 23

Taft, Robert B.—No. 19
Thaxton, H. M., L. E. Bailey and H. E. Webb—No. 41
Tomboulian, D. H.—see Cady, Willoughby M.
Tunell, G.—No. 32

Urry, William D.—No. D (Friday A.M.)

Webb, H. E.—see Thaxton, H. M.
Weber, A. H. and L. J. Eisele—No. 37
Weisskopf, V. F.—see Marshak, R. E.
Westerfield, E. C. and W. B. Pietenpol—No. 1
Whaley, R. M.—see Long, V. A.
Wheeler, Lisle L.—see Brown, S. Leroy